Wegener Center
SCIENTIFIC REPORT
101 | 2023

Investigating atmospheric blocking and related extreme events in Austria using observation-based datasets

Moritz Pichler

September 2023

Climate Change Graz
Field of Excellence
University of Graz

Wegener Center

UNI GRAZ

The Wegener Center for Climate and Global Change is an interdisciplinary, internationally recognized research and graduate education institute of the University of Graz that is pooling the University's expertise in Climate, Environmental and Global Change. It brings together research teams and scientists from fields such as geophysics and climate physics, meteorology, economics, geography, and social sciences. At the same time, close links are maintained and further developed with many national and international cooperation partners. The research interests range from monitoring, analysis, and modeling of climate and environmental change to the investigation of climate change impacts and the analysis of the human dimensions of these changes related to mitigation, adaptation, and loss & damage. More information at **www.wegcenter.at**.



Alfred Wegener (1880 – 1930), after whom the Wegener Center is named, was founding holder of the University of Graz Geophysics Chair (1924 – 1930). In his work in the fields of geophysics, meteorology, and climatology he was a brilliant scientist and scholar, thinking and acting in an interdisciplinary way, far ahead of his time with this style. The way of his ground-breaking research on continental drift is a shining role model. His sketch on the relations of continents based on traces of an ice age about 300 million years ago (left) as basis for the Wegener Center Logo is thus a continuous encouragement to explore equally innovative ways: paths emerge in that we walk them (motto of the Wegener Center).

This report is the result of a Master thesis work completed in February 2023.

SR 101 | 2023 Investigating atmospheric blocking and related extreme events in Austria using observation-based datasets

ISBN 978-3-9505053-0-6 September 2023

Suggested citation:
Pichler, M. (2023), Investigating atmospheric blocking and related extreme events in Austria using obversation-based datasets, Wegener Center Scientific Report 101-2023, Wegener Center Verlag, University of Graz, Austria, September 2023.
ISBN 978-3-9505053-0-6

(c) 2023 Wegener Center Verlag, University of Graz, Austria
The usage of images, tables, or texts of this Scientific Report is permitted for non-commercial purposes if appropriate credit is given.
For any other purposes, please contact: wegcenter@uni-graz.at

Publishing institution:
Wegener Center for Climate and Global Change, University of Graz
Brandhofgasse 5, 8010 Graz, www.wegcenter.at

Contact: Moritz Pichler
moritz.pichler@uni-graz.at

Master thesis
to obtain the degree Master of Sciences
at the University of Graz

Investigating atmospheric blocking and related extreme events in Austria using observation-based datasets

PICHLER Moritz, BSc

Graz, February 2023

Supervisor
Univ.-Prof. Mag. Dr. Andrea K. Steiner

Wegener Center for Climate and Global Change
University of Graz, Austria



"The presence of those seeking the truth is infinitely to be preferred to the presence of those who think they've found it."

— Terry Pratchett, 'Monstrous Regiment'

Abstract

Atmospheric blocking events are persistent high-pressure systems in the mid-latitudes that can block the westerly flow usually prevailing in this region. They have previously been demonstrated to be connected to extreme weather events. This thesis aims to analyze trends in the frequency of blocking events over the northern mid-latitudes and to investigate the connection between blocking and extreme weather events specifically in Austria. We used ECMWF Re-Analysis Version 5 (ERA5) data (1950–2019) and applied a blocking detection algorithm and ordinary linear regression to detect trends. The connection between blocking and extreme weather was investigated using ERA5 and WATCH Forcing Data ERA 5 (WFDE5) (1980–2018) by applying a Monte-Carlo algorithm. The resulting trends in blocking frequency vary by region and season. Since 1950, blocking frequency decreased longitudinally by 2 % per decade over the North Atlantic (January–May) and Asia (February) while it increased by 2 % and 4 % per decade over Europe (September) and East Asia (June), respectively. Some of these changes represent spatial shifts. Since 1979, regional blocking trends represent an increase over the British Isles in March and a decrease over the North Atlantic in November. We find a connection between blocking over Central and Eastern Europe and increased heatwave frequency in Austria and between blocking over Northern Europe and decreased heatwave frequency in Austria. We also demonstrate a connection between blocking over Northern Europe, the North Atlantic and Greenland and more frequent cold spells in Austria. Finally, blocking over Russia is connected to more frequent heavy precipitation events while blocking over the British Isles and the North Sea is associated with less frequent heavy precipitation events in Austria. Our findings can help stakeholders better understand changes in blocking frequency over the northern hemisphere in the recent decades and effects on extreme weather in Austria.

Zusammenfassung

Persistente Hochdruckgebiete (Blocking) in den mittleren Breiten können in dieser Region vorherrschende Westwinde blockieren und können Extremwetterereignisse auslösen. Ziel dieser Arbeit ist es, Trends in der Häufigkeit von Blocking über nördlichen mittleren Breiten und den Zusammenhang mit Extremwetterereignissen in Österreich zu untersuchen. Ein Algorithmus zur Detektion von Blocking und ein lineares Regressionsverfahren wurden auf ECMWF Re-Analysis Version 5 (ERA5)-Daten (1950 – 2019) zur Trendbestimmung angewandt. Zusammenhänge zwischen Blocking und Extremwetter wurden anhand von ERA5 und WATCH Forcing Data ERA5 (WFDE5) (1980 – 2018) mittels eines Monte-Carlo-Algorithmus untersucht. Die resultierenden Trends in der Blockinghäufigkeit variieren je nach Region und Jahreszeit. Seit 1950 nahm die Häufigkeit zonal über dem Nordatlantik (Januar-Mai) und Asien (Februar) um 2 % pro Jahrzehnt ab, während sie über Europa (September) und Ostasien (Juni) um 2 % bzw. 4 % pro Jahrzehnt zunahm. Einige dieser Änderungen sind auf räumliche Verschiebungen zurückzuführen. Seit 1979 zeigen die regionalen Trends eine Zunahme über den Britischen Inseln im März und eine Abnahme über dem Nordatlantik im November. Es konnten Zusammenhänge zwischen Blocking in Mittel- und Osteuropa und häufigeren Hitzewellen in Österreich sowie zwischen Blocking über Nordeuropa und selteneren Hitzewellen in Österreich nachgewiesen werden. Ebenso gibt es Zusammenhänge zwischen Blocking über Nordeuropa, dem Nordatlantik und Grönland und häufigeren Kältewellen in Österreich. Schließlich konnten Zusammenhänge zwischen Blocking über Russland und häufigeren Starkniederschlagsereignissen sowie zwischen Blocking über den Britischen Inseln und der Nordsee und selteneren Starkniederschlagsereignissen in Österreich gezeigt werden. Diese Ergebnisse tragen dazu bei, Veränderungen der Auftrittshäufigkeit von blockierenden Hochdrucksystemen und mögliche Auswirkungen auf Extremwetter in Österreich besser zu verstehen.

Plain Language Summary

The author is a long-standing fan of clear communication of scientific results and methods to an audience with a different background than that of the researchers themselves. Here, the research questions and main findings are summarized. For a plain language summary of the methods we used, the reader may consult Appendix C.

Research question

The weather in the midlatitudes is generally characterized by high and low pressure systems. Occasionally, theses systems stay in place for a long time, although it is not entirely clear why that happens. People have tried to find out if this kind of situation occurs more frequently now than it did in the past, with no clear conclusions. We now have access to data all the way back to 1950, and we were wondering if we could find a more definitive answer to that question using this additional data. A focus of our investigation was how such long-lasting high pressure areas can influence the development of certain extreme weather situations in Austria. This includes heatwaves, cold spells and heavy precipitation.

Results

Consistent with previous scientific work, we found out that in some regions and in some decades, the occurrence of persistent high pressure systems has increased, for example over the North Atlantic longitudes in summer, or between 120°E and 140°E in June. In other cases, their occurrence has decreased, for example over the North Atlantic longitudes in winter and spring. This means that we could not come up with a more definitive, general answer, and that it remains very difficult, if not impossible, to make an educated guess as to how the situation will develop in the future. We could show that depending on the location of a long-lasting high pressure system, it can either help or inhibit the formation of extreme weather situations in Austria. Generally, blocking systems in Central and Eastern Europe are associated with a higher chance for heatwaves to develop in Austria and with a lower chance for cold spells to develop in Austria. This is the case because persistent high pressure systems allow for clear skies and thus permit the sun to warm the affected regions. Likewise, blocking systems to the north, over Scandinavia, the North Atlantic and Greenland, are associated with a lower chance for heatwaves to develop in Austria, and with a higher chance of

cold spells to develop in Austria. In this case, cold air from the north and the east near the high pressure systems moves towards regions to the south of them. We also found that blocking events over Greenland, Iceland, the British Islands and Northern Europe are associated with a lower chance for heavy precipitation events to occur in Austria, while blocking events over Russia are associated with a higher chance of heavy precipitation events to occur in Austria. This may be the case because long-lasting high pressure systems, depending on their location, can either hinder the transport of moisture from the west towards Austria, or the transport of moisture away from Austria towards the east.

Acknowledgements

First and foremost, I deeply and sincerely thank Univ.-Prof. Mag. Dr. Andrea Steiner for the work that she has done as my supervisor. The levelheaded and constructive advice that she gave me throughout the process of writing this thesis was invaluable and there is no doubt that this thesis was greatly improved by her involvement.

I would also like to thank Dr. Lukas Brunner, MSc. for sharing the thoughts and insights he gained during his own work on atmospheric blocking during a few brief visits and Kamilya Yessimbet, MSc. for providing me with the data that I needed for my investigations.

I am very grateful to Matthias Stocker, MSc. for acting as my low-level support and friend at the Wegener Center for Climate and Global Change, and my other office colleagues, Erich and Josef, for the warm and welcoming atmosphere.

The Gemeinnützige Privatstiftung zur Förderung der Forschung auf dem Gebiet der Versicherungswirtschaft is acknowledged for their financial support, which enabled me to focus on my scientific work.

Of course, my gratitude also goes out to the rest of the Wegener Center team (including, but not limited to: Stefanie, Stephanie, Lena, Georg, Jürgen and Marc) for their friendship and for countless inspirational coffee breaks and discussions, and to all the people in Austria and abroad who I have the great privilege of counting among my friends.

I would like to express my deep gratitude to my family, most notably my parents Elisabeth and Ulrich, for their continuous support, without which none of this would have been possible in the first place. My brothers, Theo and Jakob, are acknowledged by name because (a) they are the finest pair of brothers one could possibly wish for and (b) they complained when I did not acknowledge them in my Bachelor's thesis.

Finally, I would like to mention Mag. Gabriele Jaritz, who was my Physics teacher during my last two years at school, and whose excellent classes set me on a course to study Physics — in hindsight, I can now say that it was clearly the right decision, and I am grateful for your guidance, Gabi.

There are many other names that deserve to be on this page, but for the sake of brevity, I close out with a (slightly adapted) quote:

"I don't know half of you half as well as I should like; and I have thanked less than half of you half as much as you deserve."

— Bilbo Baggins in J.R.R. Tolkien, 'The Fellowship of the Ring'; adapted.

Contents

1. Introduction **1**

2. Relevant Aspects of Atmospheric Dynamics **3**
2.1. Large-Scale Atmospheric Circulation 3
2.1.1. Hadley Cell 3
2.1.2. Polar Cell 4
2.1.3. Ferrel Cell 4
2.2. Conservative Force Fields 5
2.3. Geopotential Height 6
2.4. Pressure Coordinates 6
2.5. Atmospheric Blocking 7

3. Extreme Temperature and Precipitation **9**
3.1. Heatwaves 9
3.2. Cold Spells 10
3.3. Extreme Precipitation 10

4. Data and Methods **13**
4.1. Data 13
4.1.1. Reanalyses 13
4.1.2. ERA5 13
4.1.3. WFDE5 13
4.2. Methods 14
4.2.1. Blocking Detection and Trend Estimation 14
4.2.2. Extreme Weather Detection 15
4.2.3. Blocking Frequency Anomaly during Extreme Temperature and Precipitation Days in Austria 17
4.2.4. Extreme Weather Frequency Anomaly during Blocking days in the Northern Midlatitudes 17

5. Blocking Trends **19**
5.1. Blocking Trends, resolved in Longitude 19
5.2. Blocking Trends, resolved in 2 Dimensions 21

6. Blocking and Extreme Weather in Austria **29**
6.1. Blocking and Extreme Weather Climatologies 29
6.2. Blocking and Heatwaves in Austria 34
6.3. Blocking and Cold Spells in Austria 40

6.4. Blocking and High Precipitation in Austria 45

7. Summary and Conclusions **51**

A. Trends in Blocking Frequency in Regions Defined in Literature **55**

B. Monthly-resolved Extreme Weather Anomalies **57**

C. Plain Language: Methods **95**

Acronyms **99**

List of Figures **101**

List of Tables **105**

Bibliography **107**

1. Introduction

Atmospheric blocking of the prevailing westerly flow is an important meteorological feature in the mid-latitudes and its occurrence is closely connected to the occurrence of extreme weather events, which in turn have consequences for agricultural, economic and social systems. Brunner et al. (2018) established a connection between atmospheric blocking and extreme temperatures. For example, blocking over Scandinavia substantially increases the cold spell frequency in winter in most of Europe. Unterberger et al. (2018) found that earlier blooming (due to climate change) towards April exposes apple trees to increased risk of blocking-related late frost. In summer of 2010, a severe heatwave in the Euro-Russian region that was related to an atmospheric blocking event resulted in more that 15.000 deaths, crop failues, and hundreds of wildfires. The extent of these extreme temperatures was not easily predictable (Matsueda 2011). This highlights the problems that arise from the lack of a complete dynamical descripion of blocking mechanisms. At the same time, climate models consistently underestimate blocking frequency. Although these biases are substantially smaller in the latest climate models of Coupled Model Intercomparison Project Phase 6 (CMIP6) than, for example, in CMIP3, they are still large - especially in the European region and in winter (Davini and D'Andrea 2020).

So far, no climate change related trends were found in the frequency of occurence of blocking events (Barnes et al. 2014). Recently, the ECMWF Re-Analysis Version 5 (ERA5) back-extension was published (Bell et al. 2021). This enables us to investigate trends in blocking frequency and links to extreme events going back to 1950 — especially relevant since models remain biased and a complete dynamical theory of atmospheric blocking is still unavailable.

In this thesis, I aim to investigate the new observation-based ERA5 dataset to find trends in blocking frequency if they exist in the period 1950 – 2019. Furthermore, I aim to relate extreme weather in the Austrian region to atmospheric blocking events over the Northern Hemisphere, in particular over Europe, the North Atlantic and Greenland. Does a relation between these two phenomena exist and if so, where and during which time of the year is it most important?

After a brief overview of the relevant aspects of atmospheric dynamics in chapter 2, weather extremes (in particular heatwaves, cold spells and heavy precipitation) are defined in chapter 3. The datasets methods that were used are explained in chapter 4. Then, the results with regards to trends in blocking frequency trends are shown in chapter 5. Results regarding the connection between blocking frequency and extreme weather are shown in chapter 6. The conclusions are summarized in chapter 7.

2. Relevant Aspects of Atmospheric Dynamics

2.1. Large-Scale Atmospheric Circulation

The atmosphere is a thin gas layer around the Earth, which is a differentially heated, approximately spherical body rotating about its own axis. Because of the latitudinal difference in energy received by the atmosphere from the sun, i.e. the fact that Earth receives more solar energy per unit surface area and unit time near the equator than it does near the poles, the excess energy must be transported from the lower to the higher latitudes. Energy can be transported in three pincipal ways: through radiation, conduction of heat and transport of mass (convection). In the atmosphere, the poleward energy transport is largely due to movement of air from the low latitudes (containing more energy) towards high-latitude regions and simultaneous transport of air from high latitudes (containing less energy) towards regions in lower latitudes. On average, this circulation is organised in three cells, shown in Figure 2.1 and described in more detail in this section. The structure of the large-scale circulation of the atmosphere, including derivation of relevant forces and mechanisms can be found in standard textbooks of atmospheric physics, for example Vallis (2017)

2.1.1. Hadley Cell

Near the equator in the Intertropical Convergence Zone (ITCZ), warm air rises towards the tropopause. It cannot rise further into the stratosphere because of the warming effect caused by the ozone layer and the resulting inversion in the temperature profile, and so it is diverted polewards to the North and South. To preserve the angular momentum of the air mass that is roughly corotating with the surface of the Earth, it experiences a westward force (Coriolis force) as it travels poleward aloft. The Coriolis force is a fictitious force that appears in the non-inertial reference system corotating with the Earth. When the air has cooled sufficiently, it sinks down to the surface again in the subtropics (the well-known aridity of the subtropical climate is in large parts induced by the dry falling branch of the Hadley cell) and then flows back towards the equator. To satify the condition of angular momentum conservation, the Coriolis force again acts on the air mass, this time diverting it to the East. These average eastward surface winds have been known for a long time as *trade winds*, because they were used by trading ships. Because the underlying principle of the Hadley cell is directly tied to thermal

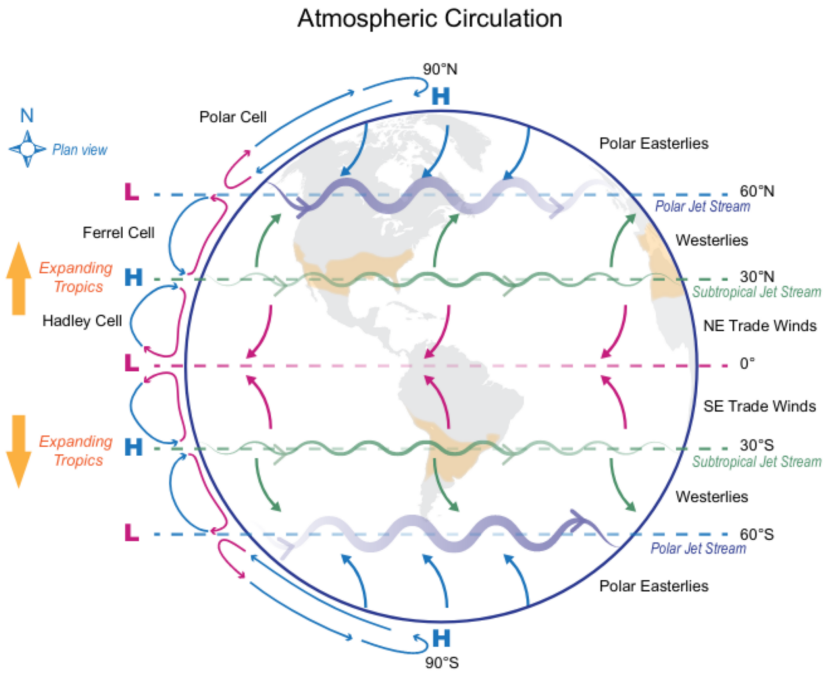


Figure 2.1.: Schematic of the large-scale atmospheric circulation, including the Hadley cell, the Ferrel cell and the Polar cell, showing meridional transport of air, average surface winds and jet streams. Adapted from Perlwitz et al. (2017).

differences between poleward and equatorward air, it is called a *thermally direct* cell.

2.1.2. Polar Cell

The polar cells at high latitudes are thermally direct cells too. Like the Hadley cell, they transport cool air towards the equator at surface level, leading to eastward winds called the *polar easterlies* while transporting warmer air towards the poles aloft. At the poleward end of the polar cell, cool air sinks towards the surface, and at the equatorward end, warmer air rises through convection.

2.1.3. Ferrel Cell

The Ferrel cell is a *thermally indirect* cell connecting the Hadley and the polar cell. Thermally indirect means that, counterintuitively, cool air seems to rise in higher latitudes to be transported equatorward and then sink in the subtropics, returning to the higher latitudes near the surface. The mechanisms behind the Ferrel cell are more complicated than those that drive the thermally direct cells, but conceptually, it is helpful to picture the circulation cells as interlocking cogs

as seen in Figure 2.2, although in reality, the Ferrel cell is driven by mid-latitude eddies and balances the momentum convergence of those eddies (Vallis 2017).

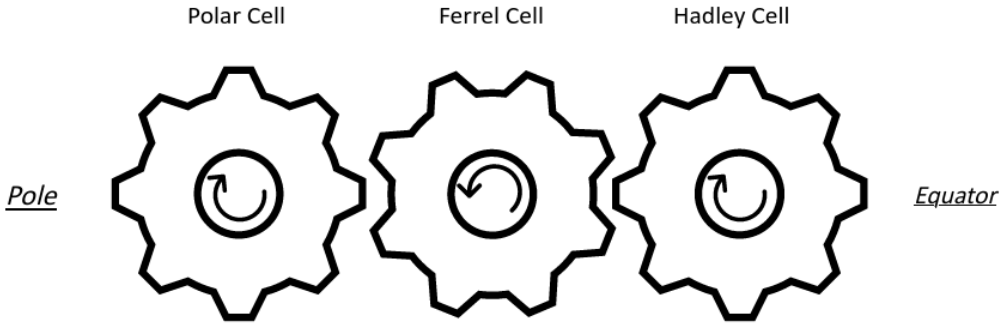


Figure 2.2.: Schematic of the three circulation cells as cogs. In a system of three linearly interconnected cogs, the middle cog must rotate in the opposite sense of the cogs on both edges.

Thus, the average surface winds in the mid-latitudes, where the Ferrel cell lies, are generally directed from the equator towards the poles and from the East to the West. Those winds are often called the *Westerlies*. Because the Ferrel cell is thermally indirect, it is weaker than its thermally direct counterparts, and so are the Westerlies. They are more of a statistical feature that emerges after averaging over time and may be disrupted or even reversed locally and on shorter time scales. For that reason, they are sometimes referred to as the *prevailing* Westerlies.

2.2. Conservative Force Fields

A conservative (or potential, or central) force field is defined as any force field $\vec{F}$ that can be expressed as the gradient field (denoted by the operator $\vec{\nabla}$) of a scalar function Φ (the negative sign is purely conventional):

$$\vec{F} = -\vec{\nabla}\Phi \tag{2.1}$$

The statement made by Equation 2.1 is completely equivalent to the following statements:

- There are no vortices in the force field ($\vec{\nabla} \times \vec{F} = 0$).
- Work done along any closed path within the force field is 0 ($\oint \vec{F} ds = 0$).
- Work done along a path between any points A and B within the force field only depends on A and B.

Not every force field that occurs in nature is a conservative force field — for example, the Coriolis force is not. However, the gravitational force and the centrifugal force are conservative, and can therefore be combined into a total force: Gravity.

2.3. Geopotential Height

Gravity, as used in the context of this thesis, is the vector sum of the gravitational force that the Earth exerts due to its mass and the centrifugal force that everything on its surface (except at the poles) feels due to the rotation of the planet. Since both the gravitational force and the centrifugal force are conservative forces (see section 2.2), one common potential that decribes gravity (the vector sum of both) can be defined as

$$\vec{F_{\mathrm{G}}}(z, \phi) = -\vec{\nabla}\Phi(z, \phi) \tag{2.2}$$

where $\vec{F_{\mathrm{G}}}$ is gravity, $\vec{\nabla}$ is the gradient operator, ϕ is the latitude, z is the altitude and Φ is the potential of gravity (the sum of the potential of the gravitational force and the potential of the centrifugal force), henceforth called *geopotential*. This can be easily inverted:

$$\Phi(\phi, z) = \int_0^z \vec{F_{\mathrm{G}}}(\phi, z')\, dz' \tag{2.3}$$

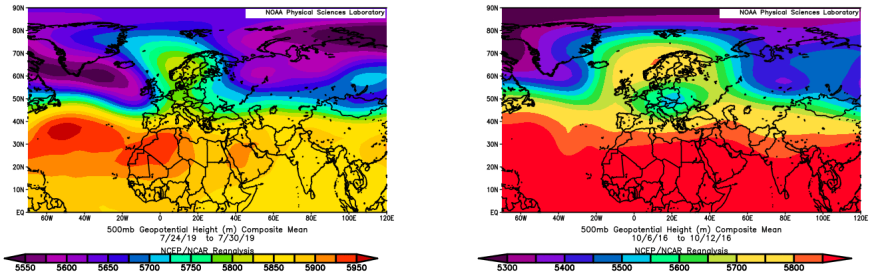
The so called *geopotential height* z_{g} is then obtained by scaling the geopotential to surface gravity g_0. Note that under the assumption that the Earth is a rotational ellipsoid, g_0 is *weakly* dependent on latitude, but otherwise constant.

$$z_{\mathrm{g}}(\phi, z) = \frac{\Phi(\phi, z)}{g_0} \tag{2.4}$$

This normalisation makes the numerical value of geopotential height more similar to that of the corresponding geometric height z and thus more intuitive.

2.4. Pressure Coordinates

In atmospheric science, altitude is often expressed using a vertical pressure coordinate, p. Switching to the pressure coordinate from the standard z coordinate simplifies a number of hydrodynamic equations that are relevant for the behaviour of the atmosphere, such as the mass conservation law and the geostrophic relations and simplifies the process of relating them to observational data, which is often given in a pressure coordinate system. In principle, any physical quantity that has a monotonous relationship with altitude can be used as altitude coordinate, and (thanks to the barometric relationship), that condition is almost universally fulfilled for pressure (Vallis 2017).



(a) Omega blocking **(b)** Rex blocking

Figure 2.3.: Examples of typical blocking situations. Images provided by the NOAA/ESRL Physical Sciences Laboratory, Boulder, Colorado from their Web site at http://psl.noaa.gov/, data from the NCEP reanalysis (Kalnay et al. 1996).

Recalling the geopotential height $z_g(\phi, z)$ from section 2.3, we can now define the partial derivative of $z_g(\phi, z)$ with respect to ϕ along a line of constant pressure (the *latitudinal gradient* along an *isobaric surface*):

$$\left(\frac{\partial z_g(\phi,z)}{\partial \phi}\right)_p = \left(\frac{\partial z_g(\phi,z)}{\partial \phi}\right)_z + \left(\frac{\partial z}{\partial \phi}\right)_p \frac{\partial z_g(\phi,z)}{\partial z} \tag{2.5}$$

2.5. Atmospheric Blocking

The climatological average of the latitudinal gradient of geopotential height on an isobaric surface as defined in Equation 2.5 is positive towards the equator. This reflects the oblateness of the Earth and the slightly stronger gravitational forces at low latitudes, due to which gases in the atmosphere are pulled towards the equator. On any isobaric surface that is sufficiently close to the Earth's surface, a reversal of the geopotential gradient points toward a surface pressure anomaly and can thus be used to detect such events. High (and low) pressure systems (i.e. anomalies in the pressure field compared to the average surface air pressure) are common in the climate system. In special cases, when the position of a high pressure system (and potentially adjacent low pressure systems) is at the right place, the mean westerly flow (see subsection 2.1.3) that prevails in the mid-latitudes can be interrupted, leading to unusually stable large-scale weather patterns — from now on referred to as *atmospheric blocking*.

A typical example of an atmospheric blocking situation is the so called Omega-blocking (Figure 2.3a), where an anticyclone and two cyclones form a system reminiscent of the namesake (uppercase) greek letter.

Another distinctive example is Rex-blocking. Here, a dipole with the cyclone to the South and an anticyclone to the North create the blocking situation with the reversed geopotential height gradient between them (Figure 2.3b). Note the long

time scale of several days over which these examples are averaged, proving how persistent these situations were.

These features share the characteristic that the geopotential height gradient is reversed, i.e. that geopotential height locally increases towards the poles instead of decreasing like the climatological average. It is this characteristic that is used to detect pressure anomalies and by extent atmospheric blocking, as described in section 4.2.

3. Extreme Temperature and Precipitation

The IPCC classifies extreme weather events as "a pattern of extreme weather that is rare at a particular place and time of year" (IPCC 2013). This definition also carries over to the 6th assessment report of the IPCC (IPCC 2021). Most well known are patterns where the intensity of an event is significantly different from the typical situation, but in principle any characteristic of a weather pattern can be unusual enough to classify it as an extreme event. For example, instead of unusual intensities, extreme events may be distinguished by an abnormal duration or size.

Many different meteorological conditions can be classified as extreme weather situations. Prominent examples are heatwaves and cold spells, but also extreme precipitation — these are also the three extremes that this thesis investigates in the context of atmospheric blocking.

3.1. Heatwaves

Broadly speaking, a heatwave is any meteorological situation in which temperatures are significantly higher than the climatological temperature in a given region, at a given time of the year. There is no general consensus of how much higher temperatures have to be, compared to the climatology, to constitute a heatwave, or how long the temperature anomaly has to persist (although there is a general consensus that it should be more than one day) — but it should at least be clear that any reasonable definition of a heatwave must take into account the location and time of the year at which the temperature anomaly occurs (Perkins and Alexander 2013).

There is a clear connection between heatwaves and excess mortality. For example (and especially relevant for this thesis), Hutter et al. (2007) found a significant effect on excess mortality of elderly humans in Vienna, and similar studies can be found for different regions of the world. Importantly, they also found reason to believe that this excess mortality was predominantly not the result of sick people whose death was inevitable within a few days and only accelerated by the effects of the heatwaves. Similarly, the World Health Organization (WHO) warns of direct (heat illness, accelerated death from diseases) and indirect (health service, risk of accidents, increased illness transmission, disruption of infrastructure) effects of extreme heat (World Health Organization 2018). Miller et al. (2021) demonstrated that heatwaves have a negative impact on the economic output of nations in

the agricultural sector, and an impact on overall economic output if they are particularly long or severe.

3.2. Cold Spells

Cold spells (also called cold waves or cold snaps) are the opposite of heatwaves. They are periods of unusally low temperatures in a certain region — but like with heatwaves, there is no general consensus of how much lower temperatures have to be, or for how many days that situation has to persist. Of course, it is reasonable to assess such thresholds regionally and dependent on the time of the year as well. Like heatwaves, cold spells are associated with an excess mortality in human populations. For example, Kyselý et al. (2011) found excess cardiovascular mortality connected to cold spells in the Czech Republic. In contrast to heatwaves, the excess mortality occured up to 13 days after the cold spell, and affected middle-aged people more than the elderly. They also found a less pronounced difference between excess mortality in males and females, reporting a much larger excess mortality for females than for males in the case of heatwaves, but not during (or after) cold spells.

Another study by deDonato et al. (2013) likewise found an excess mortality in Italian cities, but states that those who are 75 years old or older suffered the highest relative increase in excess deaths. This leads to the conclusion that the data is insufficient to make statements as to which age group suffers the most from cold spells in terms of health, but that it is clear nevertheless that there is an adverse effect on mortality overall.

In addition, extreme cold in spring regularly leads to economic damage for example for the agricultural sector in Austria, but also in other regions, therefore contributing to income variability and associated risks for farmers. One example of an exploration of potential future risks was conducted by Unterberger et al. (2018), who concluded that an advance of apple blooming towards early April could put orchards at an additional risk from blocking-related cold spells.

3.3. Extreme Precipitation

Europe was recently reminded of the potentially grim consequences of severe rainfall and flooding events when Western Europe was hit by the storm system “Bernd”, resulting in more than 180 people dead and more than 40000 affected in Germany alone on July 14th and 15th, 2021. In economic terms, more than 7 billion Euros in insurance losses were caused, most of which to residential buildings, household goods and businesses. Damages to critical infrastructure like bridges, railway routes and hospitals were reported as well (Fekete and Sandholz 2021). It is worth noting that “Bernd” was part of a severe blocking system, which does not come as a surprise: Blocking has been connected to thunderstorms during the warm season over Western and Central Europe (Mohr et al. 2019).

A notorious example of extreme precipitation in Austria occurred in June, 2009. Between June 22nd and June 25th, over 100 mm of precipitation were measured in Lower Austria, Upper Austria and Salzburg as well as Southeastern Styria and Southern Burgenland. The cause behind this torrential rainfall was a stationary low pressure system in the area. After June 25th, rainfall events kept occuring on more regional scales for almost a week (Haiden 2009). As a direct consequence of this event, about 1700 private damage reports were filed at the Styrian state government, mostly due to landslides — and indeed Styria has not nearly experienced as many landslides since 1966 (Hornich and Adelwöhrer 2010). Again, it should be pointed out that atmospheric blocking was detected over Europe starting on June 24th and lasting until June 29th, 2009 (Figure 3.1).

High precipitation periods can be assessed by creating individual thresholds for each grid point and day of the year, depending on the distribution of precipitation typical for that time and place. More difficulties remain regarding the detection and classification of periods of very little precipitation (i.e. droughts). Indeed, several different types of drought are known to literature, including the Intergovernmental Panel on Climate Change (IPCC): meteorological droughts, characterized by meteorological variables such as precipitation and temperature; agricultural droughts characterized by variables more directly connected to plant growth, such as soil moisture; and hydrological droughts, characterized by variables regarding bodies of water, such as inflow to water reservoirs (IPCC 2021).

Even if one restricts the definition of a drought to periods of low precipitation, the thresholds, as calculated for example for cold spells in the case of temperature, is useless for in the case of low precipitation. The skewness of the probability density function of daily rainfall amount means that in many places, the threshold would simply turn out to be 0. Because there is no such thing as negative precipitation, it would be impossible to ever go below that threshold. Indeed, severe droughts tend to last longer than blocking events, and establishing a connection between these two kinds of events is therefore not an easy task. For this reason, this thesis considers heavy precipitation events, but not droughts.

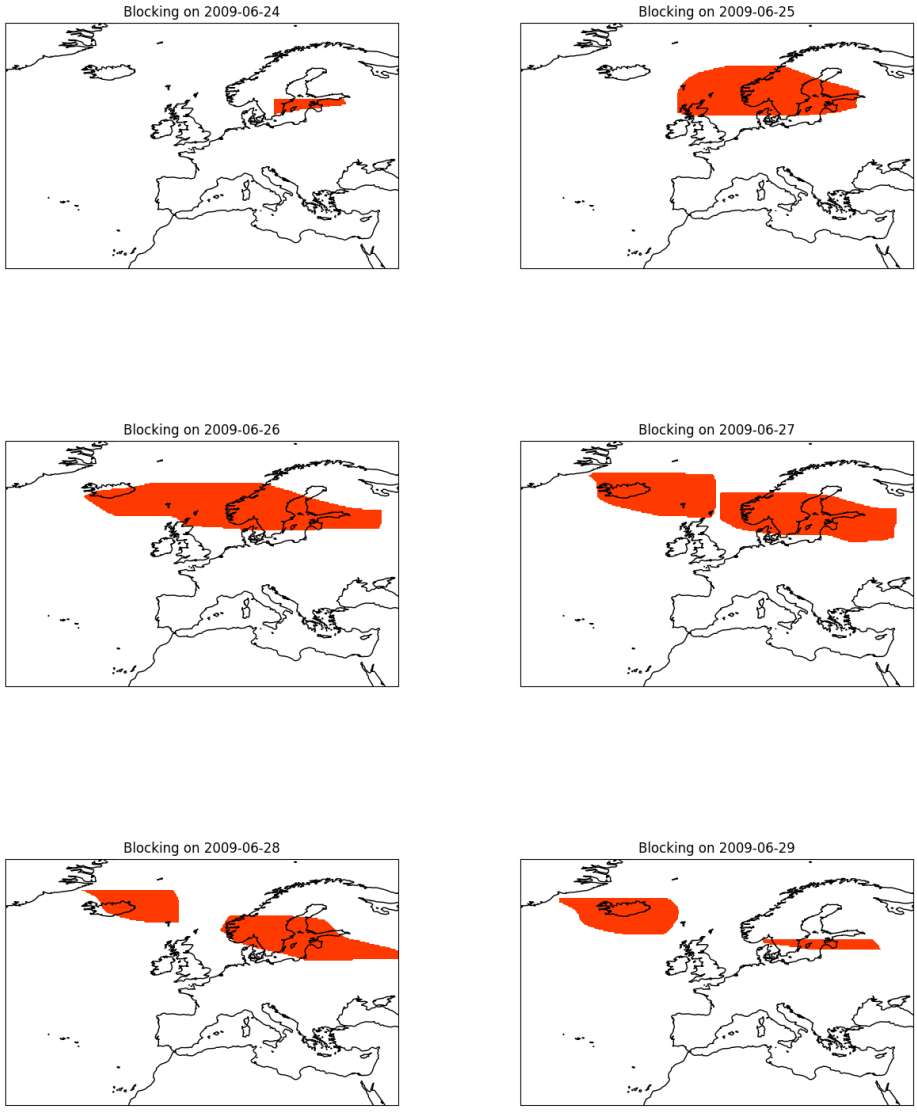


Figure 3.1.: Blocking situation between June 24th and June 29th, 2009. Shown in red are the grid points that are blocked on a given day. This period also coincides with severe rainfall in Austria, further motivating the investigation of the relationship between extreme rainfall in Austria and blocking events in Europe.

4. Data and Methods

4.1. Data

4.1.1. Reanalyses

Although a lot of observational data is available for the recent past to analyze weather and climate, the sites of those measurements are far from distributed equally across the globe. Naturally, surface stations tend to be on land, rather than over the ocean, and ocean-based observations are mainly restricted to common marine traffic routes. Satellite based measurements can suffer from limitations from the number of satellites in orbit.

Reanalyses close the resulting gaps in the data by combining the observational data and digital models, a process called *data assimilation* by the European Centre for Medium-Range Weather Forecasts (ECMWF). These datasets are produced by feeding the available observational data into a short-term weather forecasting system, although at a lower resolution than weather forecasts usually have. The outcome are 'maps without gaps': globally complete, consistent datasets (ECMWF 2020). However, it is important to keep in mind that different observing systems and assimilated data can introduce inhomogeneities over time — reanalyses are not infallible.

4.1.2. ERA5

To investigate the trends in blocking frequency across the Northern hemisphere as well as for the detection of heatwaves and coldspells in Austria, the ECMWF Re-Analysis Version 5 (ERA5) dataset (doi: 10.24381/cds.bd0915c6) on a 0.25° x 0.25° grid resolution was used, including the extension back to 1950 (Bell et al. 2021), yielding a total time coverage of 1950 – 2019.

ERA5 is a reanalysis (subsection 4.1.1) produced by ECMWF, the successor to ECMWF Re-Analysis Interim (ERA-Interim). Including the extension, it covers the time period from 1950 – present on a grid resolution of 31 km with 137 vertical levels up to the 0.01 hPa surface (section 2.4) and an hourly temporal resolution. A detailed description of the advantages of ERA5 over ERA-Interim and other previous renanalyses was given by Hersbach et al. (2020).

4.1.3. WFDE5

Applying the WATCH Forcing Data (WFD) method to ERA5 data, Cucchi et al. (2020) produced the WFDE5 dataset (doi: 10.24381/cds.20d54e34), a bias-adjusted

ERA5 based dataset specifically designed for impact studies. They found that this bias correction led to little improvement of the performance against surface observations compared to the ERA5 data. However, they did find improved agreement with observations concerning the global hydrological balance, leading to improvements towards observations in several regions including the Danube basin relative to the ERA5 data. For this reason, the WFDE5 dataset was chosen to assess high precipitation events in Austria.

4.2. Methods

4.2.1. Blocking Detection and Trend Estimation

For blocking detection, an algorithm published by Brunner et al. (2018) using a three-gradient blocking index was applied to the 500 hPa surface (section 2.4). These three gradient criteria follow the works of Davini et al. (2012) and Brunner and Steiner (2017) detecting a geopotential height gradient reversal (Equation 4.4 & Equation 4.5) while at the same time excluding low-latitude ridges (Equation 4.6). These low latitude ridges do not qualify as atmospheric blocking as they do not interrupt the westerly mean flow, but would be detected by the algorithm without the third criterion (Equation 4.6).

With $\Delta\phi = 10°lat$, the first gradient (Equation 4.1, corresponding to criterion Equation 4.4) at every grid point is computed by taking its geopotential height and subtracting it from the geopotential height of the grid point 10 degrees to the north, then dividing the result by 10 degrees. Similarly, the second gradient (Equation 4.2, corresponding to criterion Equation 4.5) is computed by subtracting the geopotential height of the grid point 10 degrees to the south, then dividing again by 10 degrees. Finally, the third gradient (Equation 4.3, corresponding to criterion Equation 4.6) is calculated by subtracting the geopotential height of the grid point 10 degrees to the south from the grid point 20 degrees to the south, then again dividing by 10 degrees. Note that for the southern hemisphere, one would have to subtract the geopotential height of grid point 10 degrees to the north from the one of the grid point 20 degrees to the north, but in this thesis, only blocking in the northern hemisphere is considered.

$$\Delta z_g^{(N)}(\lambda, \phi) := \frac{z_g(\lambda, \phi + \Delta\phi) - z_g(\lambda, \phi)}{\Delta\phi} \tag{4.1}$$

$$\Delta z_g^{(S)}(\lambda, \phi) := \frac{z_g(\lambda, \phi - \Delta\phi) - z_g(\lambda, \phi)}{\Delta\phi} \tag{4.2}$$

$$\Delta z_g^{(E)}(\lambda, \phi) := \frac{z_g(\lambda, \phi - 2 * \Delta\phi) - z_g(\lambda, \phi - \Delta\phi)}{\Delta\phi} \tag{4.3}$$

The superscripts (N), (S) and (E) describe the northward, southward and equatorward direction, respectively.

For a grid cell to be considered instantaneously blocked at a certain day, the following conditions must be satisfied:

$$\Delta z_g^{(N)} < -10 \frac{m}{^\circ lat} \tag{4.4}$$

$$\Delta z_g^{(S)} > 0 \frac{m}{^\circ lat} \tag{4.5}$$

$$\Delta z_g^{(E)} > 5 \frac{m}{^\circ lat} \tag{4.6}$$

Whenever these criteria are fulfilled for a given grid point, it is considered *instantaneously blocked* (IBs). We consider only IBs with an extent of at least 15° longitude (*extended instantaneous blocking*), and we further require that extended IB is present at the grid point for at least 3 consecutive days (*blocking*) (Brunner et al. 2018).

Subsequently each longitude was considered blocked at any given day if at least one grid point along this longitude was blocked (in the sense of extended blocking that persists for at least 3 consecutive days) at that day.

The blocking frequency for each month and each gridpoint is defined as:

$$BF = \frac{B}{D} \tag{4.7}$$

where B is the number of blocked days in a given month and D is the total number of days in that month.

Then, for all longitudes, blocking frequency was averaged over 30 years each, taking 5 year steps — i.e. , taking the 1950 – 1979 average for each longitude, then the 1955 – 1984 average and so on. This operation was carried out separately for each month of the year.

For each of those longitudes and for each month of the year, using an ordinary linear regression model, trends were computed and their statistical significance was assessed. The results are displayed in section 5.1.

To develop a deeper and more detailed understanding of these trends, they were then reassessed for each grid cell separately. Blocking frequency was averaged over each year from 1950 – 1978 (extension period) and 1979 – 2019 (time period of the original ERA5 data) and trends were detected using a linear regression model. Again, these trends were tested for statistical significance, as shown in section 5.2.

4.2.2. Extreme Weather Detection

To detect heatwaves in Austria, each gridpoint was assigned a temperature threshold. Following Russo et al. (2015), that threshold is defined for each gridpoint and each day of the year seperately by constructing the distributions of daily maximum (minimum) temperature on a given gridpoint, taking into account a window of ± 15 days around the day of the year, then taking the 90th (10th) percentile for the heatwave (cold spell) threshold. Whenever temperatures at a gridpoint fall

Table 4.1.: Definition of the Austrian region.

	lower	*upper*
longitude	9.75°	16.75°
latitude	46.75°	48.75°

above (below) these thresholds for three consecutive days, the gridpoint is said to experience a heatwave (cold spell).

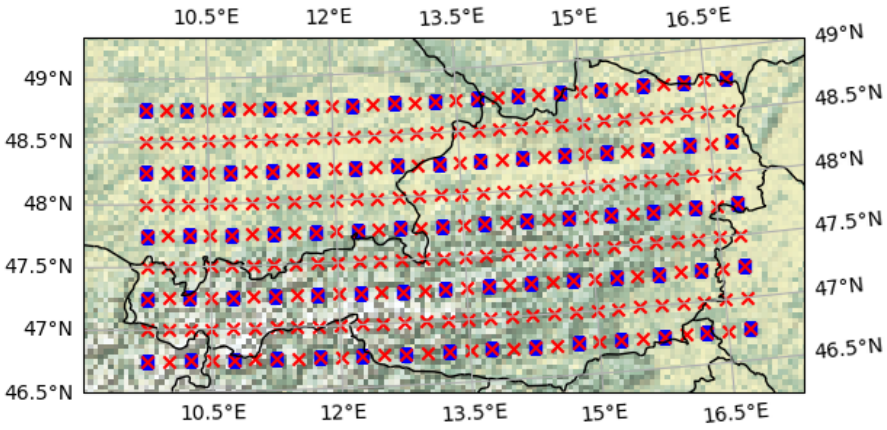


Figure 4.1.: Grid points investigated for extreme temperature (red crosses) and extreme precipitation (blue squares) in the Austrian region.

We define a heatwave (cold spell) to be experienced in Austria whenever at least one gridpoint of a 0.25° x 0.25° grid within the region defined in Table 4.1 experiences a heatwave (cold spell). The grid points within this region are shown in Figure 4.1.

High precipitation detection is conducted in a similar way. Whenever hourly accumulated rainfall exceeds the 90th percentile of the distribution of maximum hourly accumulated rainfall for a given gridpoint at a given day of the year $\pm$ 15 days, the Austrian region is considered to be experiencing a heavy precipitation event. However, days with no precipitation are not taken into account when calculating the maximum hourly accumulated rainfall distribution to reduce the skewness.

4.2.3. Blocking Frequency Anomaly during Extreme Temperature and Precipitation Days in Austria

For each gridpoint, the blocking frequency (see Equation 4.7) was subtracted from the blocking frequency during heatwaves / coldspells / high precipitation days, calculated analogously:

$$BF_{\text{anom, HW}} = \frac{B_{\text{HW}}}{D_{\text{HW}}} - BF \tag{4.8}$$

$$BF_{\text{anom, CS}} = \frac{B_{\text{CS}}}{D_{\text{CS}}} - BF \tag{4.9}$$

$$BF_{\text{anom, HP}} = \frac{B_{\text{HP}}}{D_{\text{HP}}} - BF \tag{4.10}$$

where B_{HW} / B_{CS} / B_{HP} are the number of blocked days where a heatwave / coldspell / high precipitation day in Austria (as defined in subsection 4.2.2) occurred and D_{HW} / D_{CS} / D_{HP} are the total number of days where a heatwave / coldspell / high precipitation day in Austria occurred.

Statistical significance was established by applying a Monte-Carlo method. 500 random subsamples were drawn, each comprised of the same number of days as the subsample of days where a particular extreme weather type occurred in Austria. If the blocking frequency anomaly of the subsample of days associated with a particular type of extreme weather in Austria (Equation 4.8 to Equation 4.10) exceeded the 95th percentile of the 500 blocking frequency anomalies as calculated from the 500 random subsamples on any given grid point, it is significantly positive on that grid point. Likewise, if it is lower than the 5th percentile of the 500 blocking frequency anomalies of the random subsamples, it is significantly negative.

4.2.4. Extreme Weather Frequency Anomaly during Blocking days in the Northern Midlatitudes

Likewise, we then calculated the frequency at which each investigated type of extreme weather occurs in Austria for each grid point of the Austrian region (Table 4.1, Figure 4.1):

$$HWF = \frac{HW}{D} \tag{4.11}$$

$$CSF = \frac{CS}{D} \tag{4.12}$$

$$HPF = \frac{HP}{D} \tag{4.13}$$

HWF, CSF and HPF denote heatwave frequency, cold spell frequency and heavy precipitation frequency of a grid point. HW, CS and HP denote the number

of days on which heatwaves, cold spells and heavy precipitation occurred on that grid point and D denotes the overall number of days.

We then calculated each of the extreme weather frequencies from the subsample of days where blocking occurred over regions where a significant relationship between extreme events and blocking frequency had already been established (subsection 4.2.3). We did this for (a) regions where blocking frequency was significantly *higher* on days where heatwaves / cold spells / heavy precipitation occurred in Austria and (b) regions where blocking frequency was significantly *lower* on days where heatwaves / cold spells / heavy precipitation occurred in Austria. We then compared these subsample extreme weather frequencies to the overall extreme weather frequencies:

$$HWF_{\text{anom}} = \frac{HW_{\text{B}}}{D_{\text{B}}} - HWF \tag{4.14}$$

$$CSF_{\text{anom}} = \frac{CS_{\text{B}}}{D_{\text{B}}} - CSF \tag{4.15}$$

$$HPF_{\text{anom}} = \frac{HP_{\text{B}}}{D_{\text{B}}} - HPF \tag{4.16}$$

For each grid point, HW_{B}, CS_{B} and HP_{B} denote the number of days where heatwaves / cold spells / heavy precipitation occurred in Austria and blocking was present over the aforementioned regions where the relationship was already established, and D_{B} denotes the overall days where blocking was present over these regions.

To determine statistical significance, we again applied the Monte-Carlo method, this time drawing 5000 subsamples (due to the lower amount of grid points in the Austrian region as compared to the entire northern midlatitudes, it was possible to draw more subsamples without exceeding computational resource limits). If the heatwave / cold spell / heavy precipitation frequency anomaly of the subsample of days associated with blocking occurrence over a region with an established connection to that kind of extreme weather occurrence in Austria (Equation 4.14 to Equation 4.16) exceeded the 95th percentile of the 5000 blocking frequency anomalies as calculated from the 5000 random subsamples on any given grid point, it is significantly positive on that grid point. Likewise, if it is lower than the 5th percentile of the 5000 blocking frequency anomalies of the random subsamples, it is significantly negative.

5. Blocking Trends

5.1. Blocking Trends, resolved in Longitude

In this section, we show blocking frequencies (30-year-periods, shifted by 5 years each; Figure 5.1 & Figure 5.2, upper panels) and trends in blocking frequency for the period 1950 – 2019 (Figure 5.1 & Figure 5.2, lower panels) as a function of longitude. In general, increased blocking frequency is detected over the North Atlantic and European regions and over the North Pacific region. Blocking frequency reaches roughly 15 % to 20 % in both regions in winter and spring, depending on the month. In June, blocking frequency reaches 25 % over the North Pacific and 10 % to 15 % over the North Atlantic and Europe; In July, the Pacific blocking frequency is on the order of 15 % to 20 % and the North Atlantic peak is shifted towards the Eurasian continent, reaching blocking frequencies of roughly 15 % to 20 % as well. From August to November, blocking frequency generally remains below 15 % for both regions.

The average blocking frequency over the decades reveals that the sign and the strength of changes in blocking frequency vary across longitude, month and time. For these figures, the maps in the background serve only for orientation regarding longitude.

In December, a decrease of blocking frequency over the Ural region (−1 %/decade between 30°E and 80°E) can be observed, as well as an even stronger decrease over the Pacific (up to −2 %/decade). Blocking frequency over the Atlantic and the European longitudes has largely remained the same over the whole investigated period (Figure 5.1a).

In January, blocking frequency significantly declined from roughly 10°W to 100°W (up to −2.5 %/decade) and from 130°E to 160°E (up to −1.5 %/decade). There are barely any longitudes for which a significant increase in blocking frequency was found (Figure 5.1b).

In February, a marked decline in blocking frequency of up to −2.5 %/decade is apparent from 10°E to 70°W as well as between 40°E and 180°E (up to −2.5 %/decade), meaning that blocking frequency has decreased at almost all longitudes. Like in January, there are no longitudes at which the blocking frequency has increased in a significant way (Figure 5.1c).

In March, the picture is a bit more complicated than first meets the eye. There is a clear downward trend of up to −2.5 %/decade in blocking over the investigated period as a whole from about 20°W to 70°W. To the East of that range, roughly over Europe and the British Isles, this is also true from the period 1950 – 1979 to 1965 – 1994. However, after that, blocking frequency has started to increase

again. These effects counter each other - as a result, in Figure 5.1d no significant trend can be seen in this region, but the standard errors are large in comparison to other longitudes. The opposite is true for the region from 20°E to 80°E, where blocking frequency increased in the first period, then decreased again in the second, amounting to no significant trend with a large standard error. Over the Pacific Ocean, blocking frequency increased significantly by up to 2 %/decade.

In April, a decline in blocking frequency between roughly 40°W and 70°W is observed (up to −2 %/decade). Additionally, there was an increase in blocking frequency of up to 1 %/decade in the Ural region, from 20°E to 40°E, and a slight increase of up to 1 %/decade, intermittently statistically significant, in the in the Pacific region (Figure 5.1e).

Also in May, the blocking frequency decreased around 40°W (up to −1 %/decade). There is also a decrease in blocking frequency of up to −2 %/decade over large parts of the Pacific region (Figure 5.1f). There was virtually no change in blocking frequency over the European region.

In June, the highest blocking frequencies of any month appear: More than 25 % of blocked days over the Pacific ocean. Looking at the trends, June also features the strongest trends of any month of up to 4 %/decade increase for 100°E to 150°E. There are also increases in blocking frequency (2 %/decade) around 40°W, as opposed to the first five months of the year, where blocking frequency decreased in this region. As in March, in the European region, it does not suffice to look only at the overall trends in the lower subpanel of (Figure 5.2a). During the periods 1950 – 1979 up to 1965 – 1994, blocking frequency increased, but it has been decreasing again since the 1970 – 1999 period up until the most recent period (1990 – 2019).

In July, no prominent changes in blocking frequency are apparent, except a slight decrease (1955 – 1984 to 1980 – 2009) and then increase (1980 – 2009 to 1990 – 2019) over Europe / Ural longitudes and an increase of up to 1 %/decade over the Greenland longitudes (Figure 5.2b).

In August, blocking rates are generally lower than in most other months, and the changes are subtle. While there are significant downward trends over large ranges of longitude (mostly between 0° and 140°E), they are not very strong (generally between about −0.5 %/decade to −1 %/decade), leading from an already low blocking frequency to one that is even lower, albeit only slightly (Figure 5.2c).

In September, blocking frequency over the Europe / Ural longitudes increases by up to 2 %/decade. A significant increase in blocking frequency of up to slightly above 1 %/decade can also be observed over North America (Figure 5.2d).

In October, blocking frequency peaked at European longitudes. However, this is no longer the case, due to a continuous downward trend of up to −1.5 %/decade in this region since the 1980s. Meanwhile, blocking frequency has increased over the Pacific longitudes and the Ural longitudes with a trend of up to about 1 %/decade (Figure 5.2e).

In November, blocking frequencies are, in general, rather low and not many changes have taken place over the recent decades. Most noteworthy is perhaps a

slight increase in blocking frequency of about 1 %/decade over the Pacific ocean on the Asian side (Figure 5.2f) and over the West Greenland longitudes.

Overall, we observe a decrease in blocking frequency of 2 %/decade to 3 %/decade in the North Atlantic region around 40°W. In June and July, we find an increase over the North Atlantic region of 1 %/decade to 2 %/decade, as well as a very prominent increase of 4 %/decade over eastern Asia in June. In September, there is a prominent increase of blocking frequency of roughly 2 %/decade over Europe.

5.2. Blocking Trends, resolved in 2 Dimensions

A more detailed overview of changes in blocking frequency that occurred since 1950 can be obtained by calculating this trend for each grid cell separately, i.e. by resolving these trends both in latitude and in longitude. The the mean blocking frequency was calculated for each year and each grid cell (note that the data was regridded to a 1.0°x1.0° grid to save computational resources) for each month of the year. The blocking frequency trends are shown for each month from December to November for two periods, 1950 – 1978 and 1979 – 2019, in Figure 5.3, Figure 5.4, Figure 5.5 and Figure 5.6.

The magnitude and sign of the trends in blocking frequency are highly variable in time and space. For many months in many regions, the trend direction is different for the periods 1950 – 1978 compared to 1979 – 2019. Trend directions and magnitudes are in general regionally very different. In some cases (see e.g. Figure 5.3b, 1950 – 1978 over Europe) an upward trend is accompanied by a downward trend to the north or vice versa, while in other regions, the regions with opposite trends are instead longitudinal neighbours. Thus, changes in blocking frequency typically represent spatial shifts rather than global overall increases or decreases.

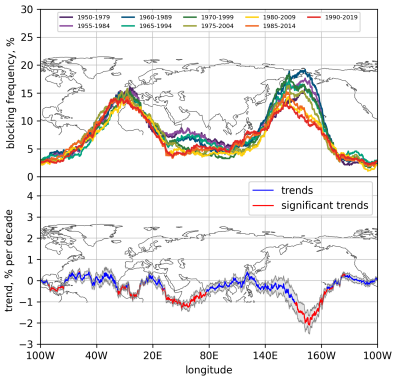
Focussing on recent trends (i.e. the 1979 – 2019 period) in the European region, there is a general decrease of up to −2 %/decade in blocking frequency over Scandinavia in February and an increase of up to 2 %/decade over the British Isles in March, of up to 2 %/decade over Scandinavia in September. A decrease of up to −3 %/decade over southern Greenland and the North Atlantic in November and no otherwise significant trends in the region during the other months are found. Note that 1 %/decade is to be interpreted as a change of 1 percentage point per decade in this context.

The period that is covered by the ECMWF Re-Analysis Version 5 (ERA5) extension (1950 – 1978) shows a very different picture, with increasing trends in blocking frequency of up to 3 %/decade over the North Atlantic, Greenland and the Pacific in December. In February, a downward trend (up to −3 %/decade) over Northern Russia and an upward trend over the North Atlantic (up to 3 %/decade) are present. In March, blocking frequency is decreasing by up to −3 %/decade over Northern Europe, and in April, it increases by up to 3 %/decade over Europe, Britain and the Atlantic. There is also an increase by up to 3 %/decade over

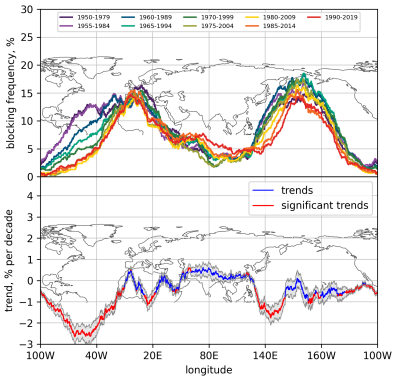
Scandinavia in June, and the same over the Pacific in July and August. In November, there is a decrease in blocking frequency of up to $-3\,\%$/decade over the British Isles.

These results demonstrate that while the longitudinal resolution of the trends (section 5.1) is suitable to provide a good overview, the details are more complicated and can only be seen in a two-dimensional view.

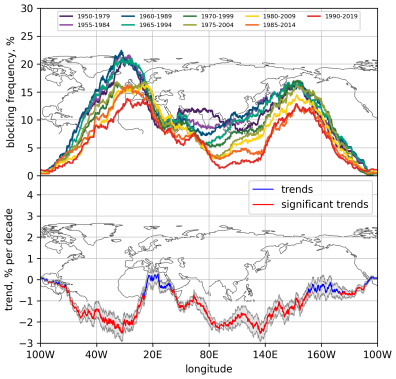
The ERA5 reanalysis data shows no clear general trends except in a few select regions, namely Scandinavia, the British Isles, Greenland, the North Atlantic and the North Pacific. Therefore, no clear global long-term trend in blocking frequency could be demonstrated to exist based on this observation-based data.



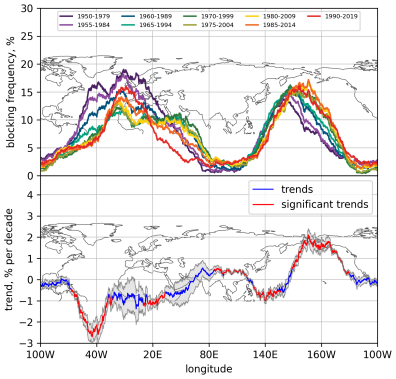
(a) December



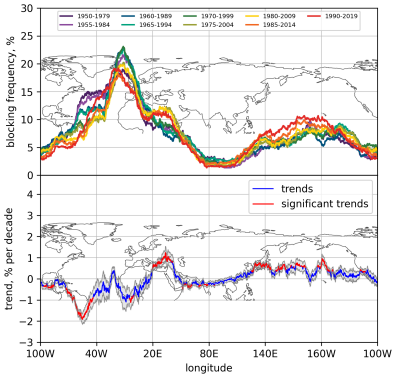
(b) January



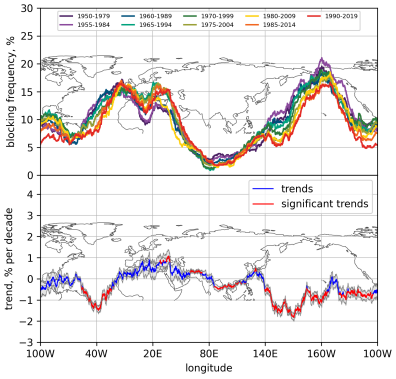
(c) February



(d) March

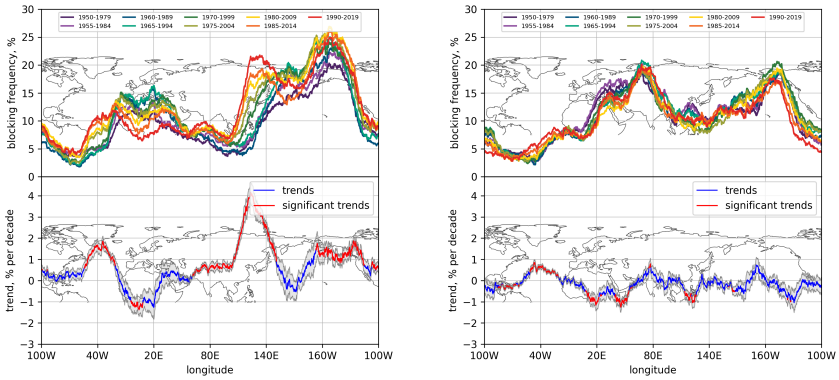


(e) April

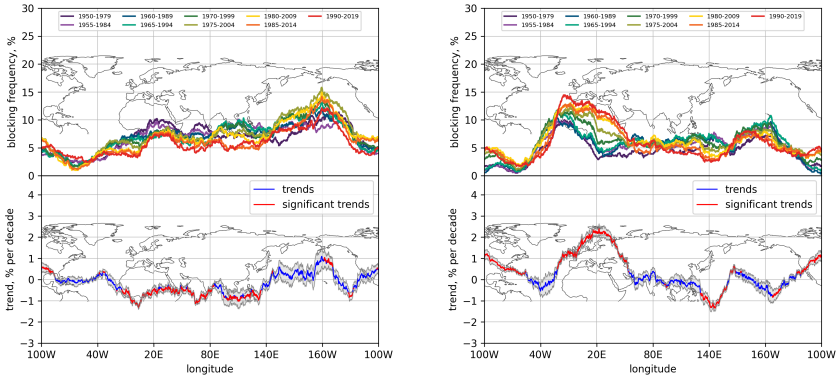


(f) May

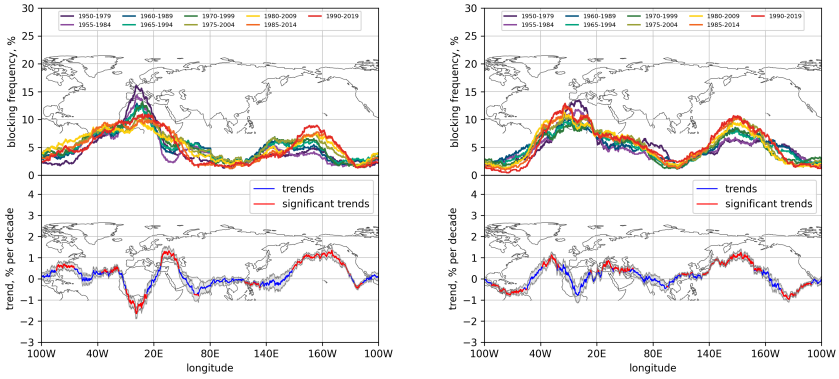
Figure 5.1.: Blocking frequency and trends from December to May (a-f). The upper subpanels show the 30-year average blocking frequency for different periods, shifted by 5 years each. The lower subpanels show the trends in blocking frequency. The grey corridor marks the standard error of the trend slope. Significant trends are shown in red (p = 0.05).



(a) June **(b)** July

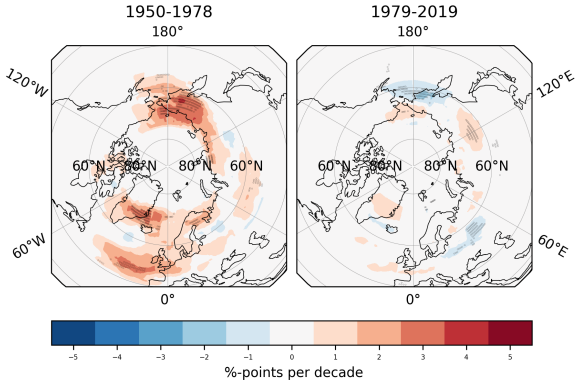


(c) August **(d)** September

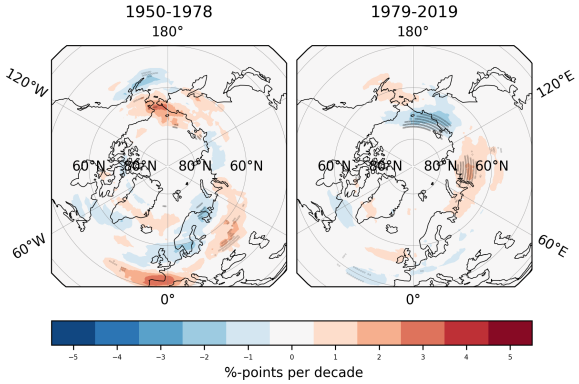


(e) October **(f)** November

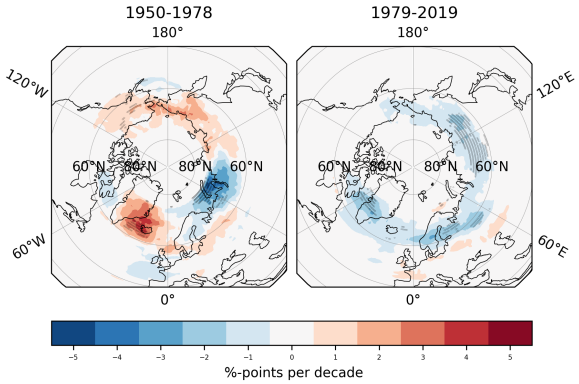
Figure 5.2.: Blocking frequency and trends from June to November (a-f). The upper subpanels show the 30-year average blocking frequency for different periods, shifted by 5 years each. The lower subpanels show the trends in blocking frequency. The grey corridor marks the standard error of the trend slope. Significant trends are shown in red (p = 0.05).



(a) December

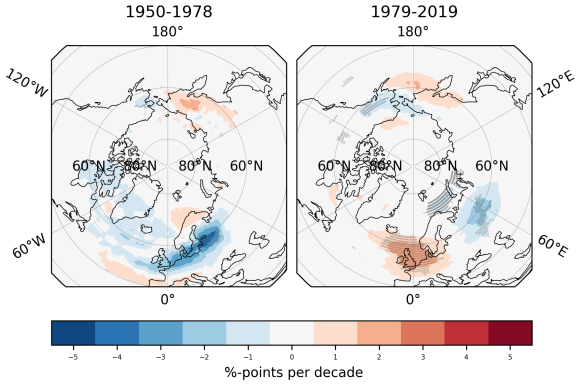


(b) January

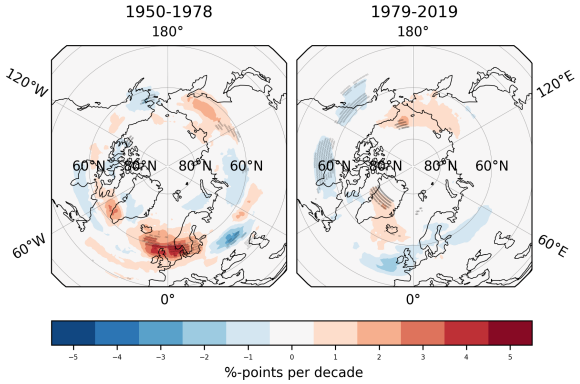


(c) February

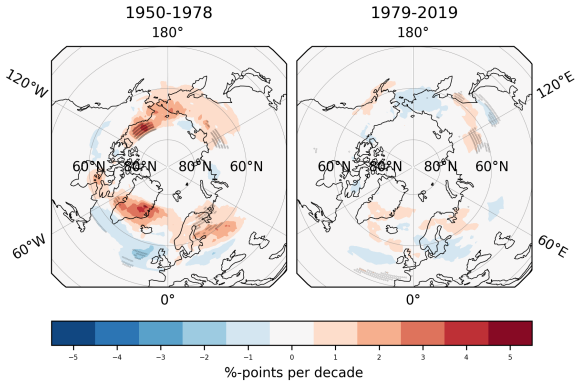
Figure 5.3.: Blocking frequency trends during winter months (2-dim). Dark crosses mark grid points for which the trend is statistically significant.



(a) March

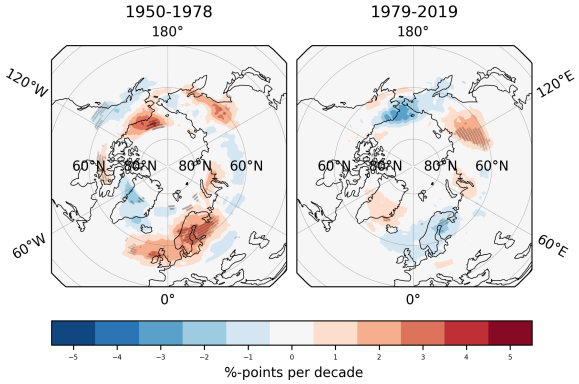


(b) April

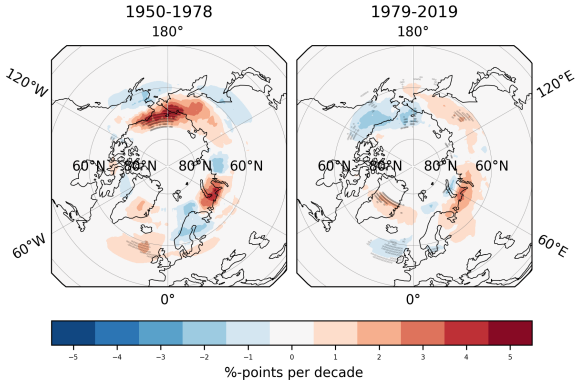


(c) May

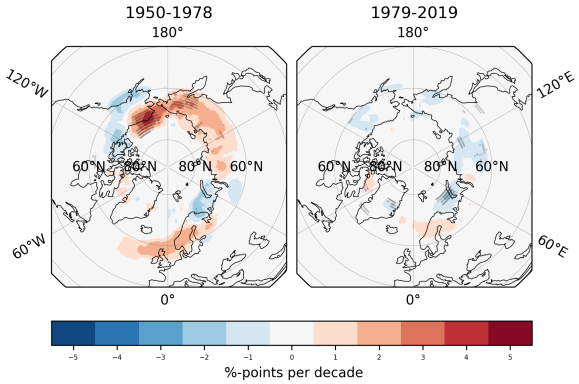
Figure 5.4.: Blocking frequency trends during spring months (2-dim). Dark crosses mark grid points for which the trend is statistically significant.



(a) June

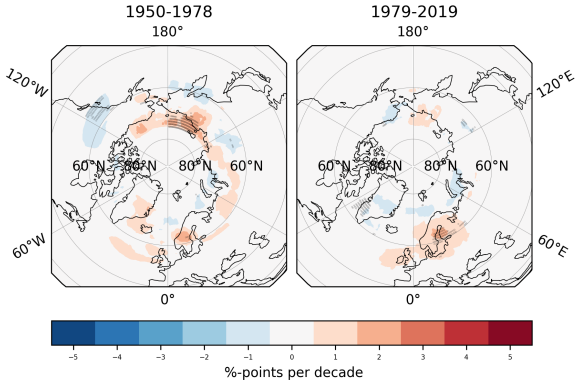


(b) July

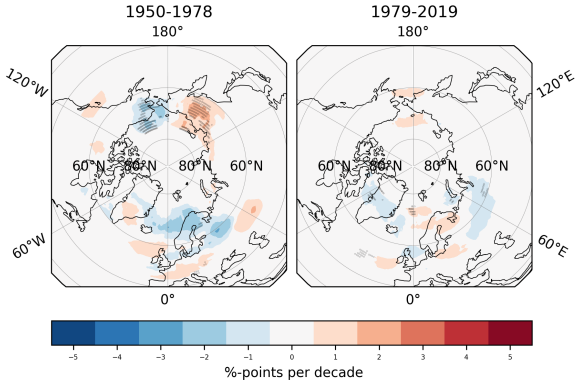


(c) August

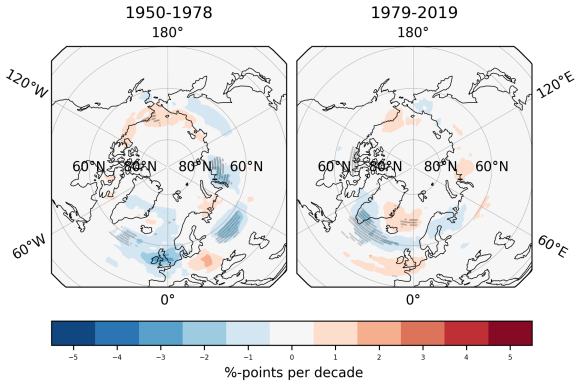
Figure 5.5.: Blocking frequency trends during summer months (2-dim). Dark crosses mark grid points for which the trend is statistically significant.



(a) September



(b) October



(c) November

Figure 5.6.: Blocking frequency trends during autumn months (2-dim). Dark crosses mark grid points for which the trend is statistically significant.

6. Blocking and Extreme Weather in Austria

6.1. Blocking and Extreme Weather Climatologies

The following sections investigate blocking occurrence in the Northern midlatitudes and potential links to extreme events in the Austrian region. All frequency anomalies were computed with respect to the overall average heatwave / cold spell / heavy precipitation / blocking frequency in the period 1980 – 2018, which is the longest common time period for all data sources at the time the calculations were conducted.

In this section, these climatologies are presented for comparison to the anomalies in the following sections. Note the different scale for heatwaves / cold spells and high precipitation.

During this period, each grid point was blocked on up to 3 % of days on average, with the highest blocking frequencies occurring over southern Scandinavia, the northern British Isles and midwestern Greenland. Each grid point was blocked up to 4 % of MJJASO days, with the highest blocking frequencies occurring over midwestern Greenland and southern Finland, and up to 4 % in NDJFMA and DJFM, respectively, with the highest blocking frequencies occurring over southern Scandinavia and the British Isles. The summer/autumn analogue to the DJFM period, JJAS, is not shown here and in the following sections because no interesting results could be found for this period (Figure 6.1).

Heatwaves occurred with a frequency of 4 % to 6 % on each grid point, with the highest frequencies occurring in the south, in western Carinthia. Each grid point experienced heatwaves 4 % to 6 % of MJJASO days, the maximum frequencies occurred in the south in parts of Carinthia and East Tyrol. Heatwaves occurred on 4 % to 5 % of NDJFMA days, with the higher frequencies generally tending to occur in the southwestern parts of Austria, and on 4 % to 6 % of DJFM days, where the highest frequencies again occurred in the south over western Carinthia (Figure 6.2).

Cold spells occurred on roughly 5 % of days across most regions of Austria. They occurred on 4 % to 5 % of MJJASO days, with the higher cold spell frequencies concentrated in the southwest (Carinthia and Tyrol). Cold spells occurred on 5 % to 7 % of NDJFMA days, with higher cold spell frequencies occurring in the north, and on 5 % to 7 % of DJFM days, with higher cold spell frequencies occurring in an even larger area of northern Austria compared to the whole NDJFMA period. The

lowest cold spell frequencies occur in the southwest (Tyrol) for both the NDJFMA and the DJFM periods (Figure 6.3).

High precipitation occurred on roughly 0.5 % of days across most of Austria. It occurred on up to roughly 0.5 % of MJJASO days, with higher frequencies of high precipitation located to the southwest (Tyrol, Carinthia, southern Salzburg, northwestern Styria) as well as to the far northeast in northeastern Lower Austria and Vienna. Grid points experienced high precipitation on up to roughly 1 % of NDJFMA days, the highest high precipitation frequencies were found to the west (Vorarlberg, Tyrol, western Upper Austria). They were blocked on up to 2 % of DJFM days, with the highest high precipitation frequencies found to the west (Vorarlberg, Tyrol, Salzburg, western Upper Austria).

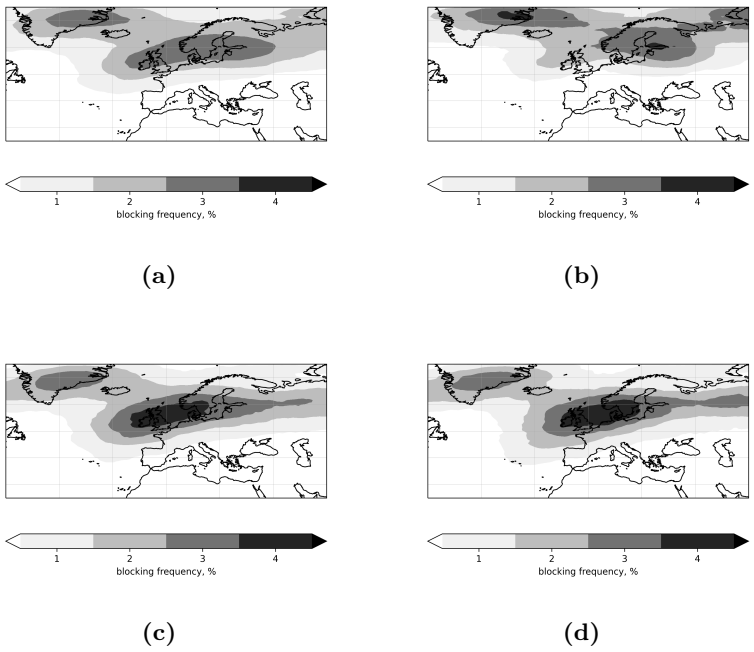


Figure 6.1.: Average blocking frequency over Europe, Greenland and the North Atlantic, calculated for the period 1980 – 2018, for (a) all year, (b) MJJASO, (c) NDJFMA and (d) DJFM.

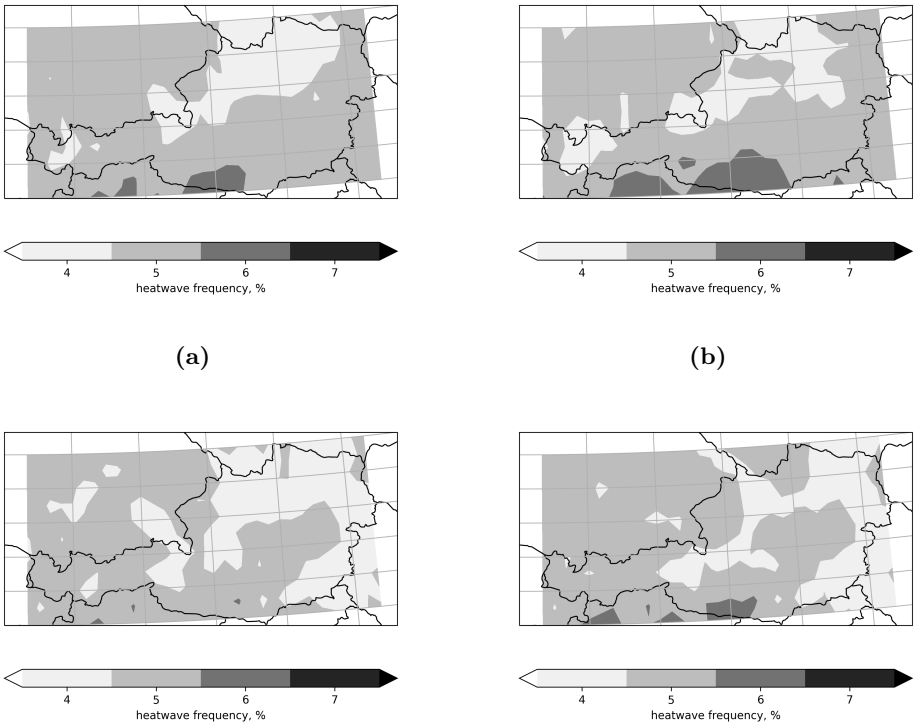


Figure 6.2.: Average heatwave frequency in Austria, calculated for the period 1980 – 2018, for (a) all year, (b) MJJASO, (c) NDJFMA and (d) DJFM.

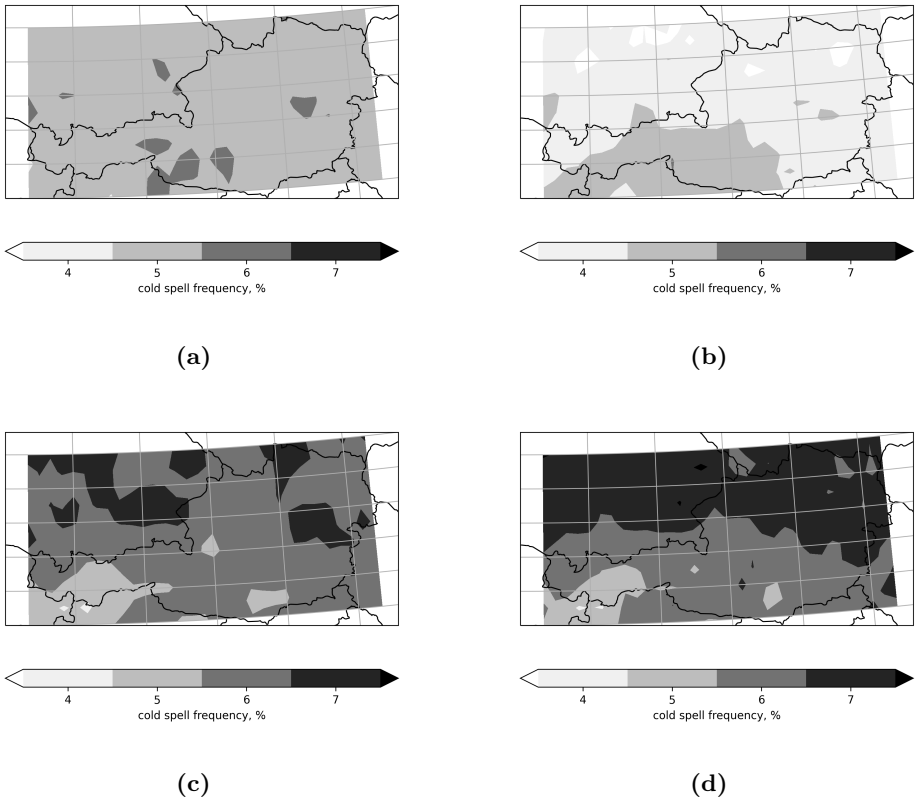


Figure 6.3.: Average cold spell frequency in Austria, calculated for the period 1980 – 2018, for (a) all year, (b) MJJASO, (c) NDJFMA and (d) DJFM.

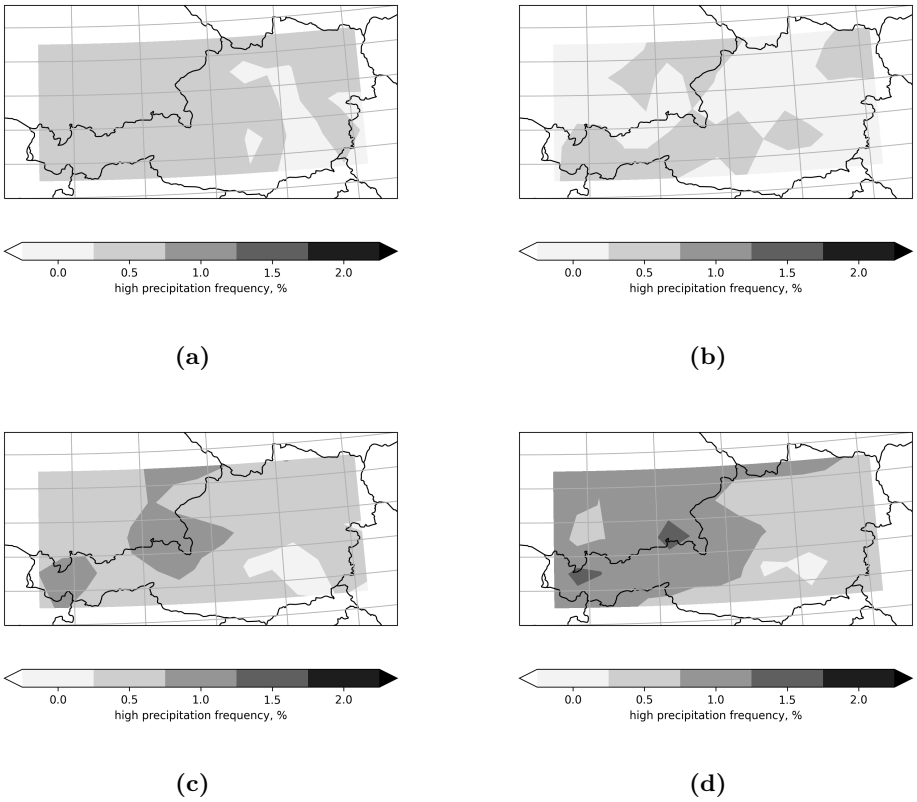


Figure 6.4.: Average high precipitation frequency in Austria, calculated for the period 1980 – 2018, for (a) all year, (b) MJJASO, (c) NDJFMA and (d) DJFM.

6.2. Blocking and Heatwaves in Austria

The blocking frequency anomaly in the subsample of days where a heatwave occurred in Austria shows a clear dipolar structure. On heatwave days in Austria, blocking occurs more frequently over Central Europe while it occurs less frequently over Northern Europe, especially Scandinavia (Figure 6.5a).

Heatwaves occur more frequently in the north and southwest of Austria on days where blocking occurs over Central Europe (Figure 6.5b). On the other hand, heatwaves occur less frequently in all of Austria when blocking occurs over Greenland and Northern Europe (Figure 6.5c). Generally, the positive heatwave frequency anomaly in Austria can be explained by the effect of radiative heating in the affected regions during blocking situations. Clear skies are a known feature of high pressure systems, and the sun will heat up a region under persistent clear skies more readily than other regions. The negative heatwave frequency anomaly is likely a result of the advection of cold air, which limits the possibility of heatwave development — the same mechanism that likely drives the positive cold spell frequency anomaly during blocking over Northern Europe (section 6.3).

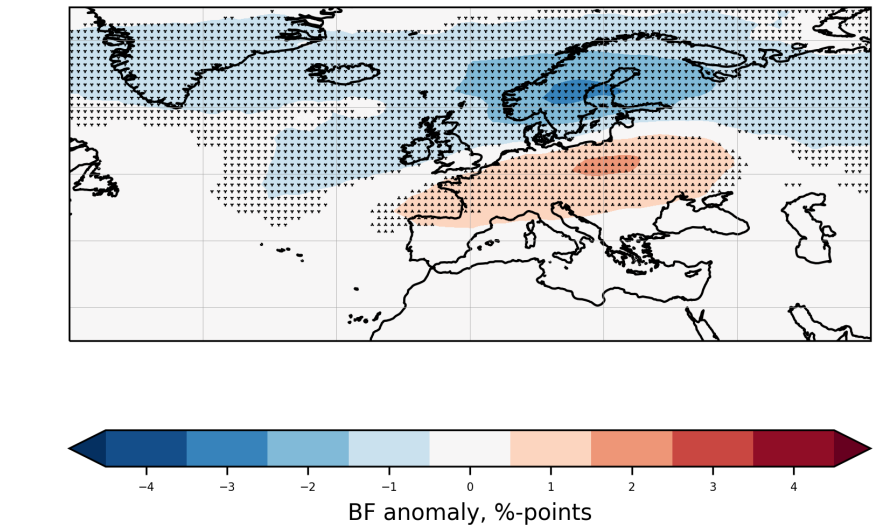
In the warmer half of the year (i.e. the months MJJASO), there is also a dipolar blocking frequency anomaly with the negative part over Greenland and Northern Europe. The positive part of this anomaly lies over Eastern Europe (Figure 6.6a).

The positive heatwave frequency anomaly associated with blocking over Eastern Europe is concentrated in the north and northeast of Austria (Figure 6.6b). The negative heatwave frequency anomaly associated with blocking over the British Isles, Greenland and Northern Europe is present over all of Austria, but seems to be weaker in the southwest (the municipalities of Tyrol and Vorarlberg; Figure 6.6c).

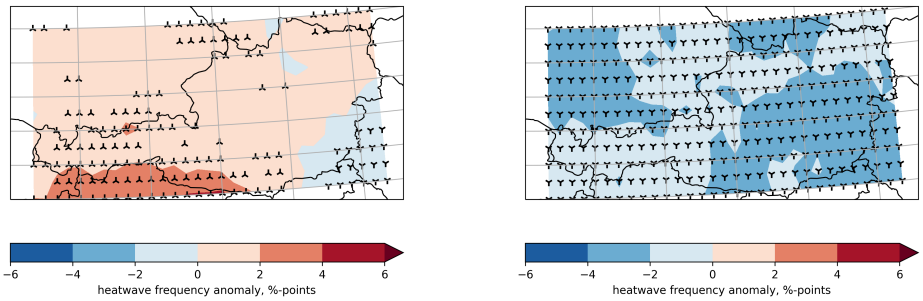
Looking at the colder half of the year (i.e. the months NDJFMA), a similar kind of dipolar blocking frequency structure is observed with a negative blocking frequency anomaly from Greenland over the North Atlantic to Northern Europe, peaking over Scandinavia, and a positive blocking frequency anomaly over Central Europe (Figure 6.7a).

On days where blocking occurs over the Central European region, there is a positive heatwave frequency anomaly over the southwest of Austria. It is even more pronounced as when considering the entire year (Figure 6.7b). On days where blocking occurs over Greenland and over Northern Europe, there is a negative heatwave frequency anomaly over all of Austria, i.e. less heatwaves than on average. (Figure 6.7c).

Special attention is paid to the extended winter season (i.e. the months DJFM), because early prolonged heatwaves my induce preliminary onset growth of crops, thus rendering them particularly vulnerable. Again, on days where heatwaves occur in Austria, blocking frequency in Greenland, the British Isles and Scandinavia is significantly decreased while the blocking frequency over Central Europe is significantly increased. On days where blocking occurs over Greenland, the British Isles and Scandinavia, heatwave frequency all over Austria is significantly decreased by -2 to -4 percentage points. On days where blocking occurs over Central Europe,

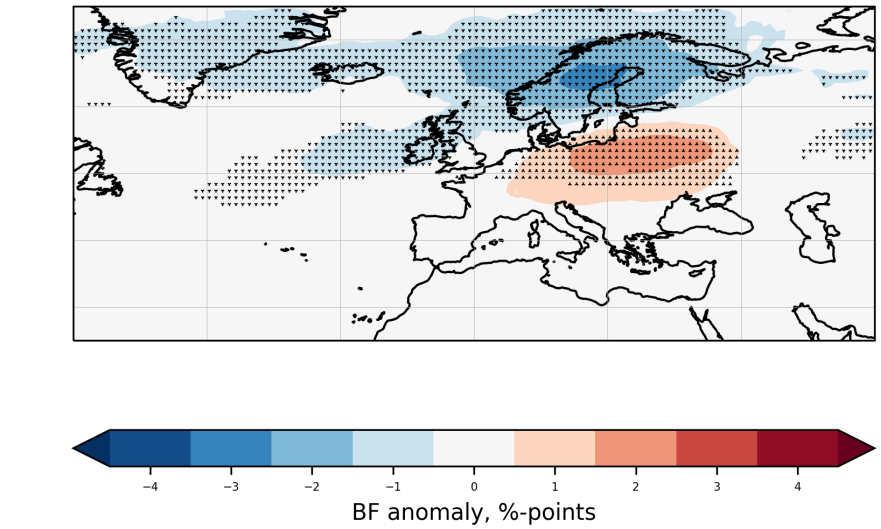


(a)

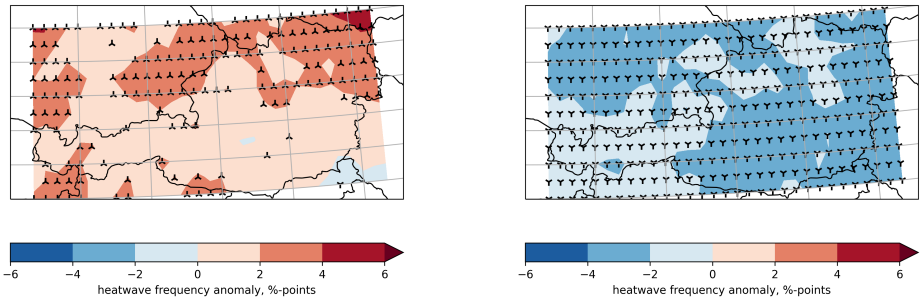


(b) **(c)**

Figure 6.5.: Blocking over the northern midlatitudes and heatwave frequency in Austria during the 1980 – 2018 period. (a) shows the blocking frequency anomaly in percentage points on days where at least one grid point in Austria is experiencing a heatwave. Marked black are the grid points for which this relationship is statistically significant. (b) shows the heatwave frequency anomaly in percentage points in Austria on days where at least 10 percent of the grid points marked as significantly positive in (a) are blocked. (c) shows the heatwave anomaly on days where at least 10 percent of the grid points marked as significantly negative in (a) are blocked.

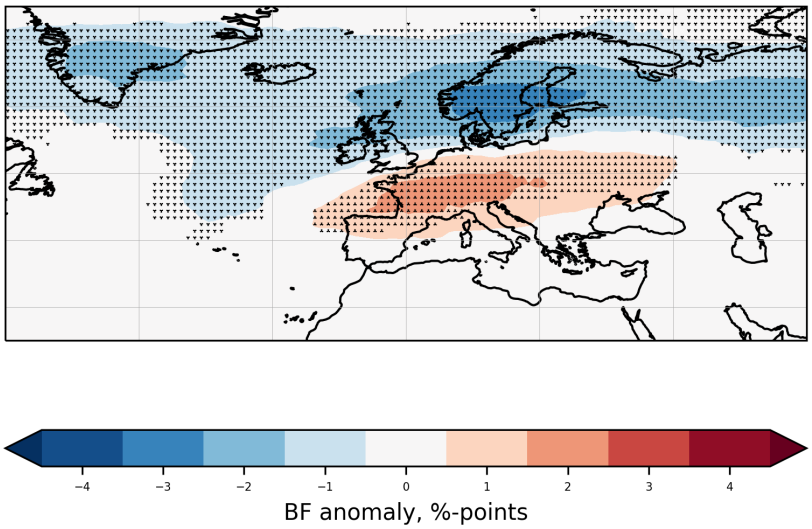


(a)

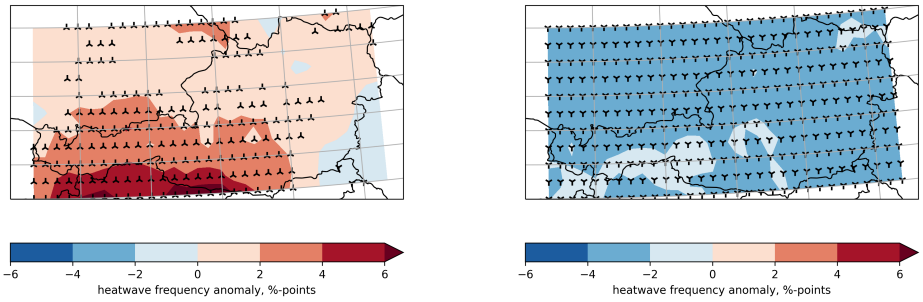


(b) (c)

Figure 6.6.: Blocking frequency over the northern midlatitudes and heatwave frequency in Austria for MJJASO (1980 – 2018). Same layout as Figure 6.5.

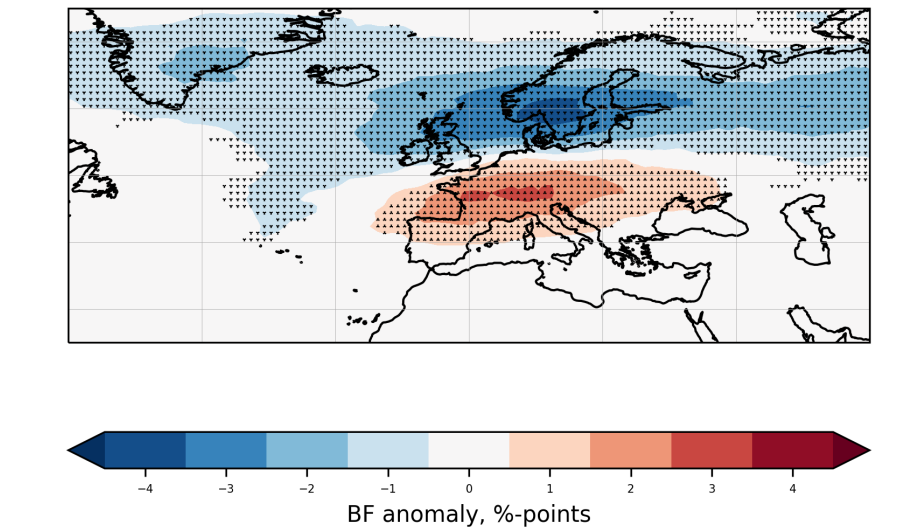


(a)

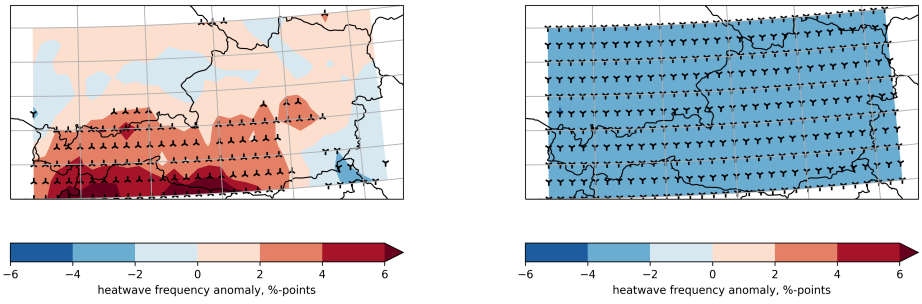


(b) **(c)**

Figure 6.7.: Blocking frequency over the northern midlatitudes and heatwave frequency in Austria for NDJFMA (1980 – 2018). Same layout as Figure 6.5.



(a)



(b) (c)

Figure 6.8.: Blocking frequency over the northern midlatitudes and heatwave frequency in Austria for DJFM (1980 – 2018). Same layout as Figure 6.5.

heatwave frequency is significantly increased by up to 6 percentage points or more in southwestern Austria.

Links between blocking and heatwave frequency were investigated for each month separately as well. These results can be found in Appendix B (Figure B.1 to Figure B.12).

6.3. Blocking and Cold Spells in Austria

On the subset of days where cold spells occur in Austria, there is a significantly positive blocking frequency anomaly (compared to the blocking frequency climatology) over Greenland, the North Atlantic and Northern Europe — especially pronounced over the British Isles and Scandinavia. This is consistent with cold air advection from the North as discussed for example by Bieli et al. (2015), Pfahl (2014), Sousa et al. (2017) and Brunner et al. (2018) (see Figure 6.9a). On the other hand, on days where blocking occurs over this Northern European region, cold spell frequency is significantly increased in all of Austria (Figure 6.9b). There is a weak negative blocking frequency anomaly over mideastern Greenland and Eastern Europe on days where cold spells occur in Austria. On the subset of days where blocking occurs in this region, cold spell frequency is slightly decreased all over Austria (Figure 6.9c).

In the warmer half of the year, the situation is different. There is a positive blocking frequency anomaly over Scandinavia during days where cold spells occur in Austria, with more cold spells than on average occurring in the northeast to southeast of Austria on days where blocking occurs in this region. There is, however, a negative blocking frequency anomaly in the northeast of Europe. This dipolar feature does not occur in the yearly average (Figure 6.9a) and in the colder half of the year (Figure 6.11a) respectively. Note that blocking in this region is conductive to heatwave development in summer (Figure 6.6a); this is consistent with inhibition of cold spell development.

For the colder half of the year NDJFMA (Figure 6.11), the picture is similar as for the whole year (Figure 6.9). There is a positive blocking frequency anomaly over Northern Europe (especially over the British Isles and Scandinavia) on cold spell days in Austria, even stronger than when the whole year is considered (Figure 6.11a). The positive cold spell frequency anomaly in Austria on days where blocking occurs in these region reaches between 4 and 6 percentage points in most of Austria. (Figure 6.11b). There is a negative blocking frequency anomaly over mideastern Greenland and Eastern Europe on days where cold spells occur in Austria (Figure 6.11a). The negative cold spell frequency anomaly on days where blocking occurs is between 2 to 4 percentage points in several regions of Austria. (Figure 6.11c).

Again, special attention is given to the extended winter period where crops may be especially vulnerable to cold spells, since this is the period of growth onset for many kinds of crops. The positive blocking frequency anomaly in this period is especially strong, reaching up to 4 percentage points over the British Isles, the North and Baltic Sea and southern Scandinavia (Figure 6.12a). The subsample of days where this region is blocked is associated with an increase in cold spells of up to more than 6 percentage points than on average in some regions of Austria (Figure 6.12b). On the other hand, blocking frequency is significantly decreased over the northern part of the Iberian peninsula and to the west of Greenland. The subsample of days where these regions are blocked is associated with a decrease in

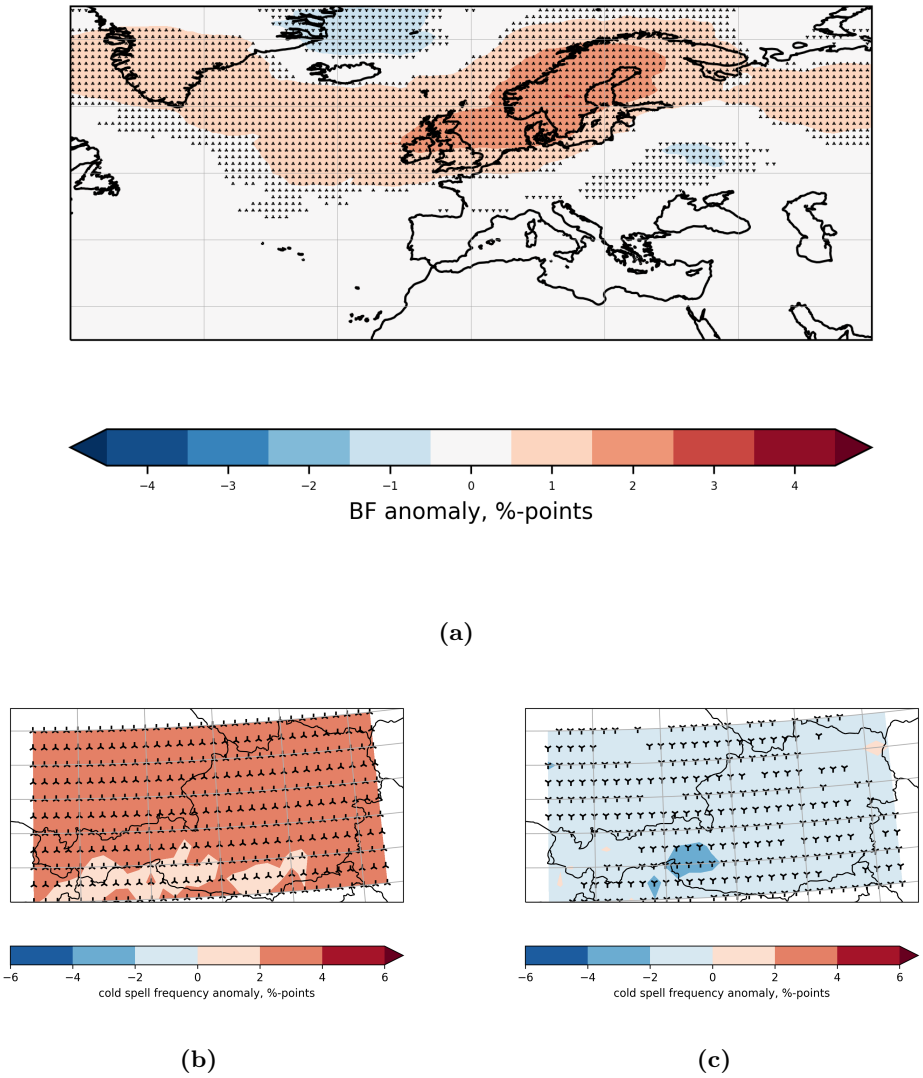


Figure 6.9.: Blocking over the northern midlatitudes and cold spell frequency in Austria during the 1980 – 2018 period. (a) shows the blocking frequency anomaly in percentage points on days where at least one grid point in Austria is experiencing a cold spell. Marked black are the grid points for which this relationship is statistically significant. (b) shows the cold spell frequency anomaly in percentage points in Austria on days where at least 10 percent of the points marked as significantly positive in (a) are blocked. (c) shows the cold spell anomaly on days where at least 10 percent of the grid points marked as significantly negative in (a) are blocked.

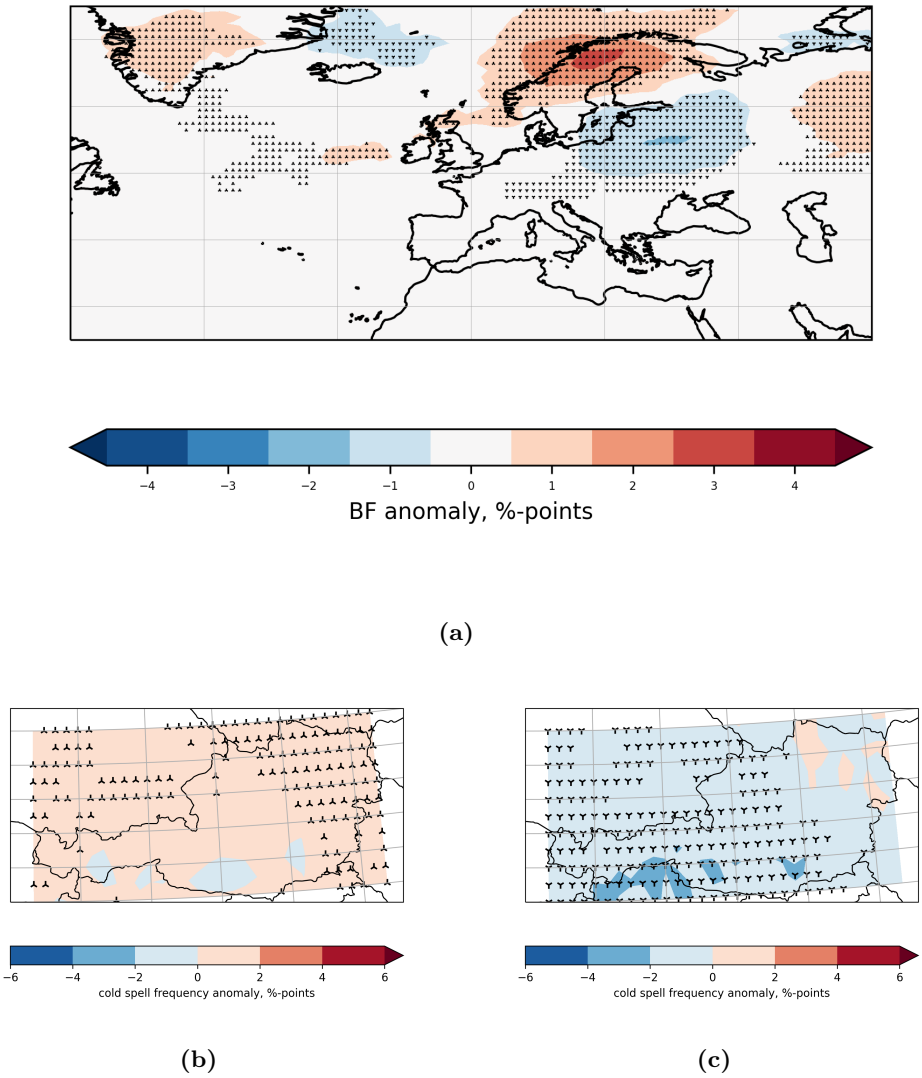
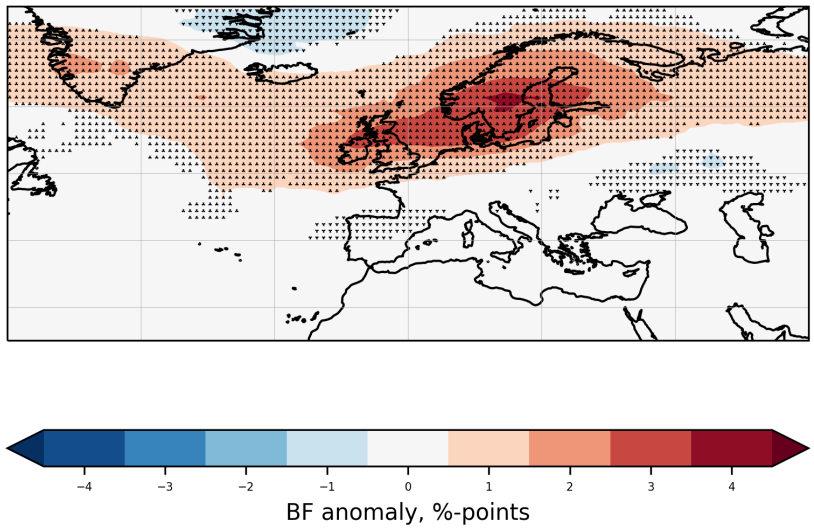


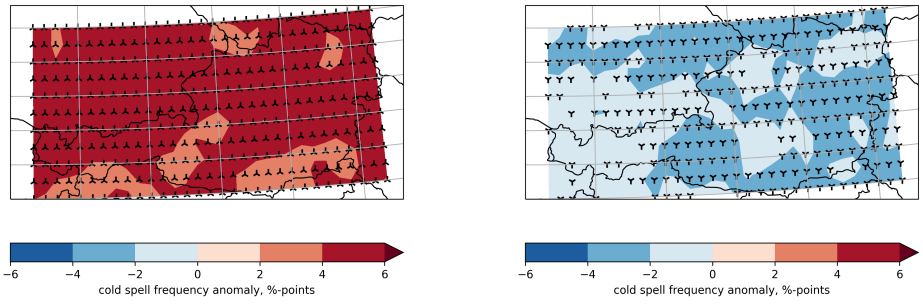
Figure 6.10.: Blocking frequency over the northern midlatitudes and cold spell frequency in Austria for MJJASO (1980 – 2018). Same layout as Figure 6.9.

cold spell frequency across Austria (Figure 6.12c), although not quite as strong as the positive anomaly of Figure 6.12b.

Links between blocking and cold spell frequency were investigated for each month separately as well. These results can be found in Appendix B (Figure B.13 to Figure B.24).



(a)



(b) **(c)**

Figure 6.11.: Blocking frequency over the northern midlatitudes and cold spell frequency in Austria for NDJFMA (1980 – 2018). Same layout as Figure 6.9.

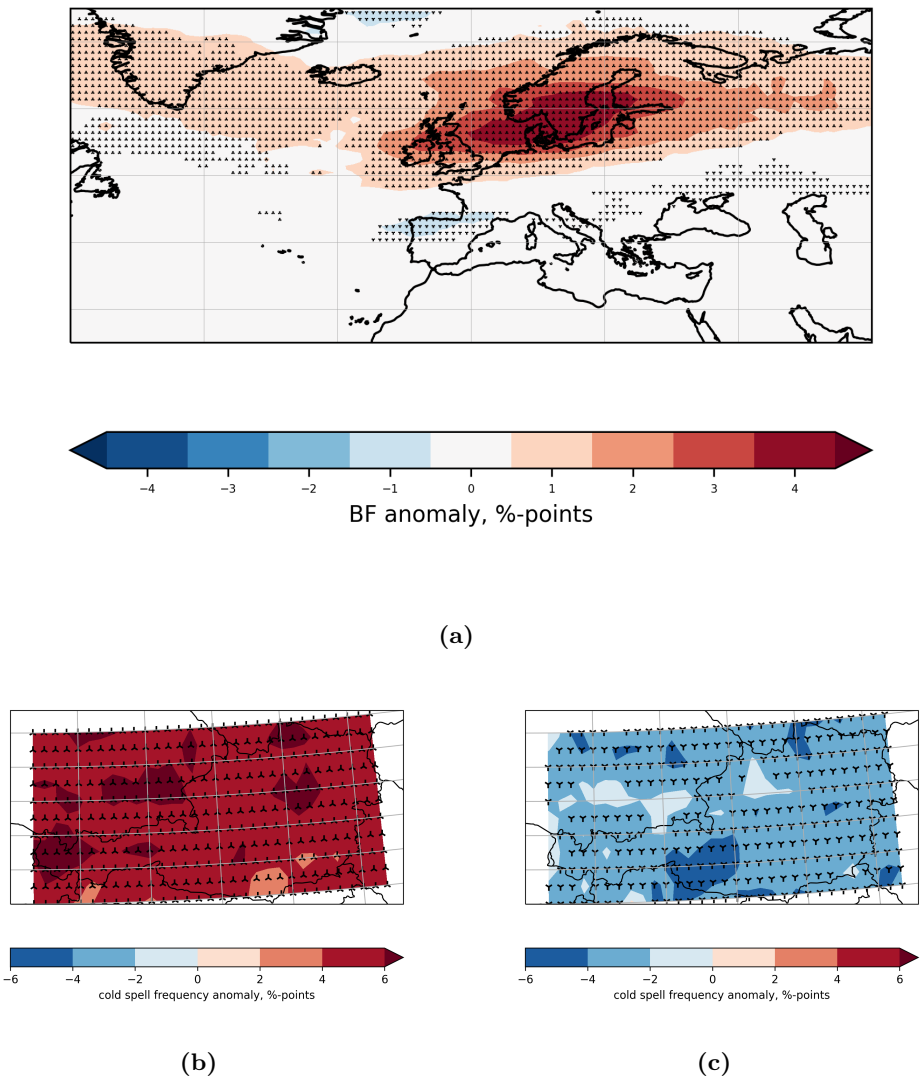


Figure 6.12.: Blocking frequency over the northern midlatitudes and cold spell frequency in Austria for DJFM (1980 – 2018). Same layout as Figure 6.9.

6.4. Blocking and High Precipitation in Austria

On the subset of days where high precipitation occurs in Austria, there is a negative blocking frequency anomaly observed over the British Isles and the North Sea area. Weaker negative blocking frequency anomalies also reside over Iceland and Finland, whereas a positive blocking frequency anomaly on this subset of days can be found over Russia, and a weaker one over parts of Norway and the Norwegian Sea.

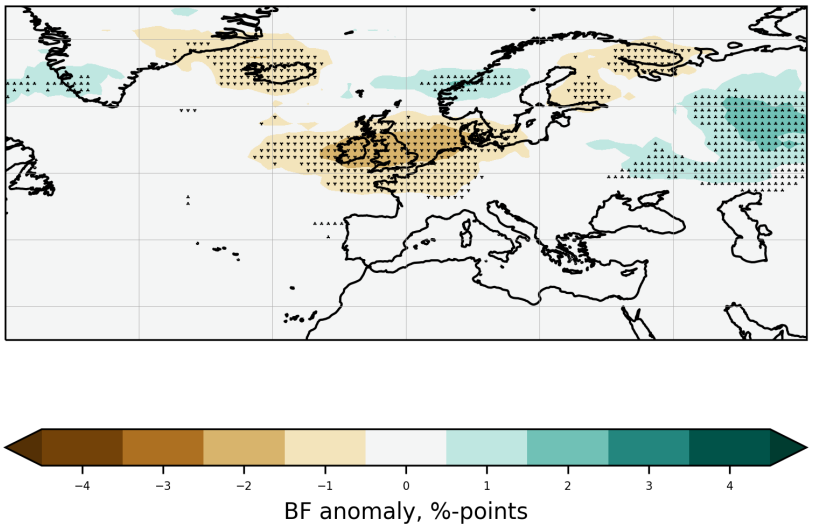
On the subsample of days where blocking occurs over the British Isles, the North Sea area, Iceland or Finland, there is a significant negative heavy precipitation frequency anomaly predominantly over the northwest of Austria (i.e. Vorarlberg, Tyrol, Salzburg, Upper Austria; Figure 6.13c). One possible explanation for this is that blocking over the British Isles and North Sea region hinders moisture from the Atlantic Ocean to reach Austria, thus limiting the ability for strong precipitation events to evolve. Note that this view is consistent with Seibert et al. (2007), who found that heavy precipitation in northwestern Austria is associated with trajectories from the Atlantic (as opposed to, for example, Vb-type situations which appear to be less affected by blocking events). Consistent with this view, we hypothesize that blocking over Russia is associated with more frequent high precipitation events in Austria because it prevents the moisture from being carried away from Austria by the Westerlies.

In the warmer half of the year (MJJASO), the connection between blocking and heavy precipitation seems less pronounced. The reason for this may be that summer precipitation tends to be organised in convective cells, i.e. thunderstorms, which depends strongly on other factors like the convective available potential energy, and thus has a weaker connection to atmospheric blocking (Figure 6.14).

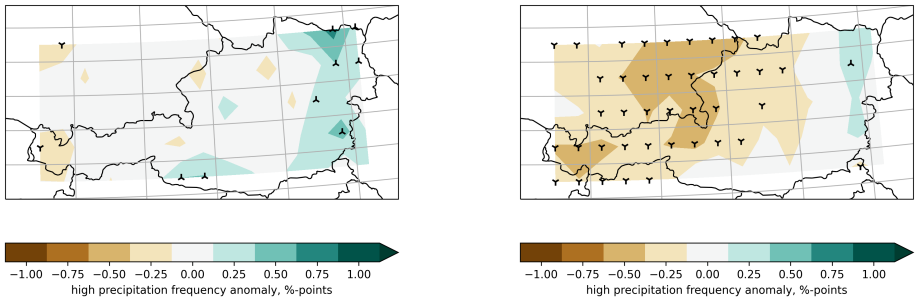
The same pattern that emerges in the yearly average is observed in the colder half of the year (NDJFMA). In fact, the connection between blocking and heavy precipitation in Austria is even stronger in this period. Regions with reduced blocking frequency span from Greenland and Iceland over the British Isles and the North Sea to Central Europe and the Baltic Sea. Blocking in this region is associated with less heavy precipitation in the northwestern parts of Austria. Higher blocking frequencies on days of heavy precipitation in Austria are found over parts of Norway, the Norwegian Sea and Russia (Figure 6.15). Blocking over that region is associated with a positive high precipitation anomaly over eastern Austria, although this anomaly is not statistically significant.

For the DJFM period, the connection between blocking frequency over the British Isles / North Sea / Baltic Sea region and low heavy precipitation frequency in the Northwest of Austria (Vorarlberg, Tyrol, Salzburg, Upper Austria) is even more pronounced, as is the direct relationship between increased blocking frequency over Russia and increased heavy precipitation frequency in the southeast of Austria (Styria, Carinthia, Burgenland; (Figure 6.16).

Links between blocking and heavy precipitation frequency were investigated for each month separately as well. These results can be found in Appendix B (Figure B.25 to Figure B.36).

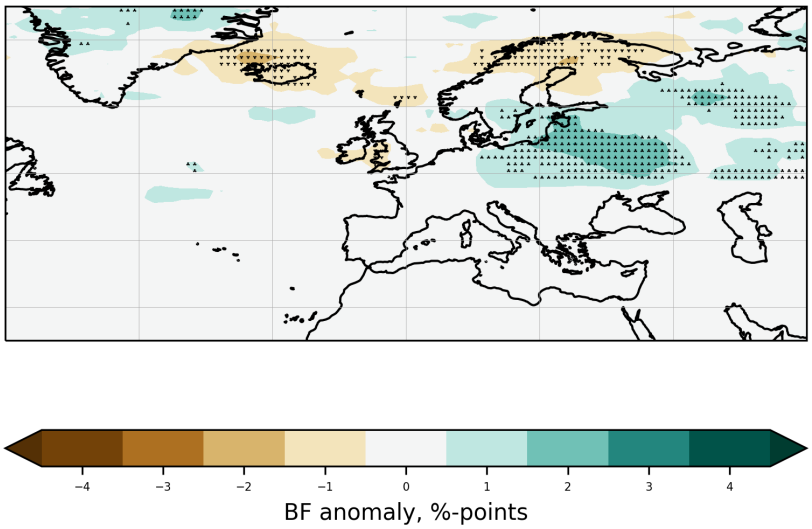


(a)

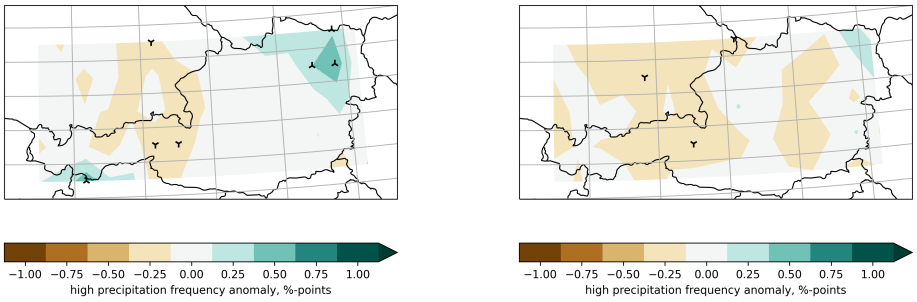


(b) (c)

Figure 6.13.: Blocking over the northern midlatitudes and heavy precipitation frequency in Austria during the 1980 – 2018 period. (a) shows the blocking frequency anomaly in percentage points on days where at least one grid point in Austria is experiencing high precipitation. Marked black are the grid points for which this relationship is statistically significant. (b) shows the high precipitation frequency anomaly in percentage points in Austria on days where at least 10 percent of the points marked as significantly positive in (a) are blocked. (c) shows the heavy precipitation anomaly on days where at least 10 percent of the grid points marked as significantly negative in (a) are blocked.

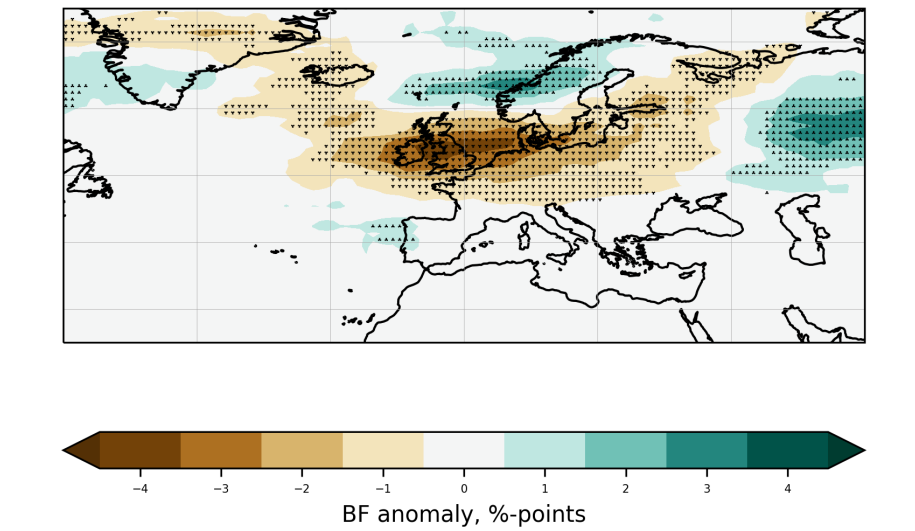


(a)

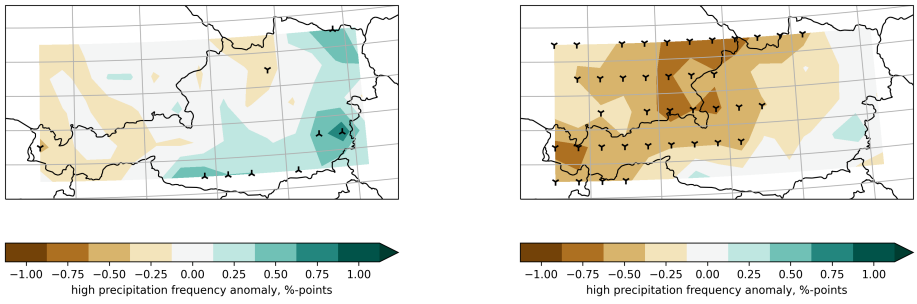


(b) **(c)**

Figure 6.14.: Blocking frequency over the northern midlatitudes and heavy precipitation frequency in Austria for MJJASO (1980 – 2018). Same layout as Figure 6.9.

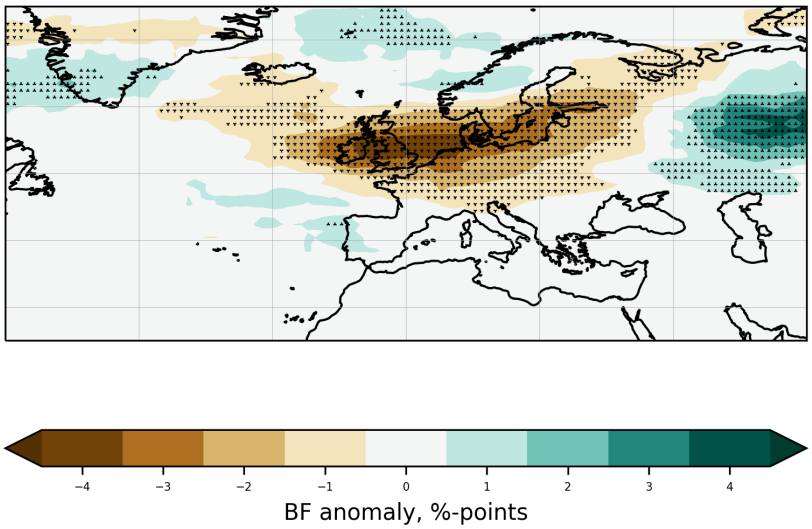


(a)

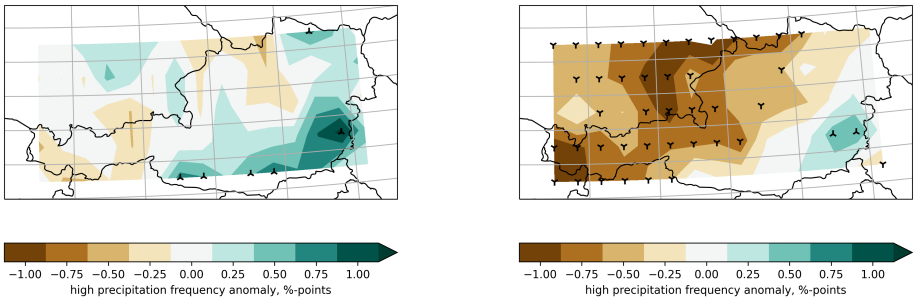


(b) (c)

Figure 6.15.: Blocking frequency over the northern midlatitudes and heavy precipitation frequency in Austria for NDJFMA (1980 – 2018). Same layout as Figure 6.9.



(a)



(b) **(c)**

Figure 6.16.: Blocking frequency over the northern midlatitudes and heavy precipitation frequency in Austria for DJFM (1980 – 2018). Same layout as Figure 6.9.

7. Summary and Conclusions

The connection to extreme weather events makes atmospheric blocking an important aspect of the Earth's climate, particularly in the northern mid-latitudes. Depending on the location of the blocking event, it can either facilitate or inhibit the formation of heatwaves, cold spells and heavy precipitation events. In this thesis, changes in the frequency of occurrence of such blocking events as well as their connection specifically to the following extreme weather types in Austria have been investigated:

- heatwave days, defined as days with a maximum temperature above the 95th percentile of the distribution of maximum temperatures found within a $\pm$ 15 days window around that day, considering the 1980 – 2018 period.
- cold spell days, defined as days with a minimum temperature below the 5th percentile of the distribution of minimum temperatures found within a $\pm$ 15 days window around that day, considering the 1980 – 2018 period.
- heavy precipitation days, defined as days with a maximum hourly precipitation above the 95th percentile of the distribution of maximum hourly precipitation found within a $\pm$ 15 days window around that day, considering the 1980 – 2018 period, not counting no precipitation days.

In previous literature, no clear, consistent trend in blocking frequency has been demonstrated to exist. We analyze reanalysis data for the period 1950 – 2019 with the hypothesis that this extension might shed new light on the matter. We found

- a general decrease of 3 percentage points per decade in the North Atlantic longitudes (roughly between 20°W and 60°W) in winter and spring, specifically in January, February, March, April and May (Figure 5.1 (a – f)).
- an increase in blocking frequency of 1 percentage points per decade to 2 percentage points per decade in June and July in the same region (Figure 5.2 (b & c)).
- a decrease in blocking frequency of 1 to 2 percentage points per decade over Asia between 40°E and 180°E in February (Figure 5.1 (c)).
- an increase of blocking frequency in June between 120°E and 140°E, by up to 4 percentage points per decade, the strongest increase in any time and place (Figure 5.2 (a)).

- an increase of roughly 2 percentage points per decade over the European longitudes in September (Figure 5.2 (d)).

Resolving blocking frequency trends in two dimensions, we find that sign and magnitude of blocking frequency trends vary across time and space. Trends for the period 1979 to 2019 show a general increase of up to 2 percentage points per decade in March over the British Isles. Blocking frequency decreases over Greenland and the North Atlantic in November.

If a global trend since 1950 does exist, it is overshadowed by the natural variability that is inherent to the system. Since climate models tend to be heavily biased with regard to atmospheric blocking, no reliable conjecture regarding the future development of blocking frequency can be made.

In this work, atmospheric blocking was detected using an algorithm that checks each point on a longitude / latitude coordinate grid for a number of criteria that must be fulfilled to be part of a blocking system. It seems plausible that tracking individual blocking systems, rather then the grid points they consist of, might yield different, more reliable results. It would also allow for a more multifaceted investigation of blocking events, as tracking blocking systems could give a solid understanding of how not just the frequency of occurrence, but also the *persistence once they have occurred* has developed over time.

The second half of this thesis is dedicated to the connection between the occurrence of blocking events and the occurrence of extreme weather events in Austria. It has been known that blocking events can trigger heatwaves at their location and cold spells to the south of their location. In this thesis, this relationship has been generally confirmed for Austria in particular, and additional information has been given as to which Austrian regions have been particularly affected:

- Blocked days connected to warm spell days in Austria show a dipole pattern of increased blocking frequency over central and eastern Europe and of decreased blocking frequency over Greenland to Northern Europe (Figure 6.5).

- For heatwaves during MJJASO, increased blocking frequency is observed over Eastern Europe. It is associated with significantly increased heat wave frequency in the northeastern parts of Austria (Figure 6.6).

- In winter and spring (NDJFMA), increased blocking frequency over central Europe is associated with increased heat wave frequency in the southern and western parts of Austria (Figure 6.7).

- Blocking connected to cold spell days in Austria shows increased blocking frequency over Greenland, the North Atlantic and, particularly, over Scandinavia (Figure 6.9).

- For cold spell days in Austria during winter and spring (NDJFMA), increased blocking frequency is observed mainly over the British Isles and Scandinavia.

Blocking in this region is connected to a significant increase in cold spells by about 4 percentage points to 6 percentage points in all of Austria (Figure 6.11).

- Blocking events in the North Sea / British Isles region seem to inhibit heavy precipitation formation especially in the colder months and in the northwest of Austria. Blocking in this region is associated with a significant decrease in heavy precipitation frequency by about -0.5 to -1 percentage points in the northwest of Austria (Figure 6.13).
- Blocking over Russia is associated with a more frequent occurrence of heavy precipitation in Austria. Blocking in this region is associated with an increase in heavy precipitation frequency by about -0.5 to -1 percentage points in the southeast of Austria (Figure 6.13).

The connection between blocking frequency and heatwave frequency in Austria can be explained by the enhanced ability of the sun to radiatively heat areas affected by stationary high pressure systems due to the frequent occurrence of clear skies in high pressure areas.

The connection between blocking frequency and cold spell frequency in Austria can be attributed to cold air advection from the polar regions towards the mid-latitudes.

A reasonable explanation for the connection between blocking frequency and heavy precipitation frequency is that blocking over the North Sea and British Isles regions prevents the prevailing Westerlies from carrying moisture towards Austria. Blocking over Russia prevents the Westerlies from carrying moisture *away* from Austria. This is supported by the fact that this connection is stronger in western Austria, where storm systems originate more often in the Atlantic, and that it is generally weaker in summer, where storms are more dependent on convective available potential energy.

While we did not find a clear global long-term trend in the observation-based reanalysis data, the most prominent observed regional trends in the period 1979 – 2019, *if* they continue, *could* have ramifications for extreme weather in Austria for the future:

- A further increase in blocking frequency over the British Isles in March (Figure 5.4a, right panel) could imply more frequent cold spells (Figure 6.7 & Figure B.3).
- A further decrease of blocking frequency over Greenland and the North Atlantic in November (Figure 5.6c, right panel) could imply more frequent heatwaves (Figure 6.7 & Figure B.11) and less frequent cold spells (Figure 6.11 & Figure B.23) in Austria in November.

In conclusion, trends in the frequency of occurrence of blocking events are regionally and temporally confined and thus no significant overarching trends could

be detected since 1950. However, trends in blocking frequency are observed for different regions and seasons. These typically represent spatial shifts of areas of high blocking frequency. It remains to be investigated if the average duration of blocking events increased, if the strength of the link between atmospheric blocking and extreme weather changed and if the severity of extreme weather connected to blocking events changed over the last decades.

There is a statistically significant relationship between atmospheric blocking and extreme weather frequency in Austria, the nature of which depends on the time of the year and the location of the blocking event. The connection between heatwaves and blocking frequency is generally dipolar, with blocking in Central and Eastern Europe being connected to higher heatwave frequency in Austria, and blocking in Northern Europe and Greenland being connected to lower heatwave frequency in Austria. Blocking in Northern Europe, the North Atlantic and Greenland is associated with an increased cold spell frequency in Austria. Blocking in the North Sea / British Isles region is associated with less frequent heavy precipitation days in the northwest of Austria, while blocking over Russia is associated with more frequent precipitation days in the southeast of Austria.

A. Trends in Blocking Frequency in Regions Defined in Literature

Various authors have investigated atmospheric blocking in the past, using more or less arbitrarily defined regions across the globe. In their work, they connected atmospheric blocking in those regions to extreme weather in Europe. No trends in blocking frequency could be detected in any of the regions as defined by Sousa et al. 2017 (Atlantic, Europe, Russia), Yao et al. 2017 (Ural), Brunner et al. 2016 (North Atlantic) and Brunner et al. 2017 (Euro-Atlantic). For the sake of completeness, the results are still shown here (Table A.1). The trends were calculated by determining the blocking frequency (i.e. days where blocking in the region occurs divided by total days of the month) for each month between 1950 and 2019, then performing an ordinary linear regression on the resulting time series.

Table A.1.: Regions investigated for trends, trends and p-values for statistical significance.

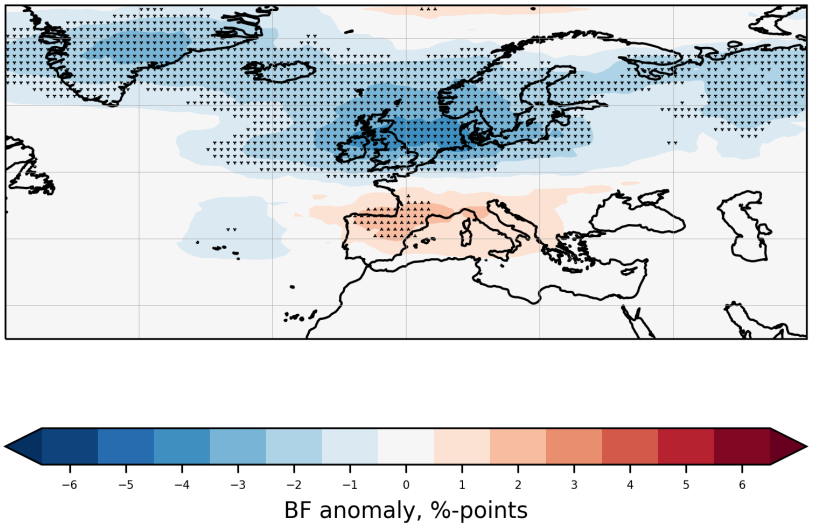
region	longitude	latitude	slope	p-value
North Atlantic[a]	30°W–10°E	30°N–72.5°N	0.0 %/year	0.24
Euro-Atlantic[b]	30°W–45°E	45°N–72.5°N	0.0 %/year	0.98
Atlantic[c]	30°W–0°	45°N–70°N	0.0 %/year	0.13
Europe[c]	0°–30°E	45°N–70°N	0.0 %/year	0.18
Russia[c]	30°E–60°E	45°N–70°N	0.0 %/year	0.83
Ural[d]	30°E–90°E	50°N–75°N	0.0 %/year	0.49

[a] Brunner et al. 2016
[b] Brunner et al. 2017
[c] Sousa et al. 2017
[d] Yao et al. 2017

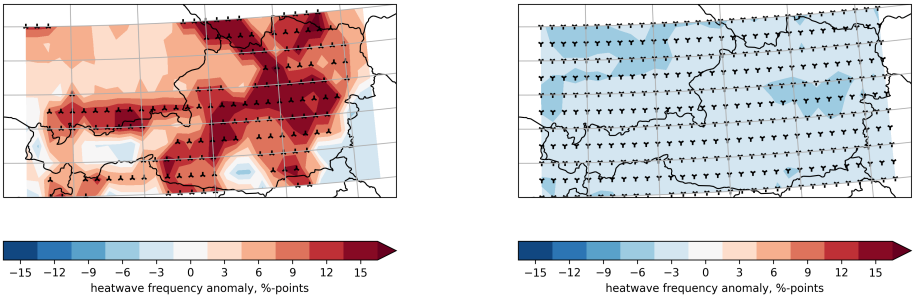
B. Monthly-resolved Extreme Weather Anomalies

All extreme weather anomalies presented in chapter 6 were calculated for each month of the year separately — the results are shown in this appendix. Note that in some cases, extreme weather frequency anomalies could not be computed because there was no region in which blocking frequency was significantly increased / reduced in the subsample of days in which this type of extreme weather occurs in Austria. A good example is the heavy precipitation frequency anomaly in Austria in October. It is worth keeping in mind that while these plots are more specific with respect to the time of the year, they are also coarser and less trustworthy, as naturally only (roughly) one twelfth of the overall available data was used for each.

Sometimes, strong anomalies are not marked as significant, while weaker anomalies in the same figure are. This is not surprising, as significance is calculated for each grid point separately, and in regions with more internal variability, anomalies must be stronger to be counted as statistically significant. However, this effect is likely to only play a minor role compared to another, much stronger criterion: Grid points with a climatological frequency of less than 1 day per year are excluded from significance testing on principle. This is necessary; consider for example the extreme case where a certain grid point was only blocked for one day in the entire period, and this blocking occurred on a day where a heatwave was detected anywhere in Austria. Naturally, this would be counted as significant, as 100 % of the blocked days at that grid point coincided with Austrian heatwave days; however, it is just as likely that it was pure coincidence. These considerations translate directly to extreme weather frequency anomalies as well and are especially relevant for this appendix, as the base sample size is much smaller; thus, situations like this are more likely to occur.

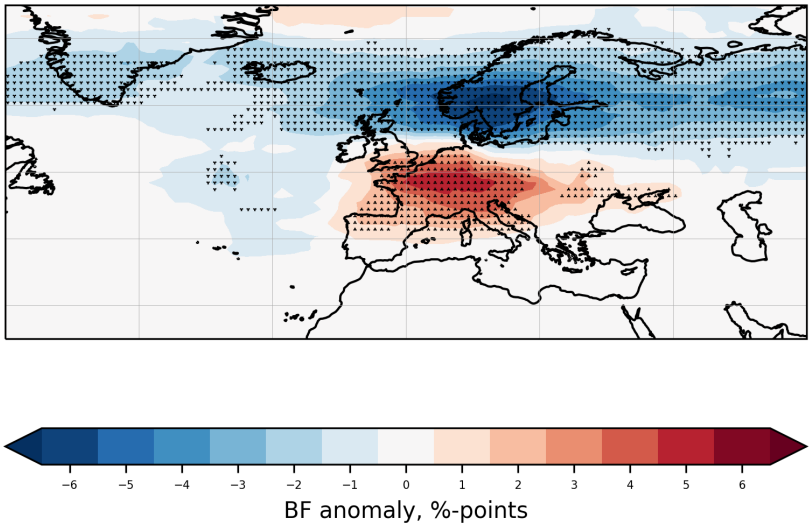


(a)

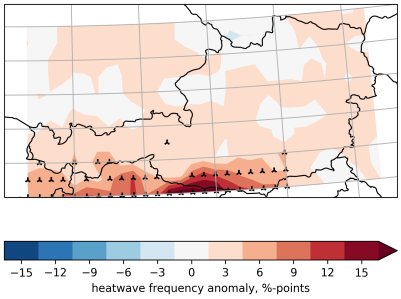


(b) **(c)**

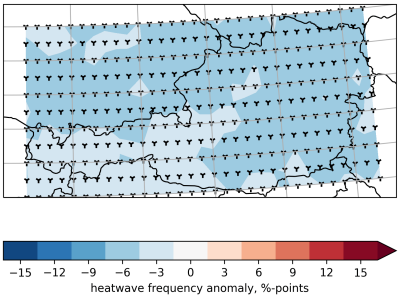
Figure B.1.: Blocking in the northern mid-latitudes and heatwave frequency in Austria in January. (a) shows the blocking frequency anomaly in percentage points on days where at least one grid point in Austria is experiencing a heatwave. Marked black are the grid points for which this relationship is statistically significant. (b) shows the heatwave frequency anomaly in percentage points in Austria on days where at least 10 percent of the points marked as significantly positive in (a) are blocked. (c) is equivalent to (b), but for the points in (a) marked as significantly negative.



(a)

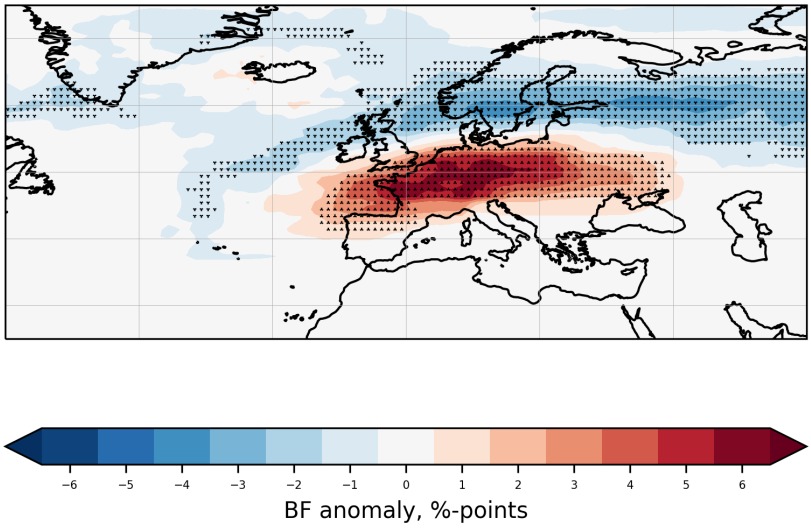


(b)

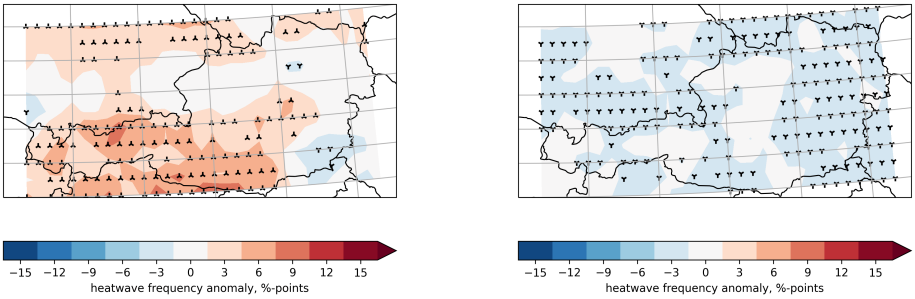


(c)

Figure B.2.: Blocking in the northern mid-latitudes and heatwave frequency in Austria in February. (a) shows the blocking frequency anomaly in percentage points on days where at least one grid point in Austria is experiencing a heatwave. Marked black are the grid points for which this relationship is statistically significant. (b) shows the heatwave frequency anomaly in percentage points in Austria on days where at least 10 percent of the points marked as significantly positive in (a) are blocked. (c) is equivalent to (b), but for the points in (a) marked as significantly negative.

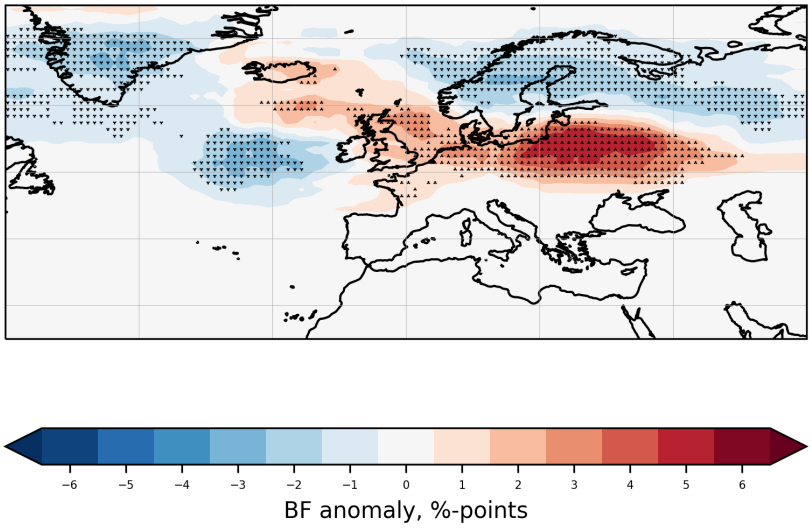


(a)

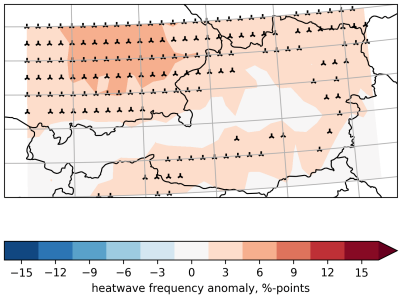


(b) **(c)**

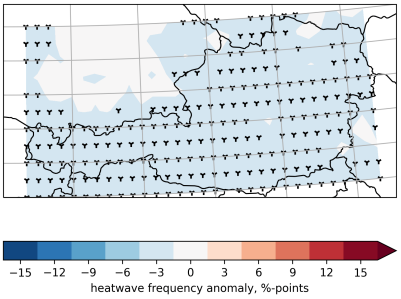
Figure B.3.: Blocking in the northern mid-latitudes and heatwave frequency in Austria in March. (a) shows the blocking frequency anomaly in percentage points on days where at least one grid point in Austria is experiencing a heatwave. Marked black are the grid points for which this relationship is statistically significant. (b) shows the heatwave frequency anomaly in percentage points in Austria on days where at least 10 percent of the points marked as significantly positive in (a) are blocked. (c) is equivalent to (b), but for the points in (a) marked as significantly negative.



(a)

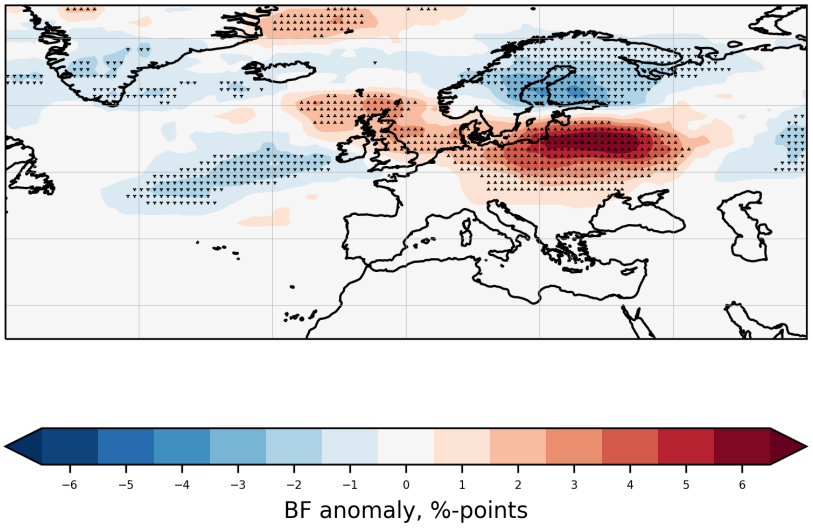


(b)

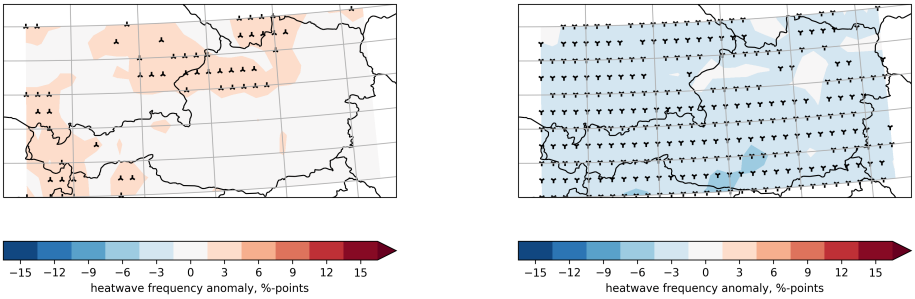


(c)

Figure B.4.: Blocking in the northern mid-latitudes and heatwave frequency in Austria in April. (a) shows the blocking frequency anomaly in percentage points on days where at least one grid point in Austria is experiencing a heatwave. Marked black are the grid points for which this relationship is statistically significant. (b) shows the heatwave frequency anomaly in percentage points in Austria on days where at least 10 percent of the points marked as significantly positive in (a) are blocked. (c) is equivalent to (b), but for the points in (a) marked as significantly negative.

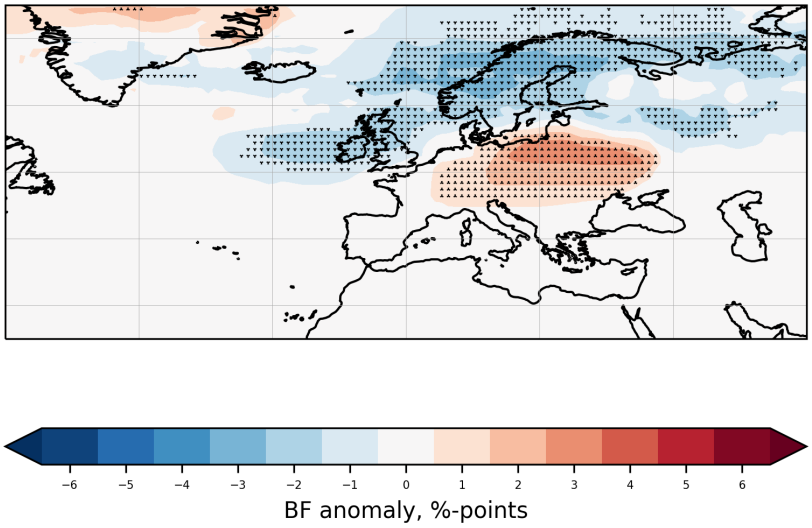


(a)

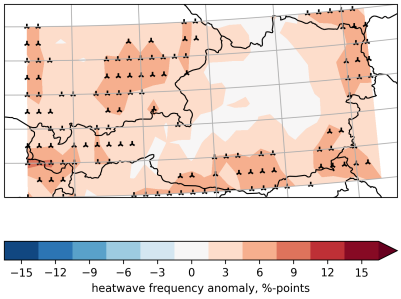


(b) **(c)**

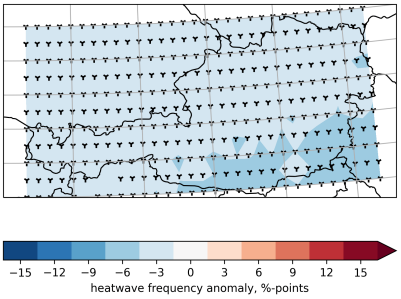
Figure B.5.: Blocking in the northern mid-latitudes and heatwave frequency in Austria in May. (a) shows the blocking frequency anomaly in percentage points on days where at least one grid point in Austria is experiencing a heatwave. Marked black are the grid points for which this relationship is statistically significant. (b) shows the heatwave frequency anomaly in percentage points in Austria on days where at least 10 percent of the points marked as significantly positive in (a) are blocked. (c) is equivalent to (b), but for the points in (a) marked as significantly negative.



(a)

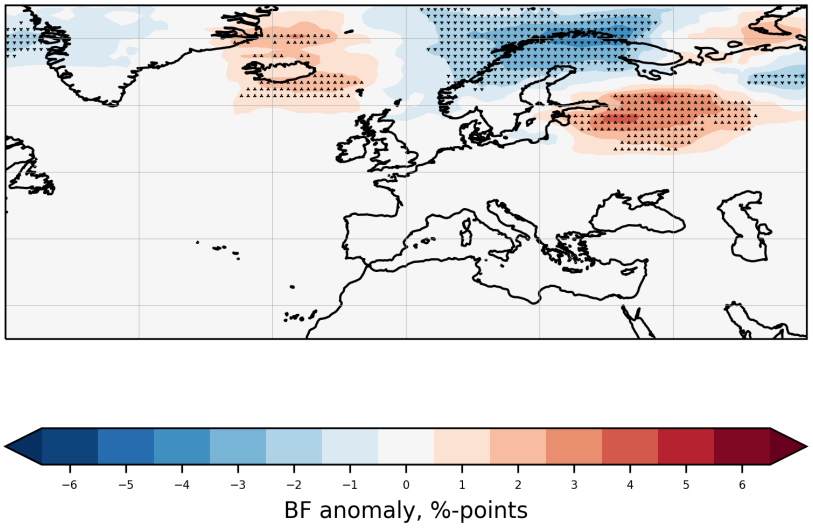


(b)

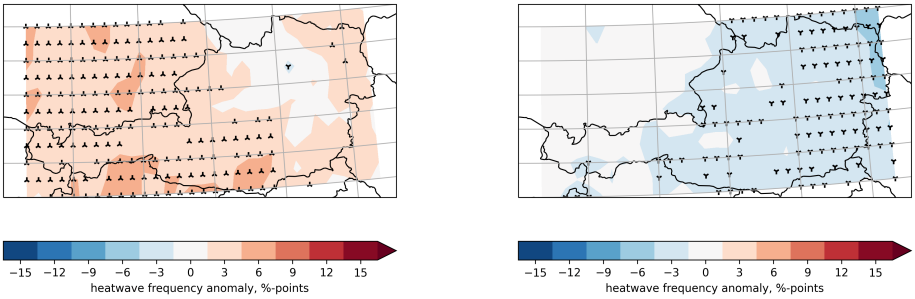


(c)

Figure B.6.: Blocking in the northern mid-latitudes and heatwave frequency in Austria in June. (a) shows the blocking frequency anomaly in percentage points on days where at least one grid point in Austria is experiencing a heatwave. Marked black are the grid points for which this relationship is statistically significant. (b) shows the heatwave frequency anomaly in percentage points in Austria on days where at least 10 percent of the points marked as significantly positive in (a) are blocked. (c) is equivalent to (b), but for the points in (a) marked as significantly negative.

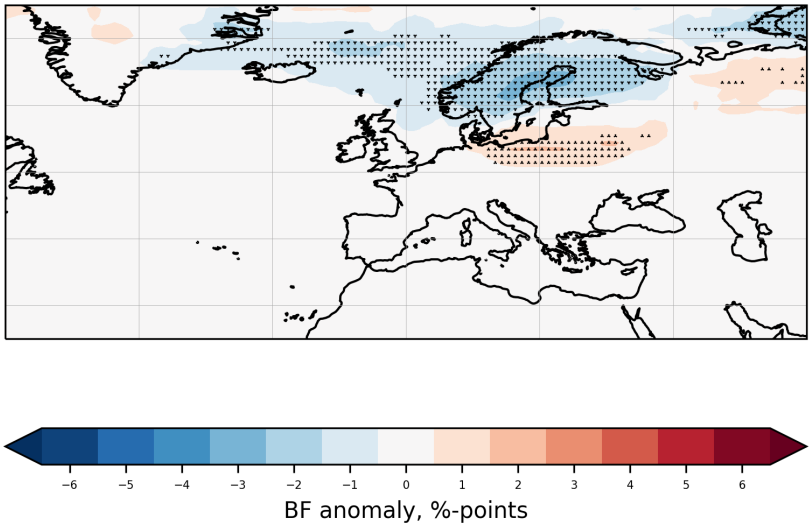


(a)

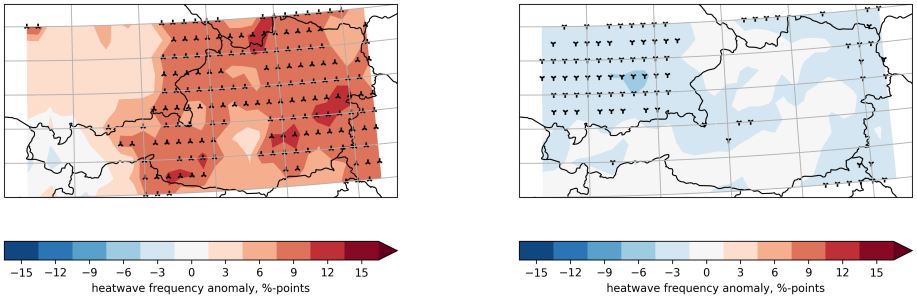


(b) **(c)**

Figure B.7.: Blocking in the northern mid-latitudes and heatwave frequency in Austria in July. (a) shows the blocking frequency anomaly in percentage points on days where at least one grid point in Austria is experiencing a heatwave. Marked black are the grid points for which this relationship is statistically significant. (b) shows the heatwave frequency anomaly in percentage points in Austria on days where at least 10 percent of the points marked as significantly positive in (a) are blocked. (c) is equivalent to (b), but for the points in (a) marked as significantly negative.

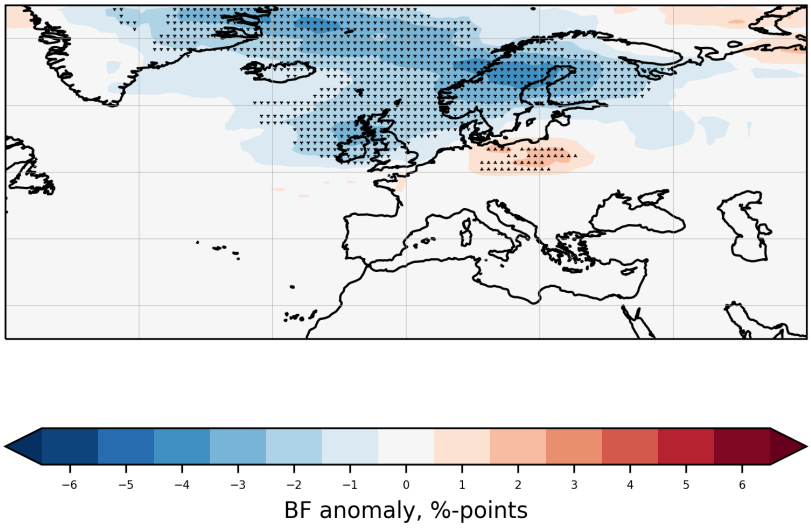


(a)

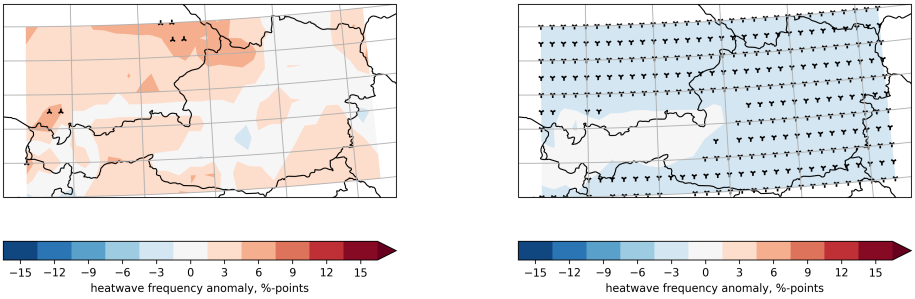


(b) **(c)**

Figure B.8.: Blocking in the northern mid-latitudes and heatwave frequency in Austria in August. (a) shows the blocking frequency anomaly in percentage points on days where at least one grid point in Austria is experiencing a heatwave. Marked black are the grid points for which this relationship is statistically significant. (b) shows the heatwave frequency anomaly in percentage points in Austria on days where at least 10 percent of the points marked as significantly positive in (a) are blocked. (c) is equivalent to (b), but for the points in (a) marked as significantly negative.

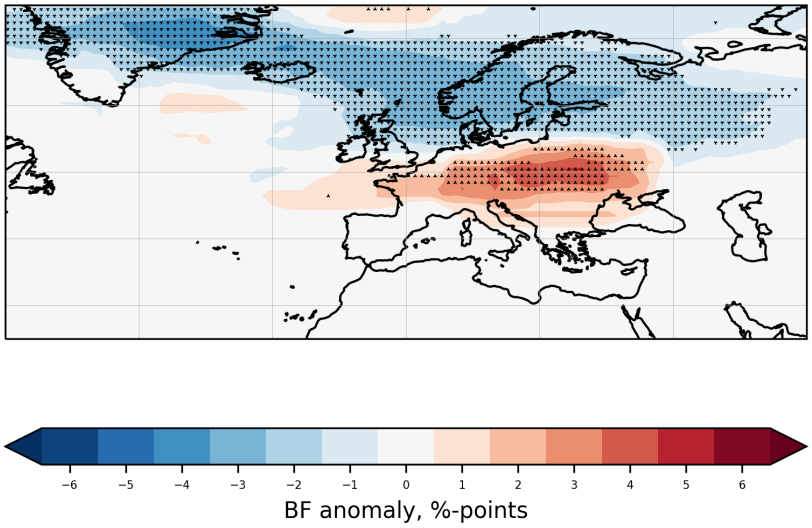


(a)

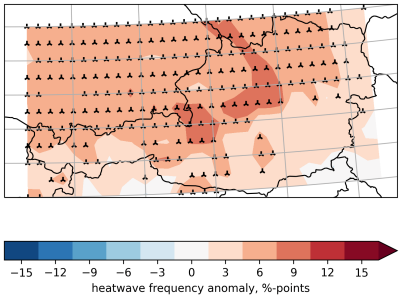


(b) **(c)**

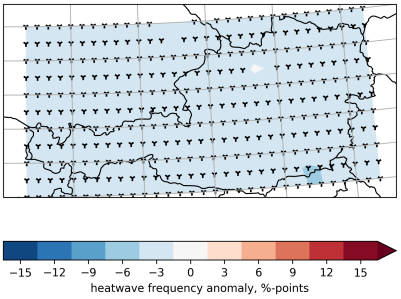
Figure B.9.: Blocking in the northern mid-latitudes and heatwave frequency in Austria in September. (a) shows the blocking frequency anomaly in percentage points on days where at least one grid point in Austria is experiencing a heatwave. Marked black are the grid points for which this relationship is statistically significant. (b) shows the heatwave frequency anomaly in percentage points in Austria on days where at least 10 percent of the points marked as significantly positive in (a) are blocked. (c) is equivalent to (b), but for the points in (a) marked as significantly negative.



(a)

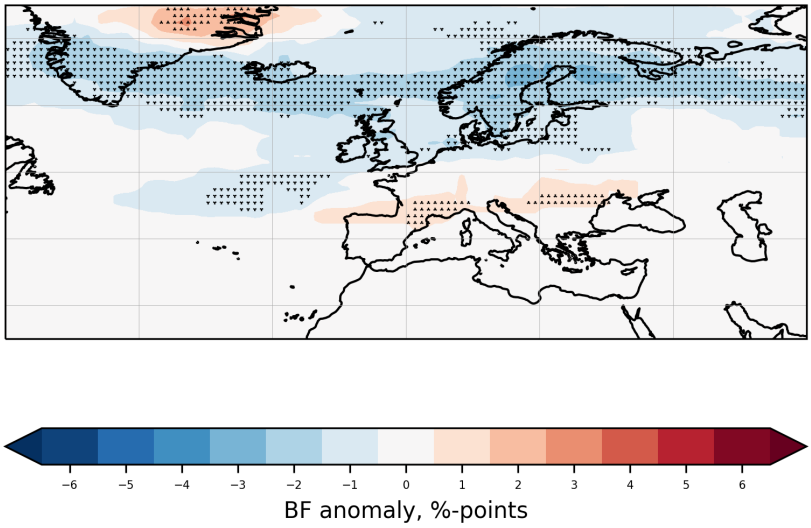


(b)

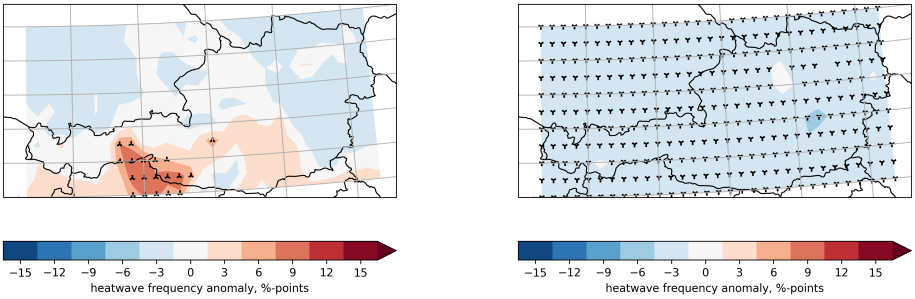


(c)

Figure B.10.: Blocking in the northern mid-latitudes and heatwave frequency in Austria in October. (a) shows the blocking frequency anomaly in percentage points on days where at least one grid point in Austria is experiencing a heatwave. Marked black are the grid points for which this relationship is statistically significant. (b) shows the heatwave frequency anomaly in percentage points in Austria on days where at least 10 percent of the points marked as significantly positive in (a) are blocked. (c) is equivalent to (b), but for the points in (a) marked as significantly negative.

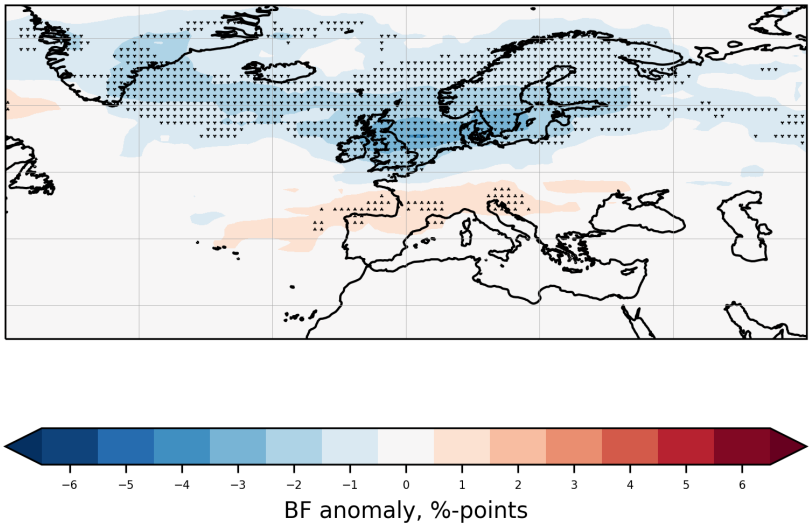


(a)

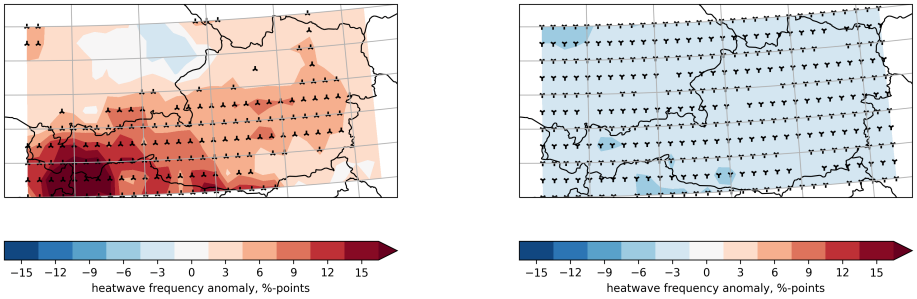


(b) **(c)**

Figure B.11.: Blocking in the northern mid-latitudes and heatwave frequency in Austria in November. (a) shows the blocking frequency anomaly in percentage points on days where at least one grid point in Austria is experiencing a heatwave. Marked black are the grid points for which this relationship is statistically significant. (b) shows the heatwave frequency anomaly in percentage points in Austria on days where at least 10 percent of the points marked as significantly positive in (a) are blocked. (c) is equivalent to (b), but for the points in (a) marked as significantly negative.

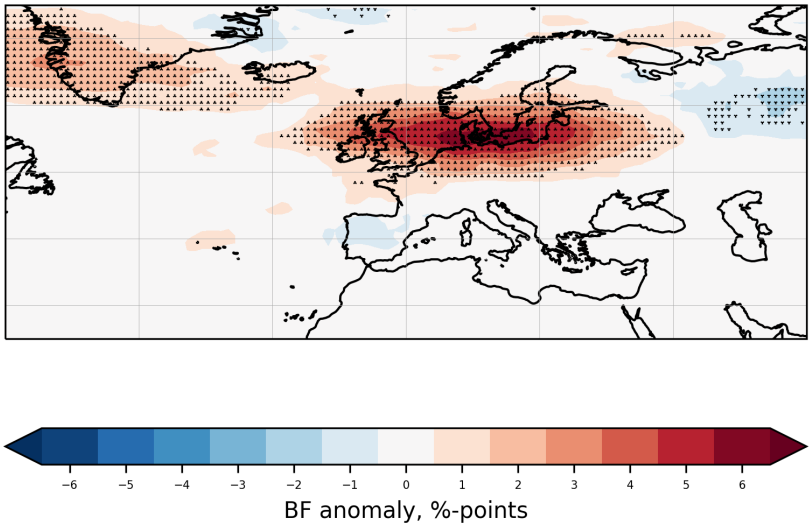


(a)

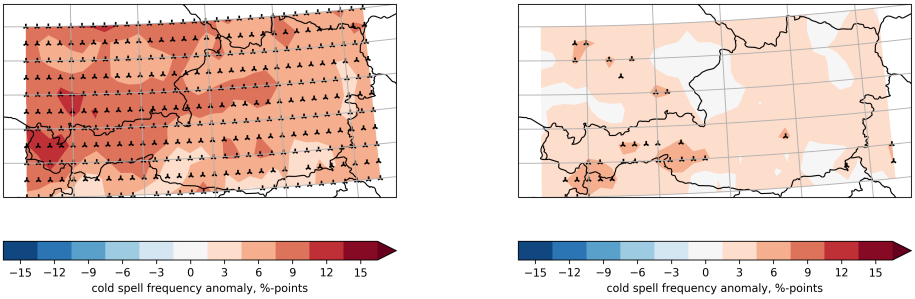


(b) **(c)**

Figure B.12.: Blocking in the northern mid-latitudes and heatwave frequency in Austria in December. (a) shows the blocking frequency anomaly in percentage points on days where at least one grid point in Austria is experiencing a heatwave. Marked black are the grid points for which this relationship is statistically significant. (b) shows the heatwave frequency anomaly in percentage points in Austria on days where at least 10 percent of the points marked as significantly positive in (a) are blocked. (c) is equivalent to (b), but for the points in (a) marked as significantly negative.

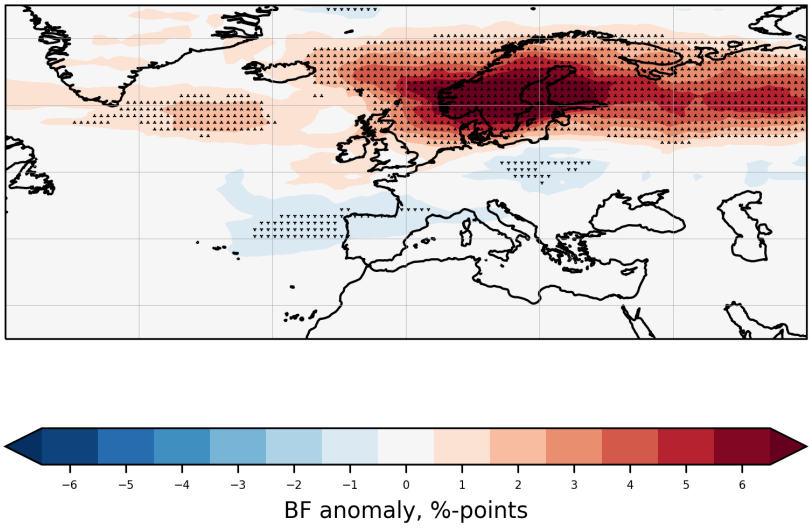


(a)

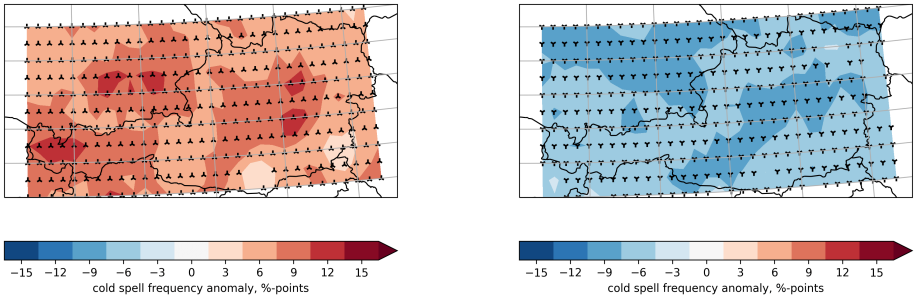


(b) **(c)**

Figure B.13.: Blocking in the northern mid-latitudes and cold spell frequency in Austria in January. (a) shows the blocking frequency anomaly in percentage points on days where at least one grid point in Austria is experiencing a heatwave. Marked black are the grid points for which this relationship is statistically significant. (b) shows the heatwave frequency anomaly in percentage points in Austria on days where at least 10 percent of the points marked as significantly positive in (a) are blocked. (c) is equivalent to (b), but for the points in (a) marked as significantly negative.

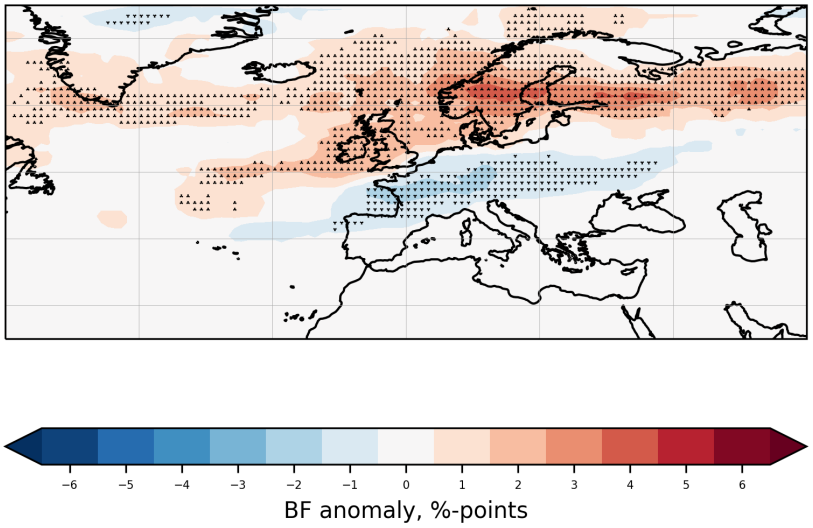


(a)

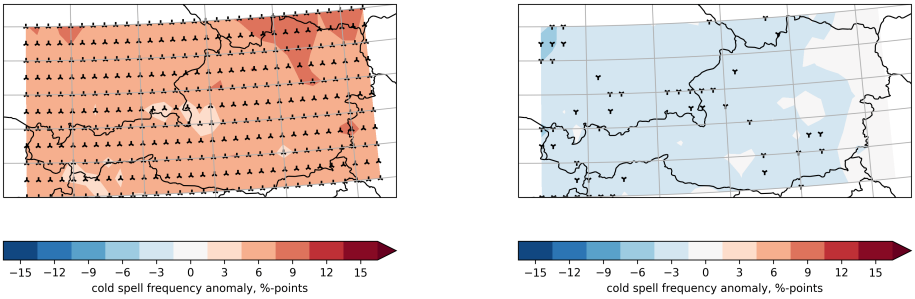


(b) **(c)**

Figure B.14.: Blocking in the northern mid-latitudes and cold spell frequency in Austria in February. (a) shows the blocking frequency anomaly in percentage points on days where at least one grid point in Austria is experiencing a heatwave. Marked black are the grid points for which this relationship is statistically significant. (b) shows the heatwave frequency anomaly in percentage points in Austria on days where at least 10 percent of the points marked as significantly positive in (a) are blocked. (c) is equivalent to (b), but for the points in (a) marked as significantly negative.

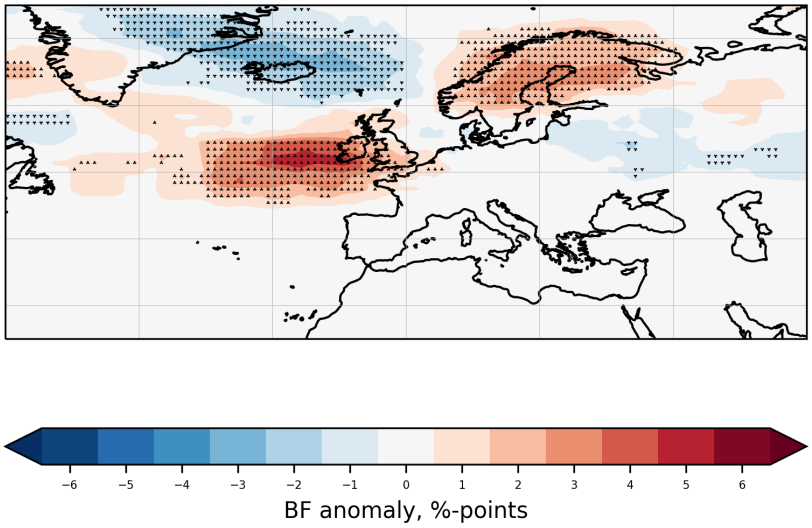


(a)

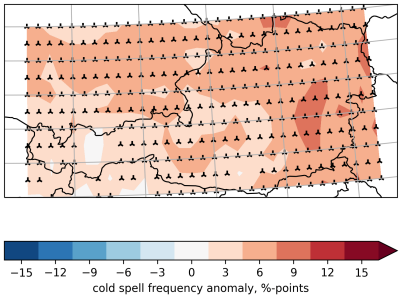


(b) **(c)**

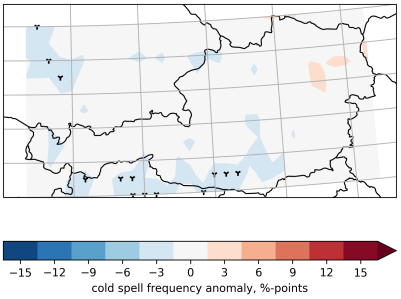
Figure B.15.: Blocking in the northern mid-latitudes and cold spell frequency in Austria in March. (a) shows the blocking frequency anomaly in percentage points on days where at least one grid point in Austria is experiencing a heatwave. Marked black are the grid points for which this relationship is statistically significant. (b) shows the heatwave frequency anomaly in percentage points in Austria on days where at least 10 percent of the points marked as significantly positive in (a) are blocked. (c) is equivalent to (b), but for the points in (a) marked as significantly negative.



(a)

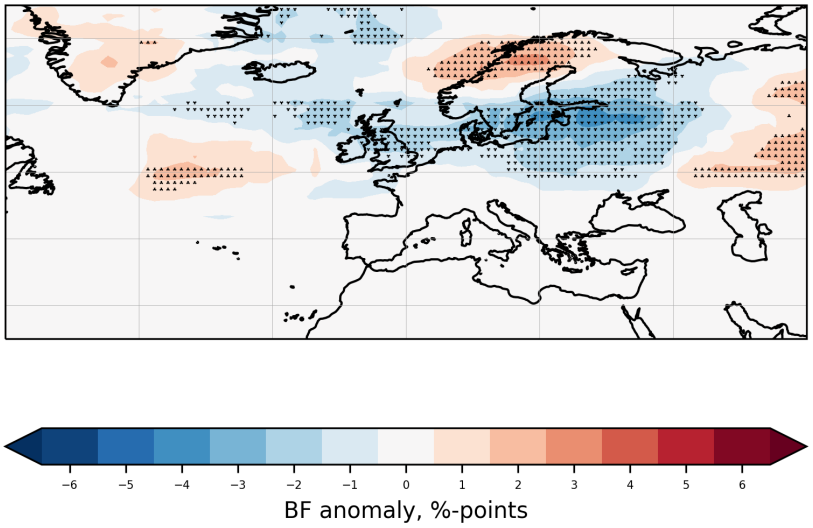


(b)

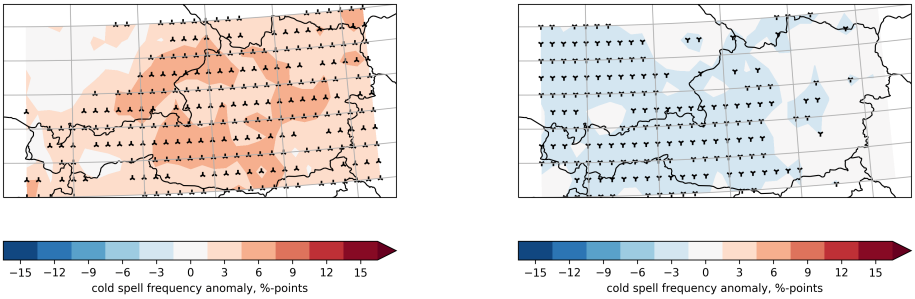


(c)

Figure B.16.: Blocking in the northern mid-latitudes and cold spell frequency in Austria in April. (a) shows the blocking frequency anomaly in percentage points on days where at least one grid point in Austria is experiencing a heatwave. Marked black are the grid points for which this relationship is statistically significant. (b) shows the heatwave frequency anomaly in percentage points in Austria on days where at least 10 percent of the points marked as significantly positive in (a) are blocked. (c) is equivalent to (b), but for the points in (a) marked as significantly negative.

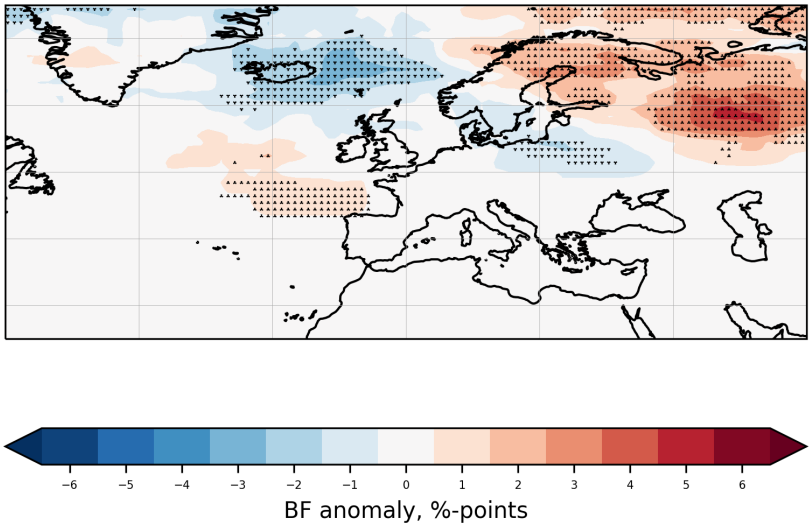


(a)

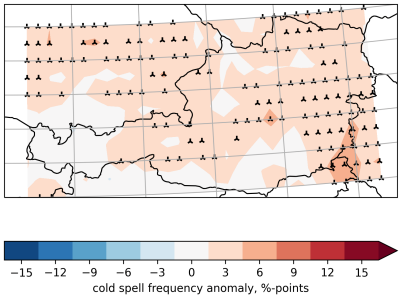


(b) **(c)**

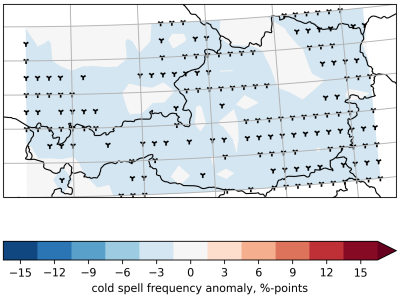
Figure B.17.: Blocking in the northern mid-latitudes and cold spell frequency in Austria in May. (a) shows the blocking frequency anomaly in percentage points on days where at least one grid point in Austria is experiencing a heatwave. Marked black are the grid points for which this relationship is statistically significant. (b) shows the heatwave frequency anomaly in percentage points in Austria on days where at least 10 percent of the points marked as significantly positive in (a) are blocked. (c) is equivalent to (b), but for the points in (a) marked as significantly negative.



(a)



(b)



(c)

Figure B.18.: Blocking in the northern mid-latitudes and cold spell frequency in Austria in June. (a) shows the blocking frequency anomaly in percentage points on days where at least one grid point in Austria is experiencing a heatwave. Marked black are the grid points for which this relationship is statistically significant. (b) shows the heatwave frequency anomaly in percentage points in Austria on days where at least 10 percent of the points marked as significantly positive in (a) are blocked. (c) is equivalent to (b), but for the points in (a) marked as significantly negative.

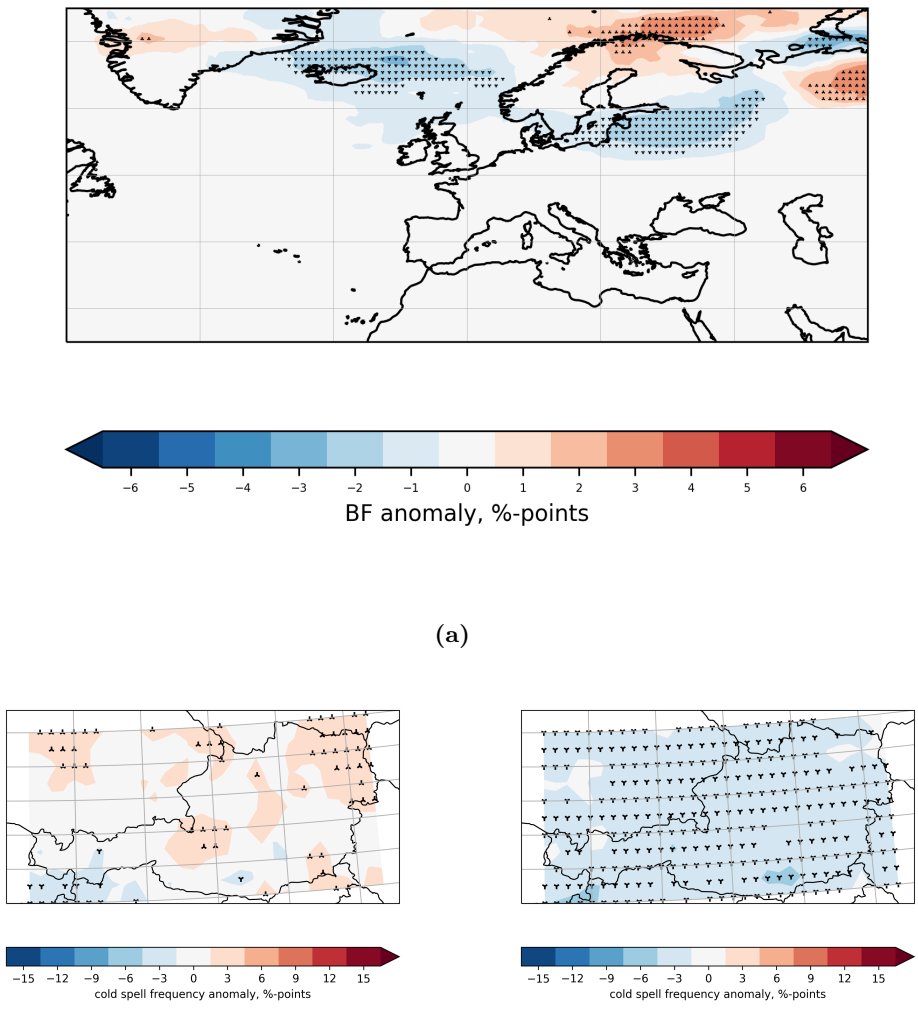
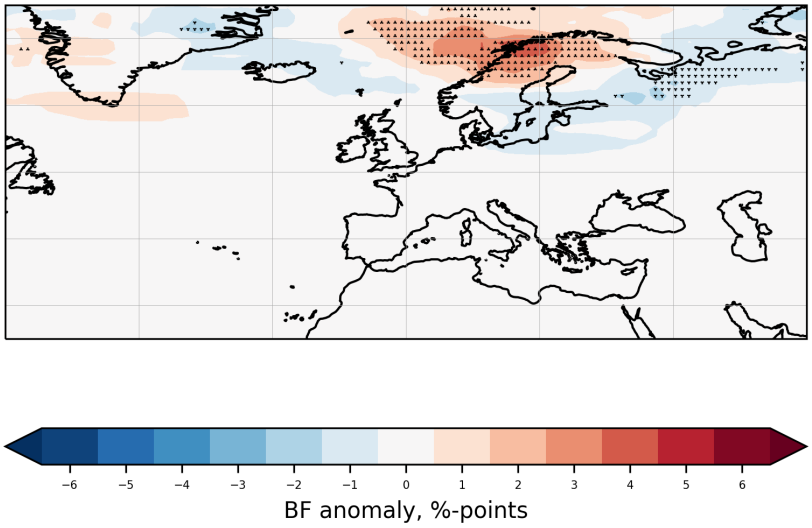
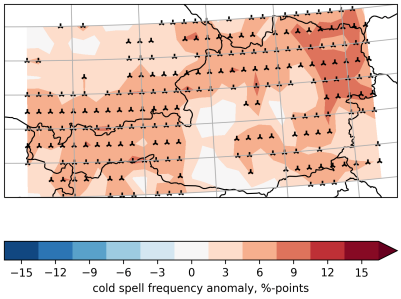


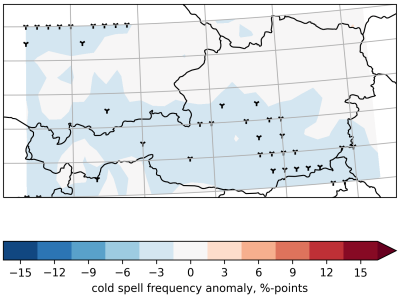
Figure B.19.: Blocking in the northern mid-latitudes and cold spell frequency in Austria in July. (a) shows the blocking frequency anomaly in percentage points on days where at least one grid point in Austria is experiencing a heatwave. Marked black are the grid points for which this relationship is statistically significant. (b) shows the heatwave frequency anomaly in percentage points in Austria on days where at least 10 percent of the points marked as significantly positive in (a) are blocked. (c) is equivalent to (b), but for the points in (a) marked as significantly negative.



(a)

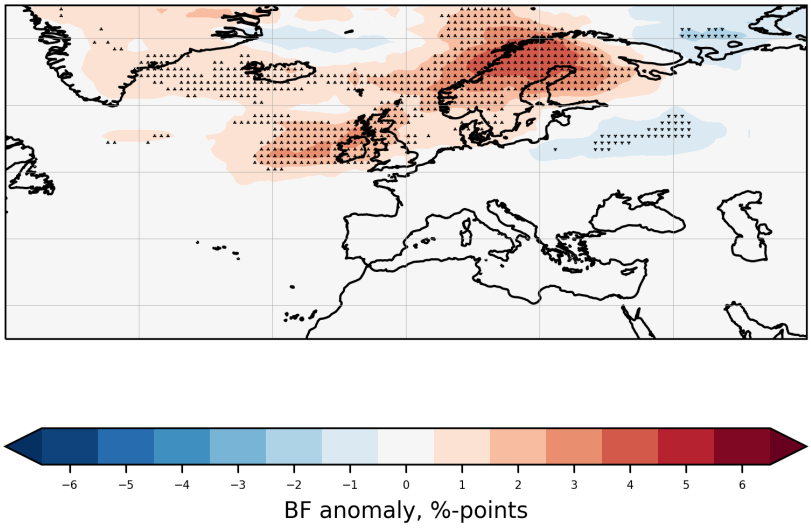


(b)

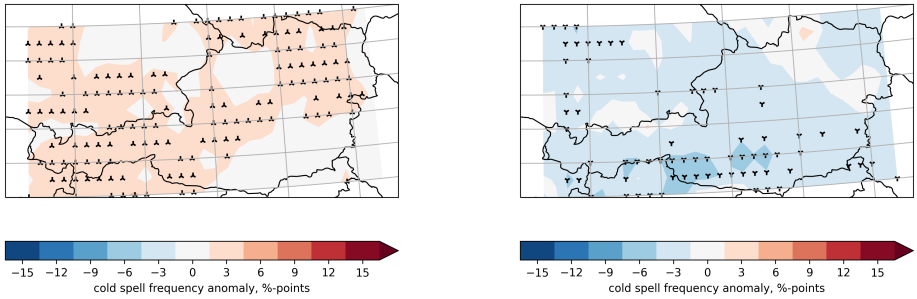


(c)

Figure B.20.: Blocking in the northern mid-latitudes and cold spell frequency in Austria in August. (a) shows the blocking frequency anomaly in percentage points on days where at least one grid point in Austria is experiencing a heatwave. Marked black are the grid points for which this relationship is statistically significant. (b) shows the heatwave frequency anomaly in percentage points in Austria on days where at least 10 percent of the points marked as significantly positive in (a) are blocked. (c) is equivalent to (b), but for the points in (a) marked as significantly negative.

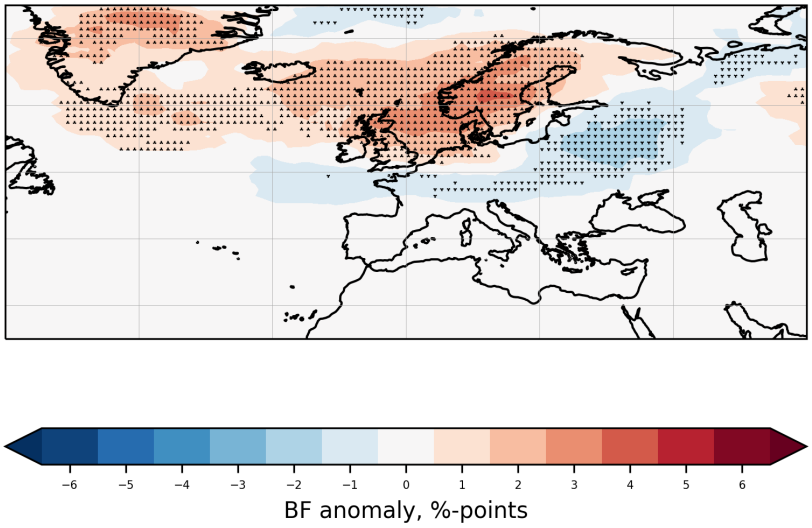


(a)

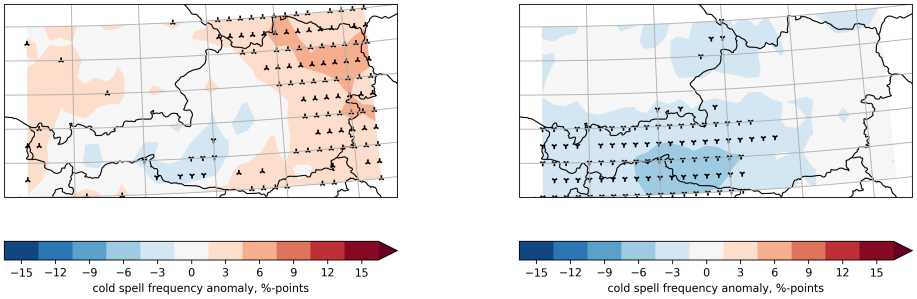


(b) **(c)**

Figure B.21.: Blocking in the northern mid-latitudes and cold spell frequency in Austria in September. (a) shows the blocking frequency anomaly in percentage points on days where at least one grid point in Austria is experiencing a heatwave. Marked black are the grid points for which this relationship is statistically significant. (b) shows the heatwave frequency anomaly in percentage points in Austria on days where at least 10 percent of the points marked as significantly positive in (a) are blocked. (c) is equivalent to (b), but for the points in (a) marked as significantly negative.

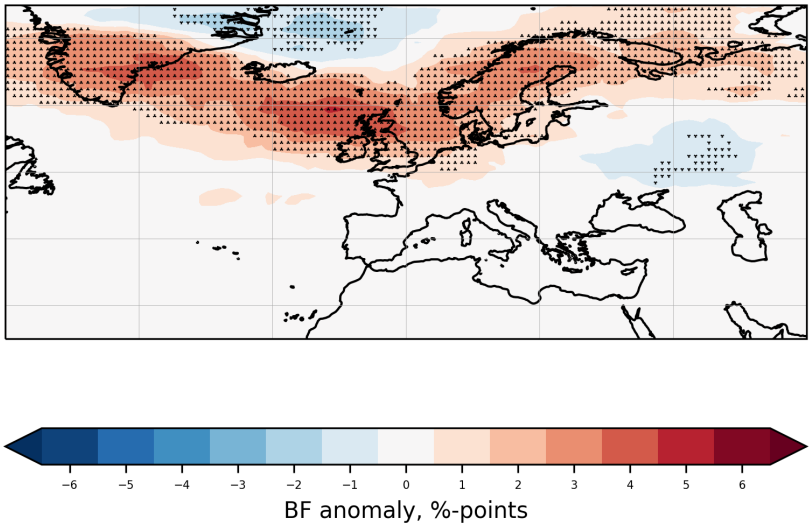


(a)

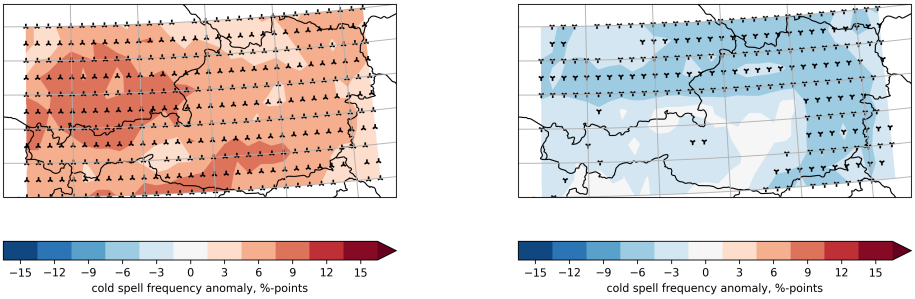


(b) **(c)**

Figure B.22.: Blocking in the northern mid-latitudes and cold spell frequency in Austria in October. (a) shows the blocking frequency anomaly in percentage points on days where at least one grid point in Austria is experiencing a heatwave. Marked black are the grid points for which this relationship is statistically significant. (b) shows the heatwave frequency anomaly in percentage points in Austria on days where at least 10 percent of the points marked as significantly positive in (a) are blocked. (c) is equivalent to (b), but for the points in (a) marked as significantly negative.

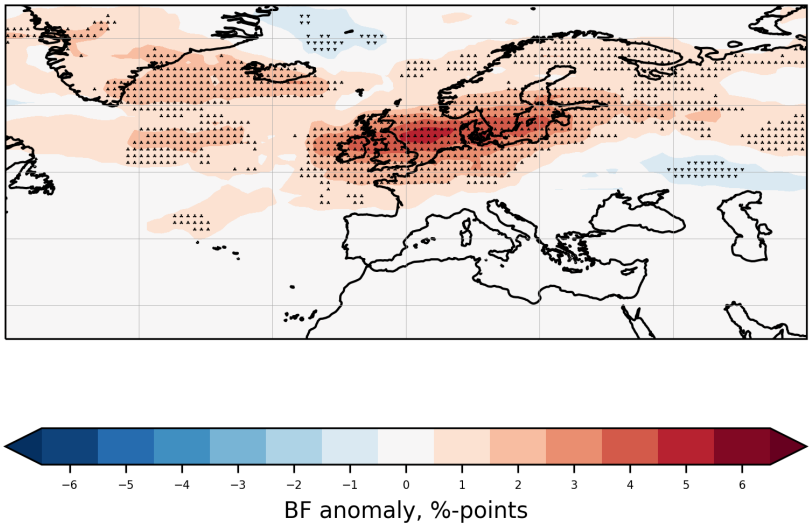


(a)

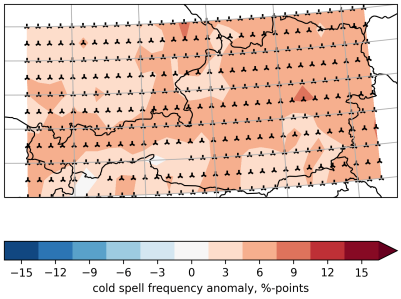


(b) **(c)**

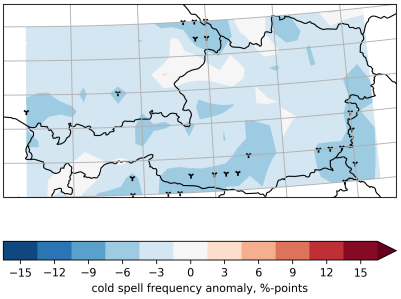
Figure B.23.: Blocking in the northern mid-latitudes and cold spell frequency in Austria in November. (a) shows the blocking frequency anomaly in percentage points on days where at least one grid point in Austria is experiencing a heatwave. Marked black are the grid points for which this relationship is statistically significant. (b) shows the heatwave frequency anomaly in percentage points in Austria on days where at least 10 percent of the points marked as significantly positive in (a) are blocked. (c) is equivalent to (b), but for the points in (a) marked as significantly negative.



(a)

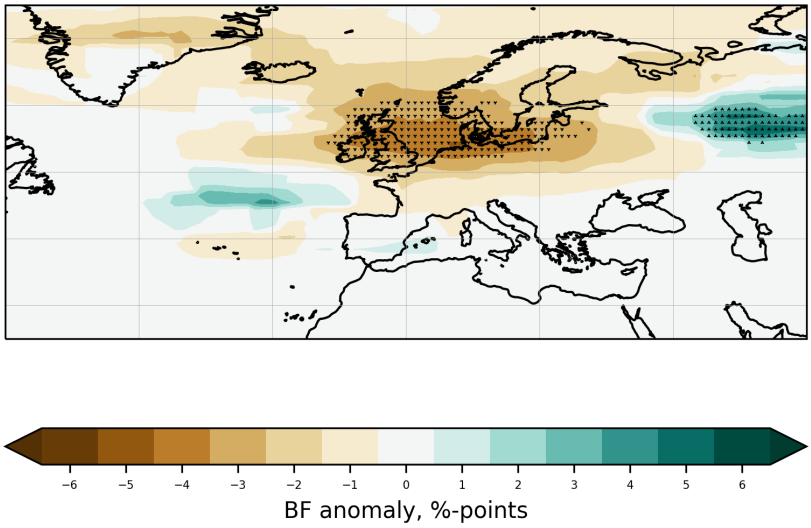


(b)

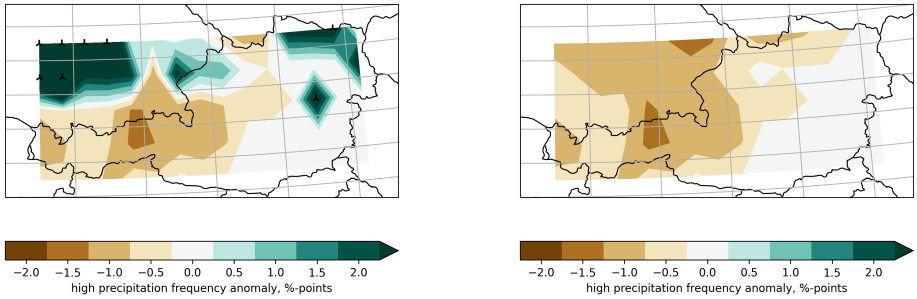


(c)

Figure B.24.: Blocking in the northern mid-latitudes and cold spell frequency in Austria in December. (a) shows the blocking frequency anomaly in percentage points on days where at least one grid point in Austria is experiencing a heatwave. Marked black are the grid points for which this relationship is statistically significant. (b) shows the heatwave frequency anomaly in percentage points in Austria on days where at least 10 percent of the points marked as significantly positive in (a) are blocked. (c) is equivalent to (b), but for the points in (a) marked as significantly negative.

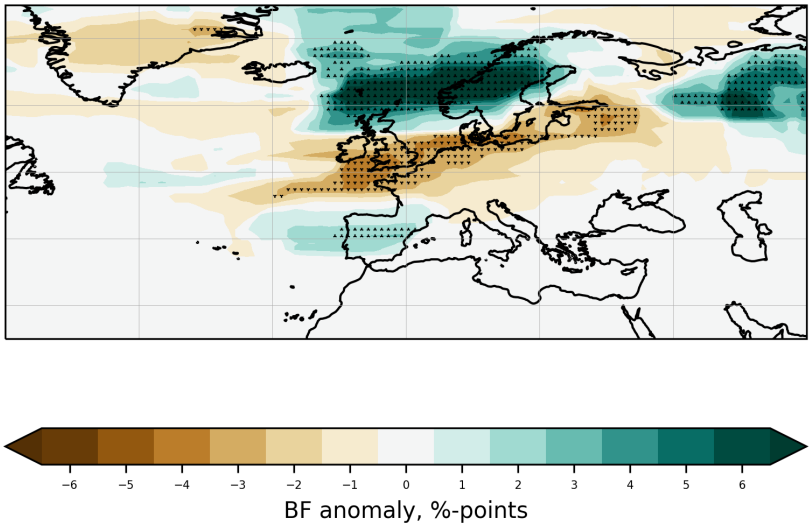


(a)

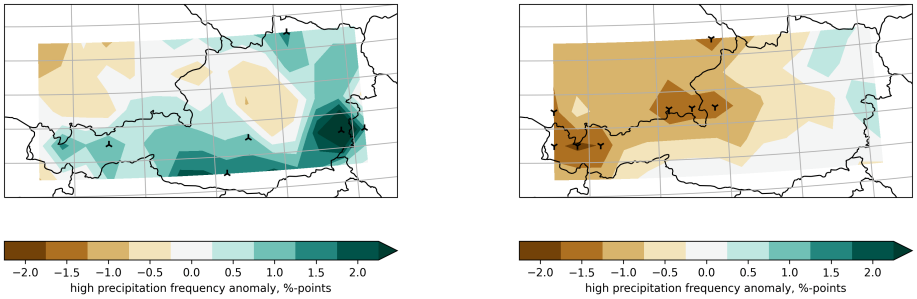


(b) **(c)**

Figure B.25.: Blocking in the northern mid-latitudes and heavy precipitation frequency in Austria in January. (a) shows the blocking frequency anomaly in percentage points on days where at least one grid point in Austria is experiencing a heatwave. Marked black are the grid points for which this relationship is statistically significant. (b) shows the heatwave frequency anomaly in percentage points in Austria on days where at least 10 percent of the points marked as significantly positive in (a) are blocked. (c) is equivalent to (b), but for the points in (a) marked as significantly negative.

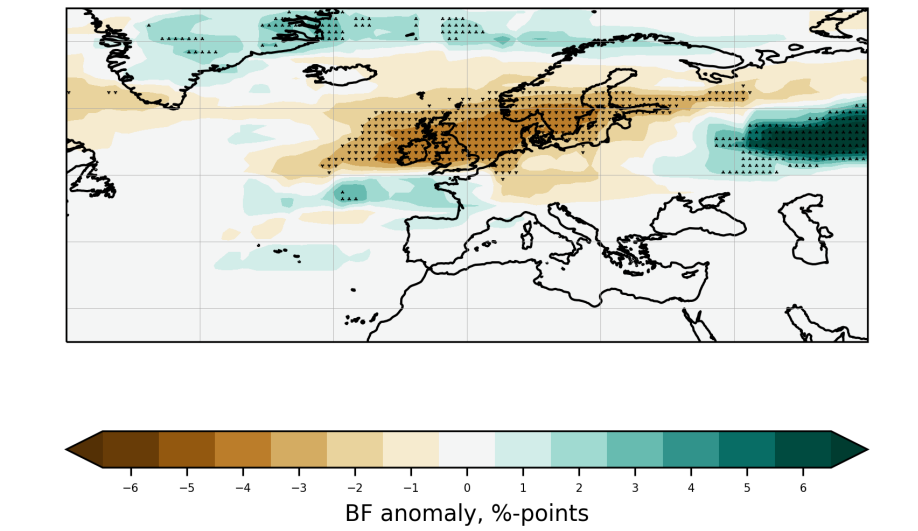


(a)

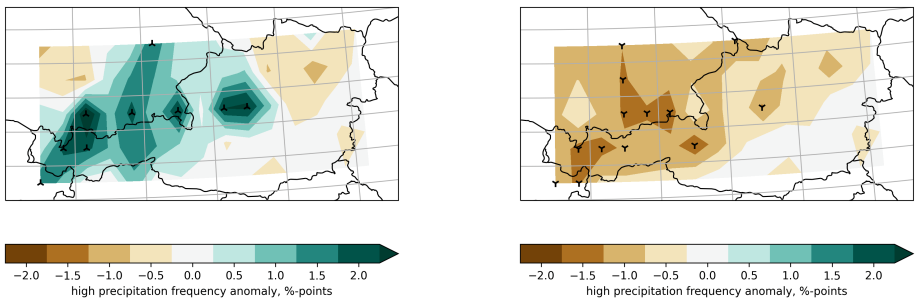


(b) **(c)**

Figure B.26.: Blocking in the northern mid-latitudes and heavy precipitation frequency in Austria in February. (a) shows the blocking frequency anomaly in percentage points on days where at least one grid point in Austria is experiencing a heatwave. Marked black are the grid points for which this relationship is statistically significant. (b) shows the heatwave frequency anomaly in percentage points in Austria on days where at least 10 percent of the points marked as significantly positive in (a) are blocked. (c) is equivalent to (b), but for the points in (a) marked as significantly negative.

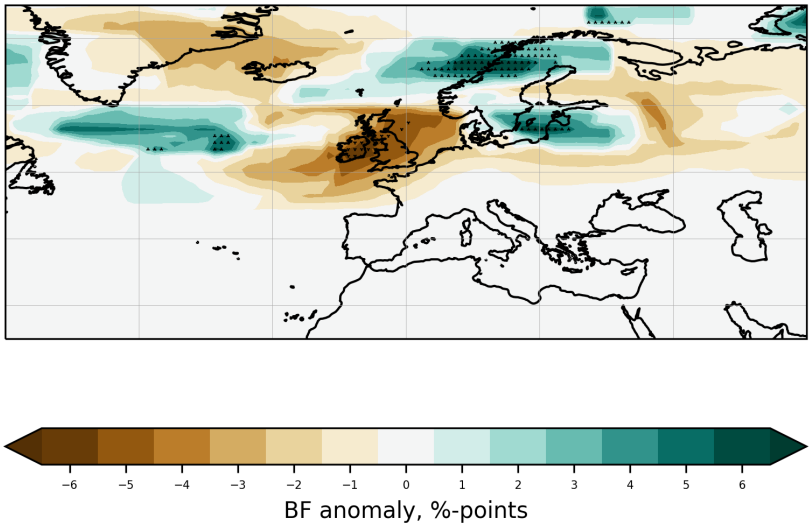


(a)

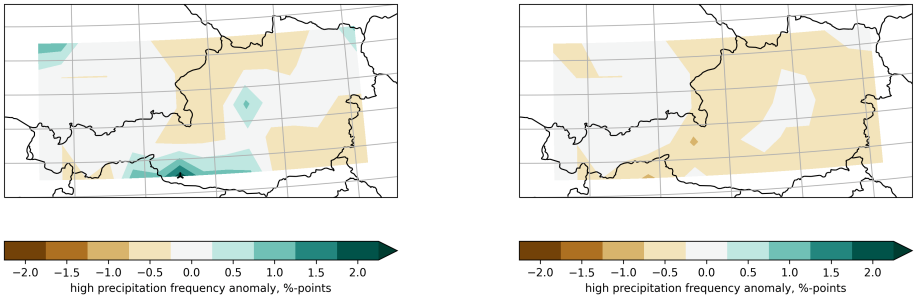


(b) **(c)**

Figure B.27.: Blocking in the northern mid-latitudes and heavy precipitation frequency in Austria in March. (a) shows the blocking frequency anomaly in percentage points on days where at least one grid point in Austria is experiencing a heatwave. Marked black are the grid points for which this relationship is statistically significant. (b) shows the heatwave frequency anomaly in percentage points in Austria on days where at least 10 percent of the points marked as significantly positive in (a) are blocked. (c) is equivalent to (b), but for the points in (a) marked as significantly negative.

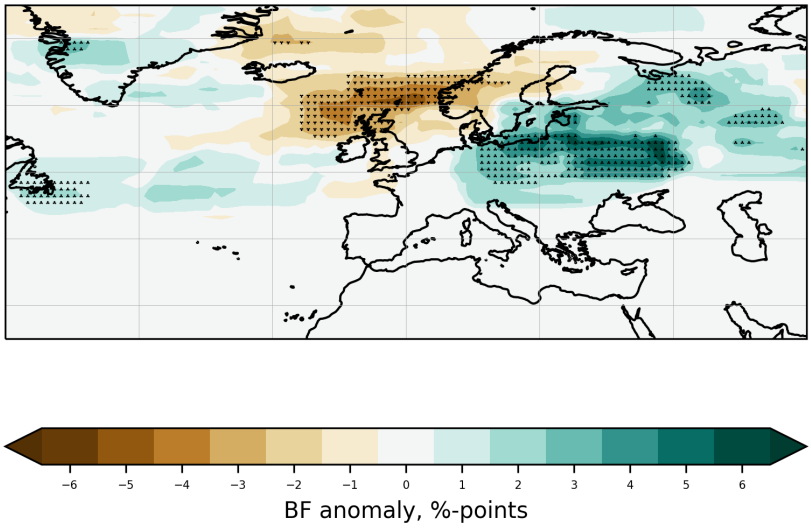


(a)

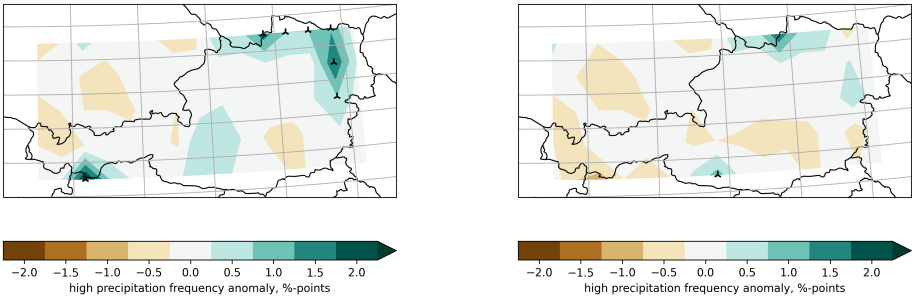


(b) **(c)**

Figure B.28.: Blocking in the northern mid-latitudes and heavy precipitation frequency in Austria in April. (a) shows the blocking frequency anomaly in percentage points on days where at least one grid point in Austria is experiencing a heatwave. Marked black are the grid points for which this relationship is statistically significant. (b) shows the heatwave frequency anomaly in percentage points in Austria on days where at least 10 percent of the points marked as significantly positive in (a) are blocked. (c) is equivalent to (b), but for the points in (a) marked as significantly negative.

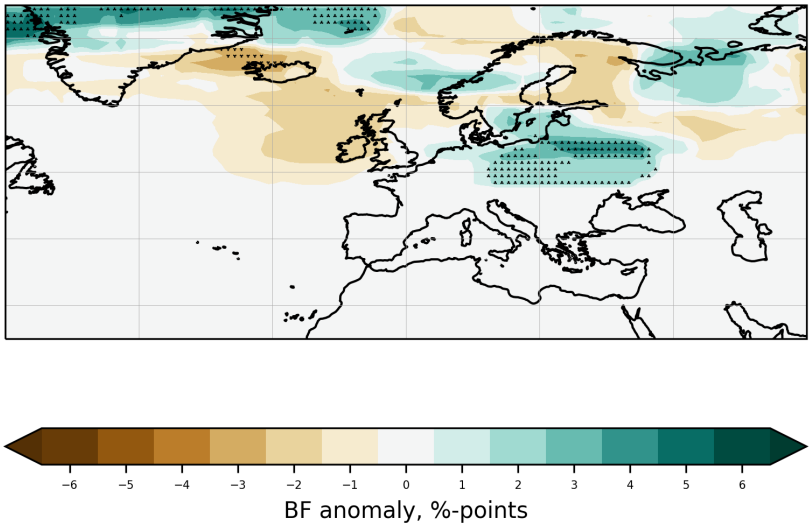


(a)

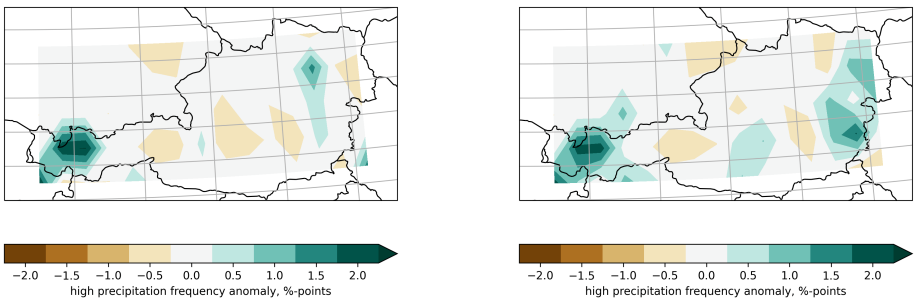


(b) **(c)**

Figure B.29.: Blocking in the northern mid-latitudes and heavy precipitation frequency in Austria in May. (a) shows the blocking frequency anomaly in percentage points on days where at least one grid point in Austria is experiencing a heatwave. Marked black are the grid points for which this relationship is statistically significant. (b) shows the heatwave frequency anomaly in percentage points in Austria on days where at least 10 percent of the points marked as significantly positive in (a) are blocked. (c) is equivalent to (b), but for the points in (a) marked as significantly negative.

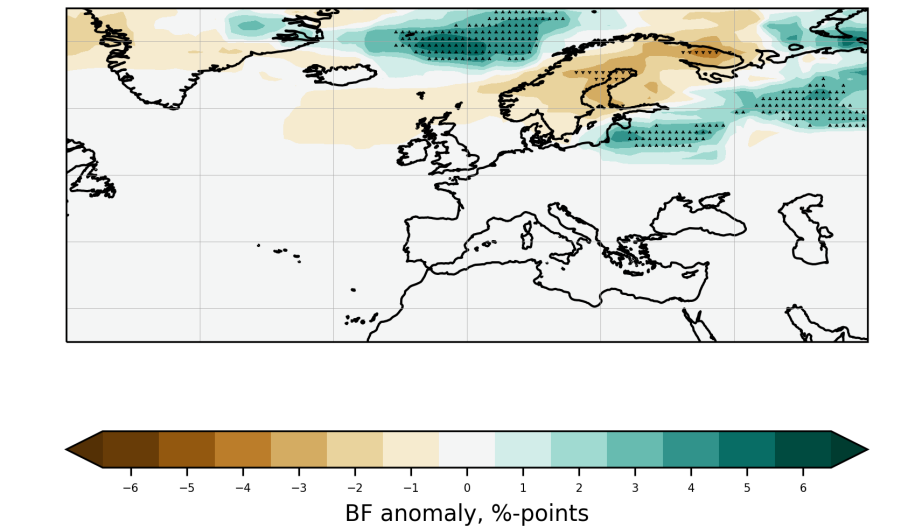


(a)

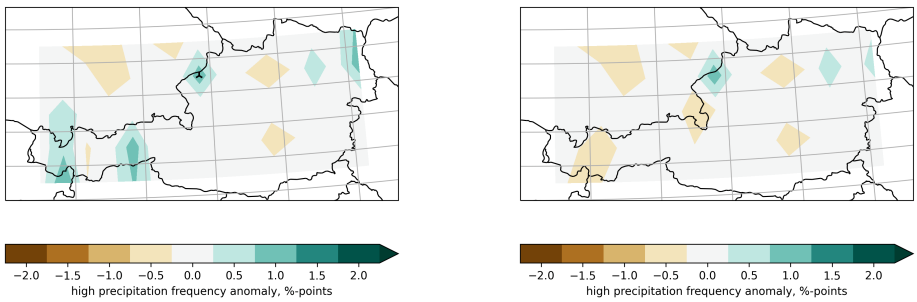


(b) **(c)**

Figure B.30.: Blocking in the northern mid-latitudes and heavy precipitation frequency in Austria in June. (a) shows the blocking frequency anomaly in percentage points on days where at least one grid point in Austria is experiencing a heatwave. Marked black are the grid points for which this relationship is statistically significant. (b) shows the heatwave frequency anomaly in percentage points in Austria on days where at least 10 percent of the points marked as significantly positive in (a) are blocked. (c) is equivalent to (b), but for the points in (a) marked as significantly negative.

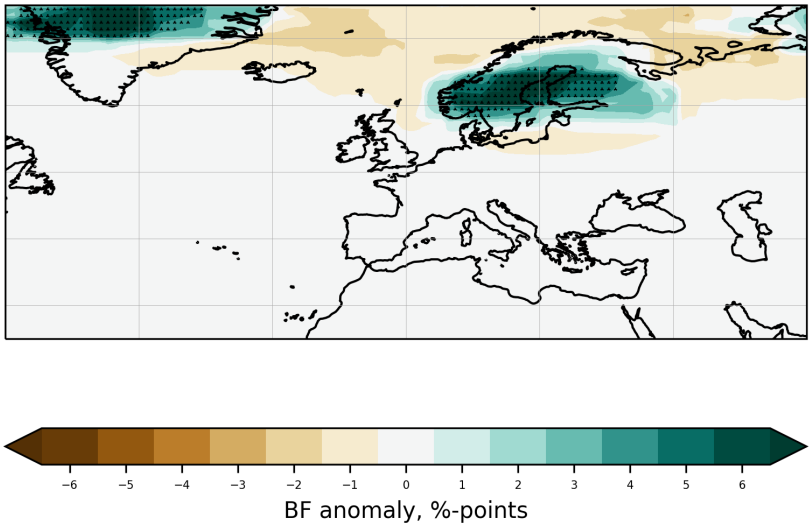


(a)

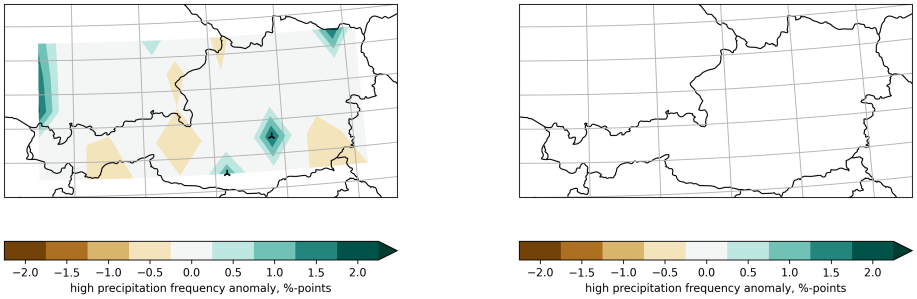


(b) **(c)**

Figure B.31.: Blocking in the northern mid-latitudes and heavy precipitation frequency in Austria in July. (a) shows the blocking frequency anomaly in percentage points on days where at least one grid point in Austria is experiencing a heatwave. Marked black are the grid points for which this relationship is statistically significant. (b) shows the heatwave frequency anomaly in percentage points in Austria on days where at least 10 percent of the points marked as significantly positive in (a) are blocked. (c) is equivalent to (b), but for the points in (a) marked as significantly negative.

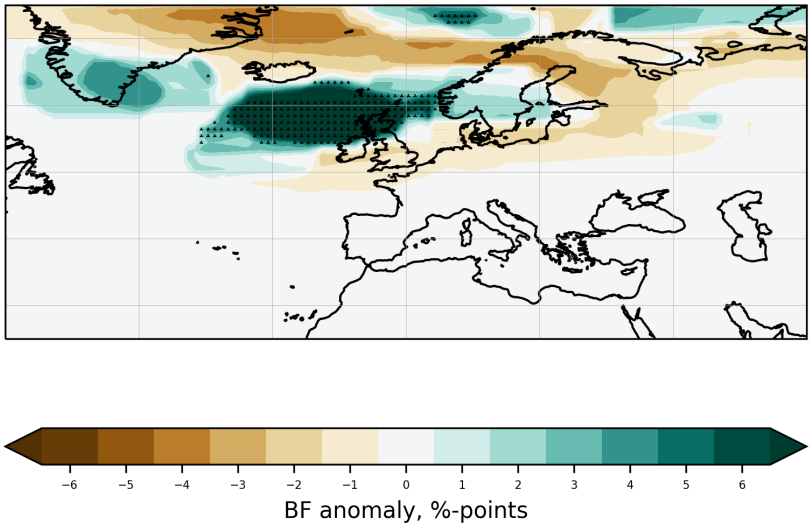


(a)

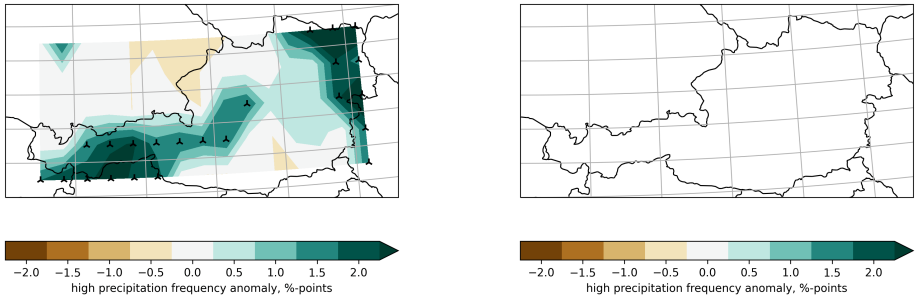


(b) **(c)**

Figure B.32.: Blocking in the northern mid-latitudes and heavy precipitation frequency in Austria in August. (a) shows the blocking frequency anomaly in percentage points on days where at least one grid point in Austria is experiencing a heatwave. Marked black are the grid points for which this relationship is statistically significant. (b) shows the heatwave frequency anomaly in percentage points in Austria on days where at least 10 percent of the points marked as significantly positive in (a) are blocked. (c) is equivalent to (b), but for the points in (a) marked as significantly negative.

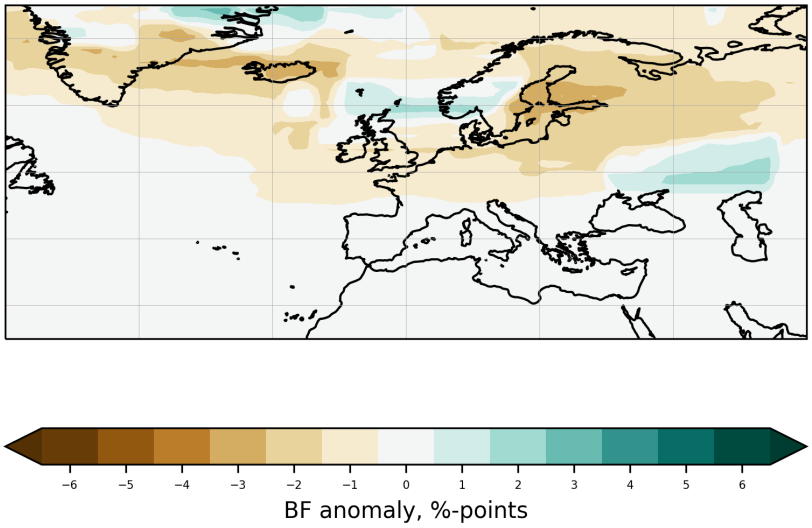


(a)

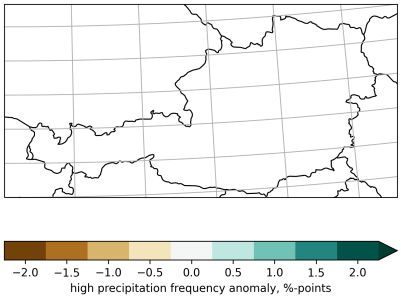


(b) **(c)**

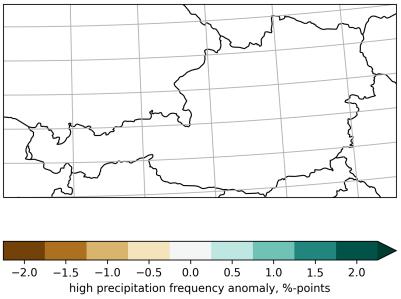
Figure B.33.: Blocking in the northern mid-latitudes and heavy precipitation frequency in Austria in September. (a) shows the blocking frequency anomaly in percentage points on days where at least one grid point in Austria is experiencing a heatwave. Marked black are the grid points for which this relationship is statistically significant. (b) shows the heatwave frequency anomaly in percentage points in Austria on days where at least 10 percent of the points marked as significantly positive in (a) are blocked. (c) is equivalent to (b), but for the points in (a) marked as significantly negative.



(a)

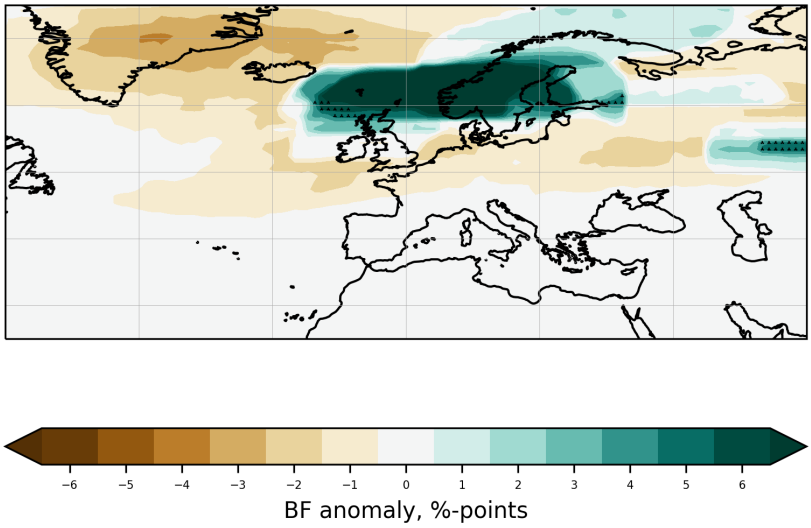


(b)

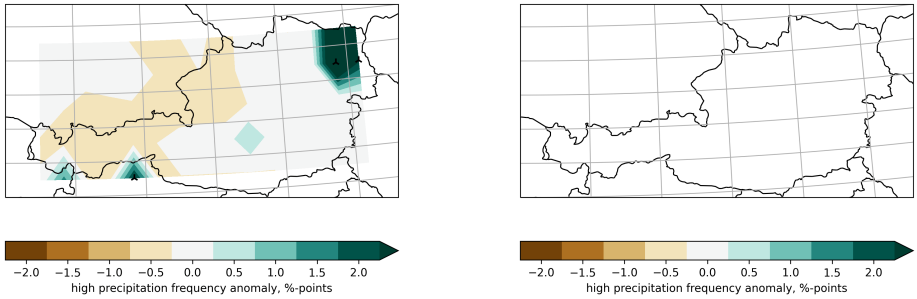


(c)

Figure B.34.: Blocking in the northern mid-latitudes and heavy precipitation frequency in Austria in October. (a) shows the blocking frequency anomaly in percentage points on days where at least one grid point in Austria is experiencing a heatwave. Marked black are the grid points for which this relationship is statistically significant. (b) shows the heatwave frequency anomaly in percentage points in Austria on days where at least 10 percent of the points marked as significantly positive in (a) are blocked. (c) is equivalent to (b), but for the points in (a) marked as significantly negative.

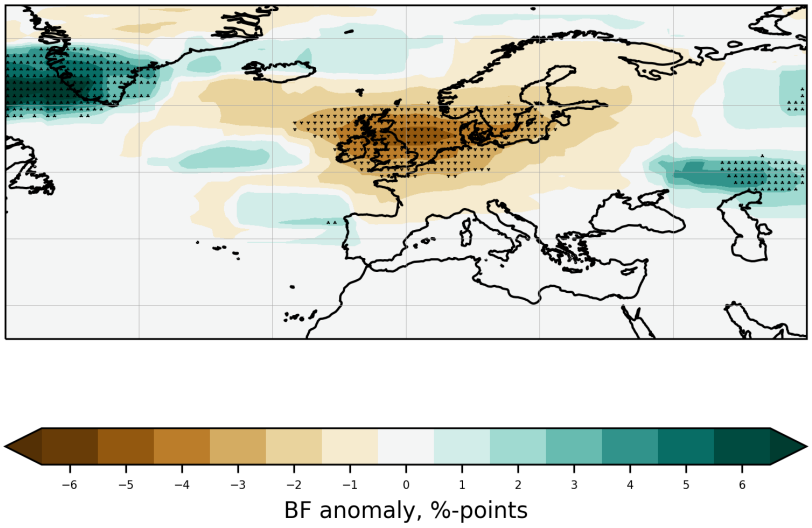


(a)

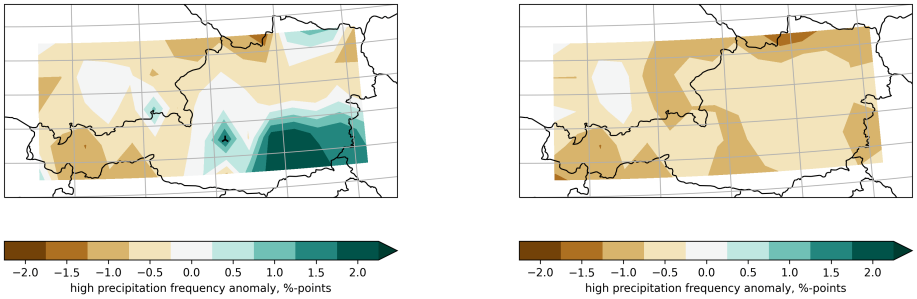


(b) **(c)**

Figure B.35.: Blocking in the northern mid-latitudes and heavy precipitation frequency in Austria in November. (a) shows the blocking frequency anomaly in percentage points on days where at least one grid point in Austria is experiencing a heatwave. Marked black are the grid points for which this relationship is statistically significant. (b) shows the heatwave frequency anomaly in percentage points in Austria on days where at least 10 percent of the points marked as significantly positive in (a) are blocked. (c) is equivalent to (b), but for the points in (a) marked as significantly negative.



(a)



(b) **(c)**

Figure B.36.: Blocking in the northern mid-latitudes and heavy precipitation frequency in Austria in December. (a) shows the blocking frequency anomaly in percentage points on days where at least one grid point in Austria is experiencing a heatwave. Marked black are the grid points for which this relationship is statistically significant. (b) shows the heatwave frequency anomaly in percentage points in Austria on days where at least 10 percent of the points marked as significantly positive in (a) are blocked. (c) is equivalent to (b), but for the points in (a) marked as significantly negative.

C. Plain Language: Methods

Determining whether or not something happens more (or less) often now than it did in the past usually involves something called "trend estimation", and it is tricky business. It is called an *estimation* because, assuming that such changes exist, we can never truly know how strong they are; But we can work out an estimate and make sure that we are convinced that it is reasonably similar to the true value. There are many (almost arbitrarily complex) methods to estimate the strength of change, which we call a *trend*, and each has its own advantages and disadvantages. In this thesis, we used a basic approach called the *first order linear regression*. This is how it works: Imagine for a moment that a friend, who is a passionate fan of the "Star Wars" movie franchise, asks you to watch the movies. Pulling up the Wikipedia entry on the franchise, you discover that there are nine whole movies in the main series; This seems like a lot of time to waste on movies that you may not like. However, you watch the first episode ("The Phantom Menace") and decide that it is not too bad after all. But how can you know that the movies do not get progressively worse? Of course, it would be a nonsensical approach to watch all the movies to determine if they do get worse; Lets say you found out that they do, you could not apply your new knowledge to save time, because you already watched all of the movies. So you might simply watch the first, fifth and ninth episode and then, based on your incomplete data, *estimate a trend* and decide not to watch the rest of the movies if it is a *downward trend*, which is to say that you estimated that they do get worse. Let us say you come up with a scale from 0 to 10 where you assign 10 stars to the first episode, as it is very good, 8 to the fifth, because you still quite liked it, and 3 to the ninth, because you thought it was horrible but still liked the soundtrack. From the first to the fifth episode, the franchise lost 2 stars in your ranking; from the fifth to the ninth, it lost 5 further stars. How much stars, per episode, do you then expect to lose on average? In other words, if you had to predict, based on your data, how many stars you would assign to, for example, the second episode if you did watch it — how could you go about this? This is exactly the kind of question that a linear regression can answer. It asks: Based on the data we have, how do we expect one phenomenon (the number of the episode) to influence some other variable (your enjoyment of the episode as expressed in stars)? We have definitive answers to the quality of the first, fifth and ninth episode, and now we estimate how much you might like the others without making you actually watch them. Take a look at Figure C.1. The episodes you have watched have been assigned a certain quality, marked with red crosses. You will notice that it is impossible to connect them with one straight line. Instead, the linear regression algorithm calculated a straight line such that

the combined distance from the points to the line is as small as it could possibly be (a linear regression algorithm does not necessarily have to use this criterion, called "least squares" criterion, for placing the line; however, it is a very reasonable one).

Tilting or shifting this line would inevitably mean that if we add up all the distances between the crosses and the line, the sum would be larger than when we do the same with the line that has been given to us by the linear regression algorithm. This means that there is no way to draw a straight line that is in better agreement with the data we already have (the red crosses). You might shift or tilt it in a way that makes it hit one of the crosses directly, but then it would be farther away from the others. The slope of this line now gives us an estimate of how much worse we would expect you to find any given episode in comparison to the previous one. This is how linear regression, in a very simple case, works. We used it to determine how much more or less long-lasting high pressure systems we expect in any given month when compared to the previous month. In case you noticed a few possible pitfalls of this strategy — for example, you might really like the sixth episode once you do decide to watch it; or even worse, there is a possibility that you would have loved all the remaining episodes, but decide not to watch them because your dissatisfaction with number nine meant that the algorithm told you they get substantially worse with every episode — you are right, and these potential problems do carry over into real world problems. In our example, we had only three data points to go off of. In reality, people strive to obtain more data before attempting to estimate trends in this way; and they are ideally very careful about statistical outliers like episode nine in our example, which fall far outside of the scope of all of the other data points, because they can unfairly influence the estimated trends especially if they occur near the beginning or the end of your sample. There are a number of tools, such as the p-value, which can be used to assess whether or not you can place confidence in the estimated trend; it is about 0.15 in our example, which would generally be regarded as too high to believe the results. To find out how this works, you will have to find an appropriate lecture and learn about null-hypotheses and statistical errors; For now, it should suffice to say that we put in the effort to find out which of the trends that we found are reasonably trustworthy.

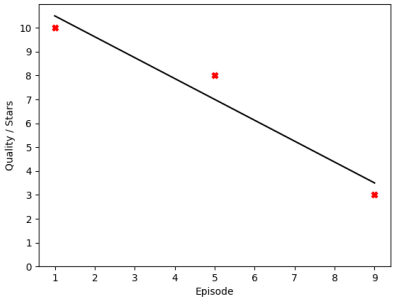


Figure C.1.: Linear regression scheme applied to fictitious ratings of "Star Wars" episodes to illustrate the general technique for the plain language summary.

Disclaimer: The ratings of the "Star Wars" episodes in this example are entirely fictitious; The author does not claim to agree with them in any way, shape or form, nor does he claim to disagree. Indeed, he hopes to avoid any heated discussion on the topic.

The connection between long-lasting high pressure systems and extreme weather in Austria was then investigated by looking at all the days where these extreme weather situations occurred in Austria and then determining in which regions there tend to be more long-lasting high pressure areas on these days compared to the normal situation. This approach has a drawback: It could be that, purely by coincidence, such high pressure systems and extreme weather situations in Austria happened at the same day without being, in fact, connected in any way. Imagine that you like to visit a bar after work every Friday to enjoy a cold glass of beer as a reward for a week's worth of hard work. You have a friend who is less proficient in the art of self-restraint: He visits the bar every day after work. One Friday, the two of you are served stale beer and engage in a casual conversation about the quality of the beer at this bar. Because you are both avid statisticians, you have kept a thorough record. Your friend calculates that about three percent of the beers he is served are stale. You arrive at a slightly higher estimate: Four percent. You and your friend might now conclude that Friday nights are bad days for ordering beer at that bar — but this conclusion is extremely dangerous and, quite possibly, false! Perhaps no stale beer is served on Mondays, and ten percent of beers served on Wednesdays are stale; You do not know, because you only looked at the estimates for the overall week and Fridays in particular. The solution to your conundrum is to ask the people around you, with less strict bar-going schedules. They simply go to this bar whenever they feel like it. If most of them report a stale-beer-estimate of roughly three percent, like your friend, then it has become dramatically more likely that Friday nights are, at a four percent rate of stale beer, indeed a bad day for going to that bar; perhaps the barkeeper on duty on Friday is not particularly good at drafting beer and you should change your order or switch to another day. But if the stale-beer-estimates reported by the other bargoers vary strongly between, lets say, zero and seven percent, then it is probably coincidence that the Friday night estimate is slightly above the average number. Perhaps the tap is defective and an average of three percent of beers come out stale no matter what the barkeeper does, and you were just unlucky enough to have been served a few more of them. This is a simplified example, but the point is that despite the slightly higher number of stale beverages you received in comparison to your friend, it is worth putting in some work to find evidence regarding the question of whether or not the phenomena *stale beer* and *Friday nights* are indeed causally connected. This method of asking many random people about their experience (i.e. *drawing random samples*) is essentially what a so called "Monte-Carlo algorithm" does. We used it to ensure that the connection we found between the high-pressure systems and extreme weather events in Austria is not purely coincidental.

Of course, it is possible that despite your best efforts to rule out coincidence, the beer tap, just by chance, happened to malfunction most often on a Friday night. This would lead you to unfairly assume that the barkeeper is not the best of his craft even after conducting your Monte-Carlo style investigation. The blight that haunts statistics is that you can never definitively rule out coincidence; You can merely work hard to push back against it.

Acronyms

CMIP6 Coupled Model Intercomparison Project Phase 6.

ERA5 ECMWF Re-Analysis Version 5.

ERA-Interim ECMWF Re-Analysis Interim.

ECMWF European Centre for Medium-Range Weather Forecasts.

IPCC Intergovernmental Panel on Climate Change.

ITCZ Intertropical Convergence Zone.

NAO North Atlantic Oscillation.

WFD WATCH Forcing Data.

WEGC Wegener Center for Climate and Global Change [University of Graz].

List of Figures

2.1. Schematic of the large-scale atmospheric circulation. 4
2.2. Schematic of the three circulation cells as cogs. 5
2.3. Examples of typical blocking situations. 7

3.1. Blocking situation between June 24th and June 29th, 2009. 12

4.1. Grid points relevant for extreme event detection. 16

5.1. Blocking frequency and trends from December to May (a-f). The upper subpanels show the 30-year average blocking frequency for different periods, shifted by 5 years each. The lower subpanels show the trends in blocking frequency. The grey corridor marks the standard error of the trend slope. Significant trends are shown in red (p = 0.05). 23
5.2. Blocking frequency and trends from June to November (a-f). The upper subpanels show the 30-year average blocking frequency for different periods, shifted by 5 years each. The lower subpanels show the trends in blocking frequency. The grey corridor marks the standard error of the trend slope. Significant trends are shown in red (p = 0.05). 24
5.3. Blocking frequency trends during winter months (2-dim). Dark crosses mark grid points for which the trend is statistically significant. 25
5.4. Blocking frequency trends during spring months (2-dim). Dark crosses mark grid points for which the trend is statistically significant. 26
5.5. Blocking frequency trends during summer months (2-dim). Dark crosses mark grid points for which the trend is statistically significant. 27
5.6. Blocking frequency trends during autumn months (2-dim). Dark crosses mark grid points for which the trend is statistically significant. 28

6.1. Blocking frequency climatology over Europe, Greenland and the North Atlantic. 30
6.2. Heatwave frequency climatology in Austria. 31
6.3. Cold spell frequency climatology in Austria. 32
6.4. High precipitation frequency climatology in Austria. 33
6.5. Blocking over the northern midlatitudes and heatwave frequency in Austria (period 1980 – 2018). 35
6.6. Blocking frequency over the northern midlatitudes and heatwave frequency in Austria for MJJASO (1980 – 2018) 36

6.7. Blocking frequency over the northern midlatitudes and heatwave frequency in Austria for NDJFMA (1980 – 2018) 37
6.8. Blocking frequency over the northern midlatitudes and heatwave frequency in Austria for DJFM (1980 – 2018) 38
6.9. Blocking over the northern midlatitudes and cold spell frequency in Austria (period 1980 – 2018). 41
6.10. Blocking frequency over the northern midlatitudes and cold spell frequency in Austria for MJJASO (1980 – 2018) 42
6.11. Blocking frequency over the northern midlatitudes and cold spell frequency in Austria for NDJFMA (1980 – 2018) 43
6.12. Blocking frequency over the northern midlatitudes and cold spell frequency in Austria for DJFM (1980 – 2018) 44
6.13. Blocking over the northern midlatitudes and heavy precipitation frequency in Austria (period 1980 – 2018). 46
6.14. Blocking frequency over the northern midlatitudes and heavy precipitation frequency in Austria for MJJASO (1980 – 2018) 47
6.15. Blocking frequency over the northern midlatitudes and heavy precipitation frequency in Austria for NDJFMA (1980 – 2018) 48
6.16. Blocking frequency over the northern midlatitudes and heavy precipitation frequency in Austria for DJFM (1980 – 2018) 49

B.1. Blocking in the northern mid-latitudes and heatwave frequency in Austria, January. 58
B.2. Blocking in the northern mid-latitudes and heatwave frequency in Austria, February. 59
B.3. Blocking in the northern mid-latitudes and heatwave frequency in Austria, March. 60
B.4. Blocking in the northern mid-latitudes and heatwave frequency in Austria, April. 61
B.5. Blocking in the northern mid-latitudes and heatwave frequency in Austria, May. 62
B.6. Blocking in the northern mid-latitudes and heatwave frequency in Austria, June. 63
B.7. Blocking in the northern mid-latitudes and heatwave frequency in Austria, July. 64
B.8. Blocking in the northern mid-latitudes and heatwave frequency in Austria, August. 65
B.9. Blocking in the northern mid-latitudes and heatwave frequency in Austria, September. 66
B.10. Blocking in the northern mid-latitudes and heatwave frequency in Austria, October. 67
B.11. Blocking in the northern mid-latitudes and heatwave frequency in Austria, November. 68

B.12. Blocking in the northern mid-latitudes and heatwave frequency in Austria, December. 69
B.13. Blocking in the northern mid-latitudes and cold spell frequency in Austria, January. 70
B.14. Blocking in the northern mid-latitudes and cold spell frequency in Austria, February. 71
B.15. Blocking in the northern mid-latitudes and cold spell frequency in Austria, March. 72
B.16. Blocking in the northern mid-latitudes and cold spell frequency in Austria, April. 73
B.17. Blocking in the northern mid-latitudes and cold spell frequency in Austria, May. 74
B.18. Blocking in the northern mid-latitudes and cold spell frequency in Austria, June. 75
B.19. Blocking in the northern mid-latitudes and cold spell frequency in Austria, July. 76
B.20. Blocking in the northern mid-latitudes and cold spell frequency in Austria, August. 77
B.21. Blocking in the northern mid-latitudes and cold spell frequency in Austria, September. 78
B.22. Blocking in the northern mid-latitudes and cold spell frequency in Austria, October. 79
B.23. Blocking in the northern mid-latitudes and cold spell frequency in Austria, November. 80
B.24. Blocking in the northern mid-latitudes and cold spell frequency in Austria, December. 81
B.25. Blocking in the northern mid-latitudes and heavy precipitation frequency in Austria, January. 82
B.26. Blocking in the northern mid-latitudes and heavy precipitation frequency in Austria, February. 83
B.27. Blocking in the northern mid-latitudes and heavy precipitation frequency in Austria, March. 84
B.28. Blocking in the northern mid-latitudes and heavy precipitation frequency in Austria, April. 85
B.29. Blocking in the northern mid-latitudes and heavy precipitation frequency in Austria, May. 86
B.30. Blocking in the northern mid-latitudes and heavy precipitation frequency in Austria, June. 87
B.31. Blocking in the northern mid-latitudes and heavy precipitation frequency in Austria, July. 88
B.32. Blocking in the northern mid-latitudes and heavy precipitation frequency in Austria, August. 89
B.33. Blocking in the northern mid-latitudes and heavy precipitation frequency in Austria, September. 90

B.34. Blocking in the northern mid-latitudes and heavy precipitation frequency in Austria, October. 91
B.35. Blocking in the northern mid-latitudes and heavy precipitation frequency in Austria, November. 92
B.36. Blocking in the northern mid-latitudes and heavy precipitation frequency in Austria, December. 93

C.1. Linear regression scheme applied to fictitious ratings of "Star Wars" episodes to illustrate the general technique for the plain language summary. 96

List of Tables

4.1. Definition of the Austrian region. 16

A.1. Regions investigated for trends, trends and p-values for statistical significance. 55

Bibliography

Barnes, E. A., E. Dunn-Sigouin, G. Masato, and T. Woollings (2014). "Exploring recent trends in Northern Hemisphere blocking". *Geophys. Res. Lett.* 41. DOI: 10.1002/2013GL058745.

Bell, B., H. Hersbach, A. Simmons, P. Berrisford, P. Dahlgren, A. Horányi, J. Muñoz-Sabater, J. Nicolas, R. Radu, D. Schepers, C. Soci, S. Villaume, J.-R. Bidlot, L. Haimberger, J. Woollen, C. Buontempo, and J.-N. Thépautt (2021). "The ERA5 global reanalysis: Preliminary extension to 1950". *Q. J. R. Meteor. Soc.* 147.741, pp. 4186–4227. DOI: 10.1002/qj.4174.

Bieli, M., S. Pfahl, and H. Wernli (2015). "A Lagrangian investigation of hot and cold temperature extremes in Europe". *Q. J. R. Meteor. Soc.* 141.686, pp. 98–108. DOI: 10.1002/qj.2339.

Brunner, L., G. C. Hegerl, and A. K. Steiner (2017). "Connecting atmospheric blocking to European temperature extremes in spring". *J. Climate* 30.2, pp. 585–594. DOI: 10.1175/JCLI-D-16-0518.1.

Brunner, L., N. Schaller, J. Anstey, J. Sillmann, and A. K. Steiner (2018). "Dependence of Present and Future European Temperature Extremes on the Location of Atmospheric Blocking". *Geophys. Res. Lett.* 45, pp. 6311–6320. DOI: 10.1029/2018GL077837.

Brunner, L. and A. K. Steiner (2017). "A global perspective on atmospheric blocking using GPS radio occultation – one decade of observations". *Atmos. Meas. Tech.* 10, pp. 4727–4745. DOI: 10.5194/amt-10-4727-2017.

Brunner, L., A. K. Steiner, B. Scherllin-Pirscher, and M. W. Jury (2016). "Exploring atmospheric blocking with GPS radio occultation observations". *Atmos. Chem. Phys.* 16.7, pp. 4593–4604. DOI: 10.5194/acp-16-4593-2016.

Cucchi, M., G. P. Weedon, A. Amici, N. Bellouin, S. Lange, H. M. Schmied, H. Hersbach, and C. Buontempo (2020). "WFDE5: bias-adjusted ERA5 reanalysis data for impact studies". *Earth Sys. Sci. Data* 12.3, pp. 2097–2120. DOI: 10.5194/essd-12-2097-2020.

Davini, P., C. Cagnazzo, S. Gualdi, and A. Navarra (2012). "Bidimensional diagnostics, variability, and trends of Northern Hemisphere blocking". *J. Climate* 25, pp. 6496–6509. DOI: 10.1175/JCLI-D-12-00032.1.

Davini, P. and F. D'Andrea (2020). "From CMIP3 to CMIP6: Northern Hemisphere Atmospheric Blocking Simulation in Present and Future Climate". *J. Climate* 33.23, pp. 10021–10038. DOI: 10.1175/JCLI-D-19-0862.1.

deDonato, F. K., M. Leone, D. Noce, M. Davoli, and P. Michelozzi (2013). "The Impact of the February 2012 Cold Spell on Health in Italy Using Surveillance Data". *PLOS ONE* 8.4, e61720. DOI: 10.1371/journal.pone.0061720.

ECMWF (2020). *Fact Sheet: Reanalysis*. URL: https://www.ecmwf.int/en/about/media-centre/focus/2020/fact-sheet-reanalysis (visited on 04/20/2022).

Fekete, A. and S. Sandholz (2021). "Here Comes the Flood, but Not Failure? Lessons to Learn after the Heavy Rain and Pluvial Floods in Germany 2021". *Water* 13.21, pp. 1–20. DOI: 10.3390/w13213016.

Haiden, T. (2009). *Meteorologische Analyse des Niederschlags von 22.-25. Juni 2009*. Tech. rep. Zentralanstalt für Meteorologie und Geodynamik. URL: http://www.wetterberatung.net/docs/aktuell/2009-06-30_Meteorologische%20Analyse%20HOWA2009.pdf.

Hersbach, H. et al. (2020). "The ERA5 global reanalysis". *Q. J. R. Meteor. Soc.* 146.730, pp. 1999–2049. DOI: 10.1002/qj.3803.

Hornich, R. and R. Adelwöhrer (2010). "Landslides in Styria in 2009". *Geomech. and Tunnelling* 3.5. DOI: 10.1002/geot.201000042.

Hutter, H.-P., H. Moshammer, P. Wallner, B. Leitner, and M. Kundi (2007). "Heatwaves in Vienna: effects on mortality". *Wien. Klin. Wochenschr.* 119, pp. 223–227. DOI: 10.1007/s00508-006-0742-7.

IPCC (2013). *Climate Change 2013: The Physical Science Basis. Contribution of Working Group I to the Fifth Assessment Report of the Intergovernmental Panel on Climate Change*. Ed. by T. F. Stocker, D. Qin, G.-K. Plattner, M. Tignor, S. K. Allen, J. Boschung, A. Nauels, Y. Xia, V. Bex, and P. M. Midgley. Cambridge, United Kingdom and New York, NY, USA: Cambridge University Press. 1535 pp.

– (2021). *Climate Change 2021: The Physical Science Basis. Contribution of Working Group I to the Sixth Assessment Report of the Intergovernmental Panel on Climate Change*. Ed. by M.-D. V., P. Zhai, A. Pirani, S. L. Connors, C. Péan, S. Berger, N. Caud, Y. Chen, L. Goldfarb, M. I. Gomis, M. Huang, K. Leitzell, E. Lonnoy, J. B. R. Matthews, T. K. Maycock, T. Waterfield, O. Yelekçi, R. Yu, and B. Zhou. in press. Cambridge, United Kingdom and New York, NY, USA: Cambridge University Press.

Kalnay, E., M. Kanamitsu, R. Kistler, W. Collins, D. Deaven, L. Gandin, M. Iredell, S. Saha, G. White, J. Woollen, Y. Zhu, A. Leetmaa, R. Reynolds, M. Chelliah, W. Ebisuzaki, W. Higgins, J. Janowiak, K. C. Mo, C. Ropelewski, J. Wang, R. Jenne, and D. Joseph (1996). "The NCEP/NCAR 40-Year Reanalysis Project". *Bull. Amer. Meteor. Soc.* 77.3, pp. 437–471. DOI: 10.1175/1520-0477(1996)077<0437:TNYRP>2.0.CO;2.

Kyselý, J., E. Plavcová, H. Davídkovová, and J. Kynčl (2011). "Comparison of hot and cold spell effects on cardiovascular mortality in individual population groups in the Czech Republic". *Clim. Res.* 49, pp. 113–129. DOI: 10.3354/cr01014.

Matsueda, M. (2011). "Predictability of Euro-Russian blocking in summer of 2010". *Geophys. Res. Lett.* 38.6, L06801. DOI: 10.1029/2010GL046557.

Miller, S., K. Chua, J. Coggins, and H. Mohtadi (2021). "Heat Waves, Climate Change, and Economic Output". *J. Eur. Econ. Assoc.* 19.5, pp. 2658–2694. DOI: 10.1093/jeea/jvab009.

Mohr, S., J. Wandel, S. Lenggenhager, and O. Martius (2019). "Relationship between atmospheric blocking and warm-season thunderstorms over western and central Europe". *Q. J. R. Meteor. Soc.* 145.724, pp. 3040–3056. DOI: 10.1002/qj.3603.

Perkins, S. E. and L. V. Alexander (2013). "On the Measurement of Heat Waves". *J. Climate* 26, pp. 4500–4517. DOI: 10.1175/JCLI-D-12-00383.1.

Perlwitz, J., T. Knutson, and A. N. LeGrande (2017). "Large-scale circulation and climate variability". In: *Climate Science Special Report: Fourth National Climate Assessment, Volume I*. Ed. by D. Wuebbles, D. Fahey, K. Hibbard, D. Dokken, B. Stewart, and T. Maycock. U.S. Global Change Research Program, pp. 161–184. DOI: 10.7930/J0RV0KVQ.

Pfahl, S. (2014). "Characterising the relationship between weather extremes in Europe and synoptic circulation features". *Nat. Hazard. Earth Sys.* 14.6, pp. 1461–1475. DOI: 10.5194/nhess-14-1461-2014.

Russo, S., J. Sillmann, and E. M. Fischer (2015). "Top ten European heatwaves since 1950 and their occurrence in the coming decades". *Environ. Res. Lett.* 10.12, p. 124003. DOI: 10.1088/1748-9326/10/12/124003.

Seibert, P., A. Frank, and H. Formayer (2007). "Synoptic and regional patterns of heavy precipitation in Austria". *Theor. Appl. Climatol.* 87, pp. 139–153. DOI: 10.1007/s00704-006-0198-8.

Sousa, P. M., R. M. Trigo, D. Barriopedro, P. M. M. Soares, A. M. Ramos, and M. L. R. Liberato (2017). "Responses of European precipitation distributions and regimes to different blocking locations". *Climate Dyn.* 48.3, pp. 1141–1160. DOI: 10.1007/s00382-016-3132-5.

Unterberger, C., L. Brunner, S. Nabernegg, K. Steininger, A. K. Steiner, E. Stabentheiner, S. Monschein, and H. Truhetz (July 2018). "Spring frost risk for regional apple production under a warmer climate". *PLOS ONE* 13.7, pp. 1–18. DOI: 10.1371/journal.pone.0200201.

Vallis, G. K. (2017). *Atmospheric and Ocean Dynamics*. 2nd ed. Cambridge, United Kingdom: Cambridge University Press. ISBN: 978-1-10706550-5. DOI: 10.1017/9781107588417.

World Health Organization (2018). *Heat and Health*. URL: https://www.who.int/news-room/fact-sheets/detail/climate-change-heat-and-health (visited on 01/13/2023).

Yao, Y., D. Luo, A. Dai, and I. Simmonds (2017). "Increased Quasi Stationarity and Persistence of Winter Ural Blocking and Eurasian Extreme Cold Events in Response to Arctic Warming. Part I: Insights from Observationsal Analysis". 30.10, pp. 3549–3568. DOI: 10.1175/JCLI-D-16-0261.1.

Atmospheric blocking events are persistent high-pressure systems in the midlatitudes that can block the westerly flow usually prevailing in this region. They have previously been demonstrated to be connected to extreme weather events. This thesis aims to analyze trends in the frequency of blocking events over the northern mid-latitudes and to investigate the connection between blocking and extreme weather events specifically in Austria. We used ECMWF Re-Analysis Version 5 (ERA5) data (1950–2019) and applied a blocking detection algorithm and ordinary linear regression to detect trends. The connection between blocking and extreme weather was investigated using ERA5 and WATCH Forcing Data ERA 5 (WFDE5) (1980–2018) by applying a Monte-Carlo algorithm. The resulting trends in blocking frequency vary by region and season. Since 1950, blocking frequency decreased longitudinally by 2% per decade over the North Atlantic (January–May) and Asia (February) while it increased by 2% and 4% per decade over Europe (September) and East Asia (June), respectively. Some of these changes represent spatial shifts. Since 1979, regional blocking trends represent an increase over the British Isles in March and a decrease over the North Atlantic in November. We find a connection between blocking over Central and Eastern Europe and increased heatwave frequency in Austria and between blocking over Northern Europe and decreased heatwave frequency in Austria. We also demonstrate a connection between blocking over Northern Europe, the North Atlantic and Greenland and more frequent cold spells in Austria. Finally, blocking over Russia is connected to more frequent heavy precipitation events while blocking over the British Isles and the North Sea is associated with less frequent heavy precipitation events in Austria. Our findings can help stakeholders better understand changes in blocking frequency over the northern hemisphere in the recent decades and effects on extreme weather in Austria.

Persistente Hochdruckgebiete (Blocking) in den mittleren Breiten können in dieser Region vorherrschende Westwinde blockieren und können Extremwetterereignisse auslösen. Ziel dieser Arbeit ist es, Trends in der Häufigkeit von Blocking über nördlichen mittleren Breiten und den Zusammenhang mit Extremwetterereignissen in Österreich zu untersuchen. Ein Algorithmus zur Detektion von Blocking und ein lineares Regressionsverfahren wurden auf ECMWF Re-Analysis Version 5 (ERA5)-Daten (1950 – 2019) zur Trendbestimmung angewandt. Zusammenhänge zwischen Blocking und Extremwetter wurden anhand von ERA5 und WATCH Forcing Data ERA5 (WFDE5) (1980 – 2018) mittels eines Monte-Carlo-Algorithmus untersucht. Die resultierenden Trends in der Blockinghäufigkeit variieren je nach Region und Jahreszeit. Seit 1950 nahm die Häufigkeit zonal über dem Nordatlantik (Januar-Mai) und Asien (Februar) um 2% pro Jahrzehnt ab, während sie über Europa (September) und Ostasien (Juni) um 2% bzw. 4% pro Jahrzehnt zunahm. Einige dieser Änderungen sind auf räumliche Verschiebungen zurückzuführen. Seit 1979 zeigen die regionalen Trends eine Zunahme über den Britischen Inseln im März und eine Abnahme über dem Nordatlantik im November. Es konnten Zusammenhänge zwischen Blocking in Mittel- und Osteuropa und häufigeren Hitzewellen in Österreich sowie zwischen Blocking über Nordeuropa und selteneren Hitzewellen in Österreich nachgewiesen werden. Ebenso gibt es Zusammenhänge zwischen Blocking über Nordeuropa, dem Nordatlantik und Grönland und häufigeren Kältewellen in Österreich. Schließlich konnten Zusammenhänge zwischen Blocking über Russland und häufigeren Starkniederschlagsereignissen sowie zwischen Blocking über den Britischen Inseln und der Nordsee und selteneren Starkniederschlagsereignissen in Österreich gezeigt werden. Diese Ergebnisse tragen dazu bei, Veränderungen der Auftrittshäufigkeit von blockierenden Hochdrucksystemen und mögliche Auswirkungen auf Extremwetter in Österreich besser zu verstehen.

SR 101 | 2023 Investigating atmospheric blocking and related extrem events in Austria using observation-based datasets
Wegener Center Verlag, University of Graz, Austria. ISBN 978-3-9505053-0-6